The Abdus Salam
International Centre for Theoretical Physics

United Nations
Educational, Scientific and
Cultural Organization

IAEA
International Atomic Energy Agency

2142-3

Advanced Conference on Seismic Risk Mitigation and Sustainable Development

10 - 14 May 2010

Fault Zone Physical Processes Controlling Earthquake Nucleation and Dynamic Earthquake Rupture

James R. Rice

Harvard University
Dept. Earth & Planetary Sciences
USA

Presentation for conference on
Seismic Risk Mitigation and Sustainable Development
Abdus Salam International Centre for Theoretical Physics
Trieste, Italy, 10-14 May 2010

Fault Zone Physical Processes Controlling Earthquake Nucleation and Dynamic Earthquake Rupture

James R. Rice (Harvard Univ.)

Collaborators on studies discussed:

Massimo Cocco (INGV, Rome), ***Nora DeDontney*** (Harvard), ***Renata Dmowska*** (Harvard), ***Eric M. Dunham*** (Stanford), ***Nadia Lapusta*** (Caltech), ***Kristine M. Larson*** (Colorado), ***Yajing Liu*** (Woods Hole), ***Hiroyuki Noda*** (Caltech), ***Alan W. Rempel*** (Oregon), ***John W. Rudnicki*** (Northwestern), ***Paul Segall*** (Stanford), ***Victor C. Tsai*** (USGS), ***Robert C. Viesca-Falguières*** (Harvard)

Outline:

- Rate and state dependent friction, slow slip rates
  - Lab and physical basis.
  - Crustal loading, earthquake nucleation and event sequences.
  - Aseismic deformation transients in subduction zones.
  - Dieterich [*JGR,* 1994] derivation of Omori law; change in earthquake rates.

- Thermal weakening by dynamic shear along mature fault zones
  - Structure and physical state of maturely slipped faults
  - Dynamic thermal weakening processes during seismic slip
    - -- flash-heating of microscale contact asperities
    - -- thermal pressurization of pore fluids
    - -- thermal decomposition (e.g., of clays, serpentine, carbonates)
  - Self-healing rupture modes and earthquakes at low overall stress levels

Rate / state friction definitions & parameters:

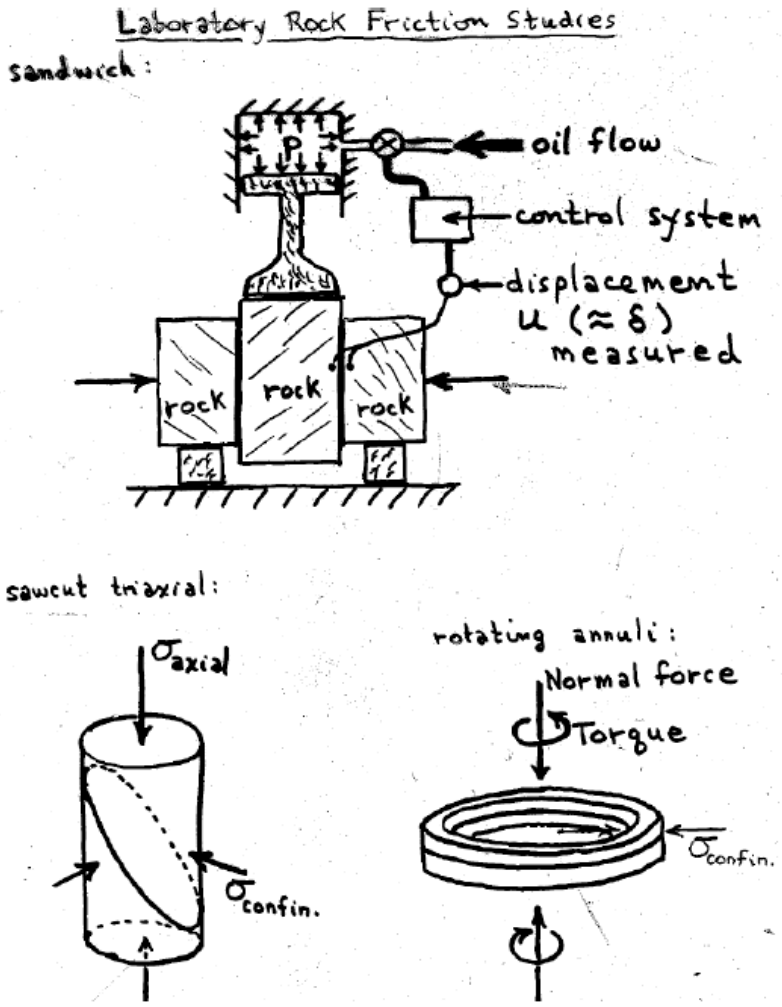

Dieterich & Kilgore data, granite gouge at room *T*:

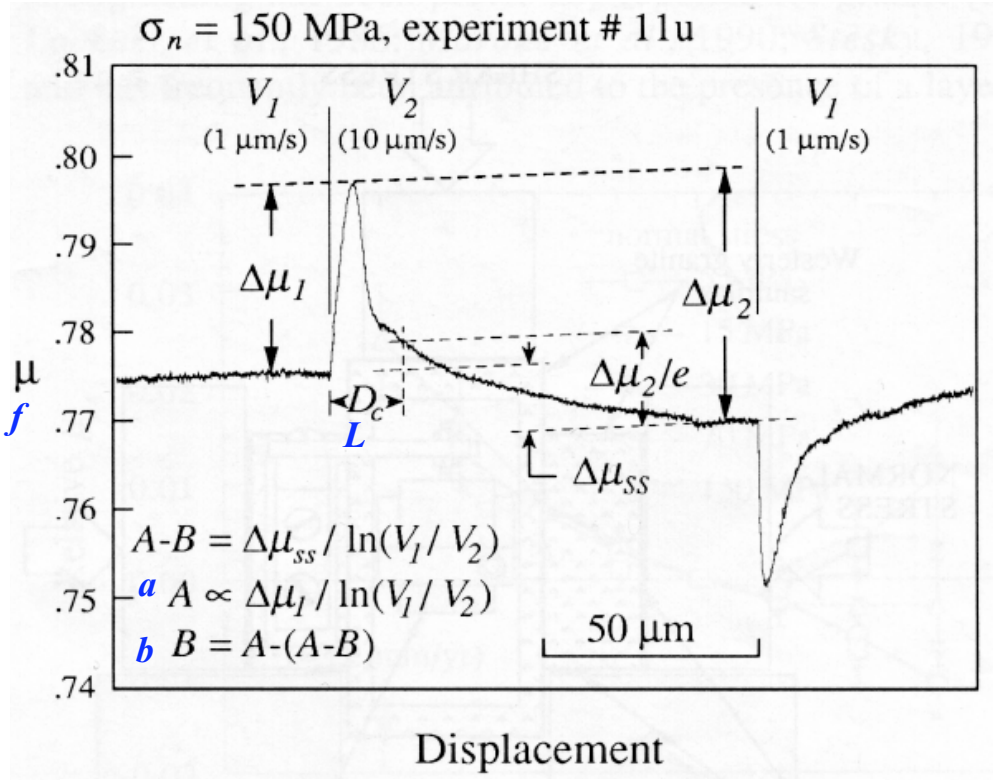

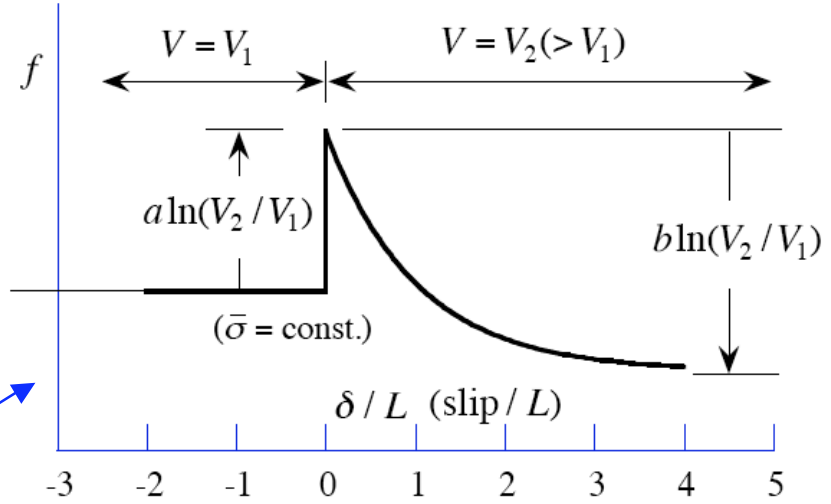

Diagram to describe rate/state equations

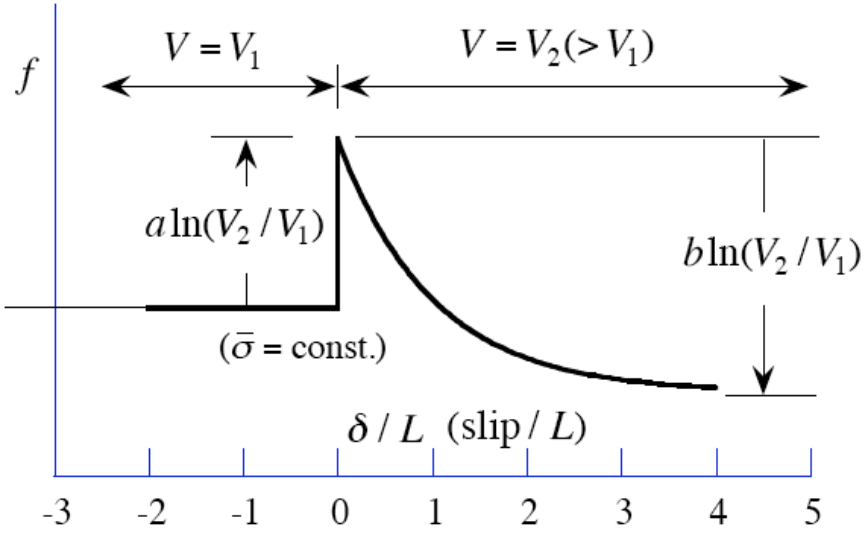

- f = friction coefficient $= \dfrac{\tau}{(\sigma - p)} = \dfrac{\tau}{\bar{\sigma}}$ (shear stress; effective stress; pore pressure; normal stress)
- δ = slip
- $V = \dfrac{\partial \delta}{\partial t}$ = slip rate
- L = slip to renew asperity contact population

- $a = V\left(\dfrac{\partial f}{\partial V}\right)_{\text{instantaneous}} > 0$ always.
- $f_{ss}(V)$ = steady state value of f
- $a - b = V\left(\dfrac{df_{ss}(V)}{dV}\right)$;

  $a - b > 0 \Rightarrow$ *stable* and

  $a - b < 0 \Rightarrow$ *potentially unstable*.

- Unstable slip patch size $\approx 4h^*$:

$$h^* = \frac{2\mu L}{\pi(1-\nu)(b-a)_{\max}\bar{\sigma}}$$

$$4h^* \approx 1.0 \text{ km} \times \frac{L}{40\ \mu\text{m}} \times \frac{1.0 \text{ MPa}}{\bar{\sigma}}$$

Note: *Dilatancy* with increase of V also stabilizes in *fluid-saturated* gouge); significant effect when $(b-a)_{\max}\bar{\sigma}$ is small [Segall & Rice, *JGR*, 1995]

- Commonly adopted model, with one state variable (called $\theta \approx$ avg. asperity contact lifetime):

$$f = f_o + a\ln(V/V_o) + b\ln(V_o\theta/L)\ , \quad d\theta/dt = 1 - V\theta/L \qquad \text{("ageing" law)}$$

At a given temperature T, a, b, L, f_o and V_o are constants (one of f_o and V_o chosen arbitrarily)

$$\theta_{ss}(V) = L/V\ , \quad f_{ss}(V) = f_o + (a-b)\ln(V/V_o)$$

Temperature dependence of friction parameters:

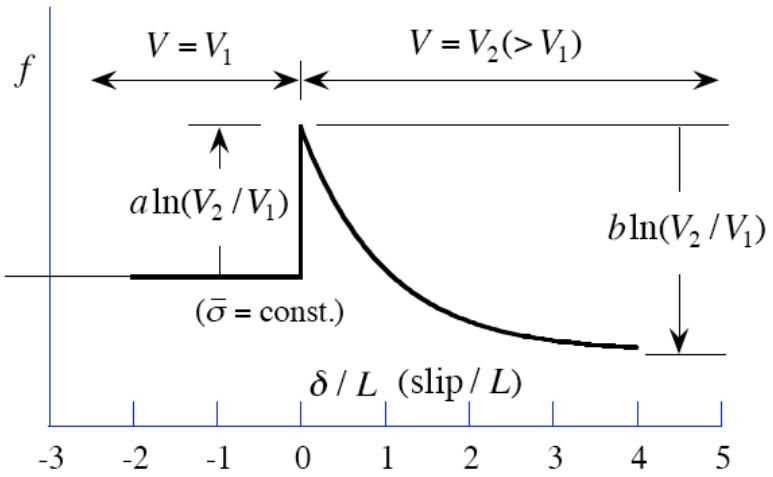

f = friction coefficient $= \tau / (\sigma - p) = \tau / \bar{\sigma}$.

δ = slip, $V = \partial\delta / \partial t$ = slip rate.

L = slip to renew asperity contact population.

$a = V[\partial f / \partial V]_{\text{instantaneous}} > 0$ always.

$a - b = V df_{ss}(V) / dV$ can be > 0 (*stable*)

or < 0 (*potentially unstable*).

Unstable slip patch size $\approx 4h^*$;

$h^* = 2\mu L / [\pi(1-\nu)(b-a)_{\max}\bar{\sigma}]$,

$$4h^* \approx 1.0 \text{ km} \times \frac{L}{40\ \mu\text{m}} \times \frac{1.0 \text{ MPa}}{\bar{\sigma}}$$

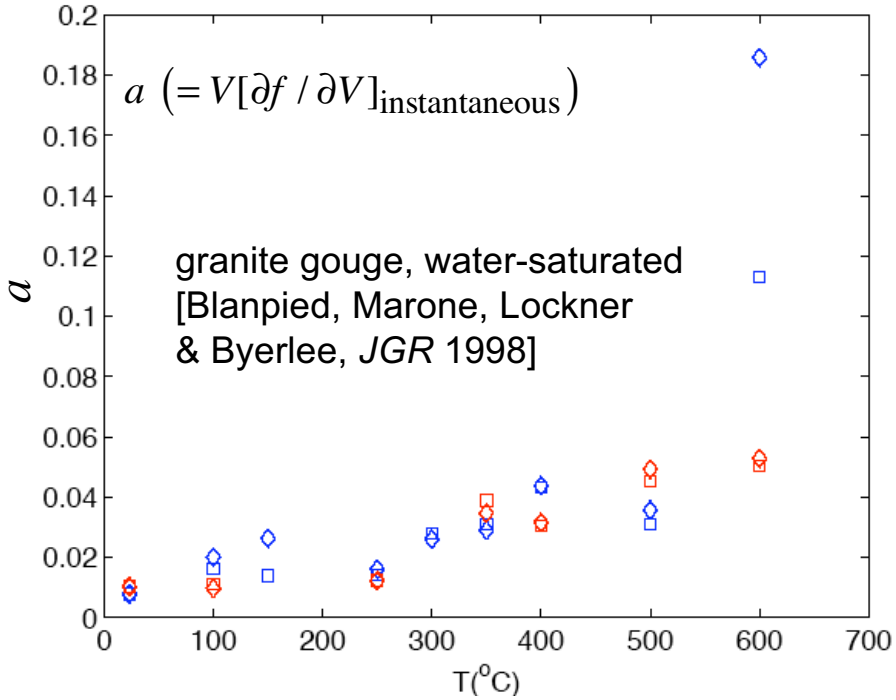

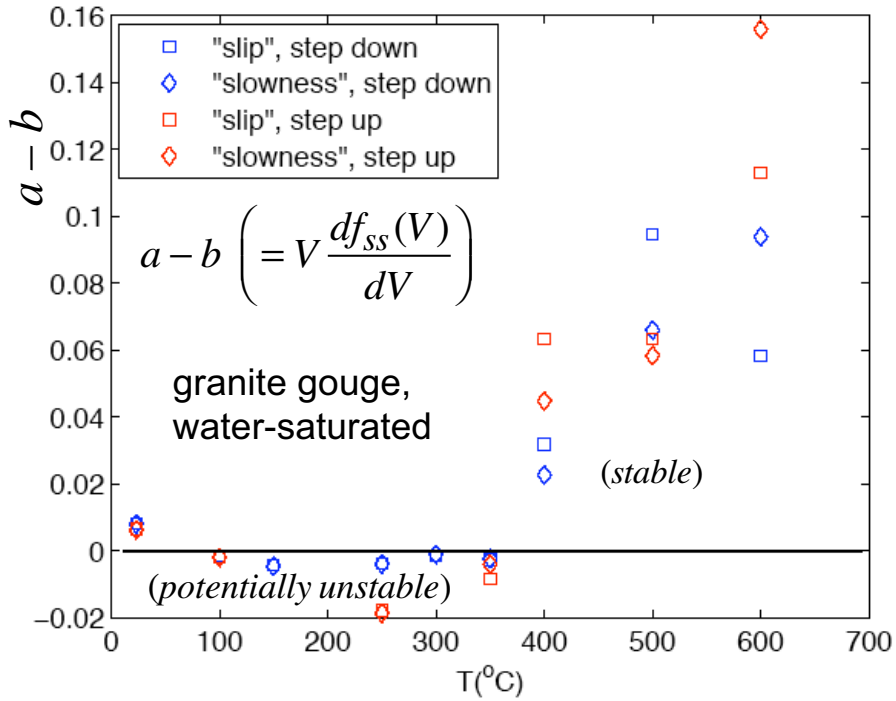

Application to study of nucleation and early propagation of rupture in a strike-slip fault model (Lapusta & Rice [*JGR*, 2003])

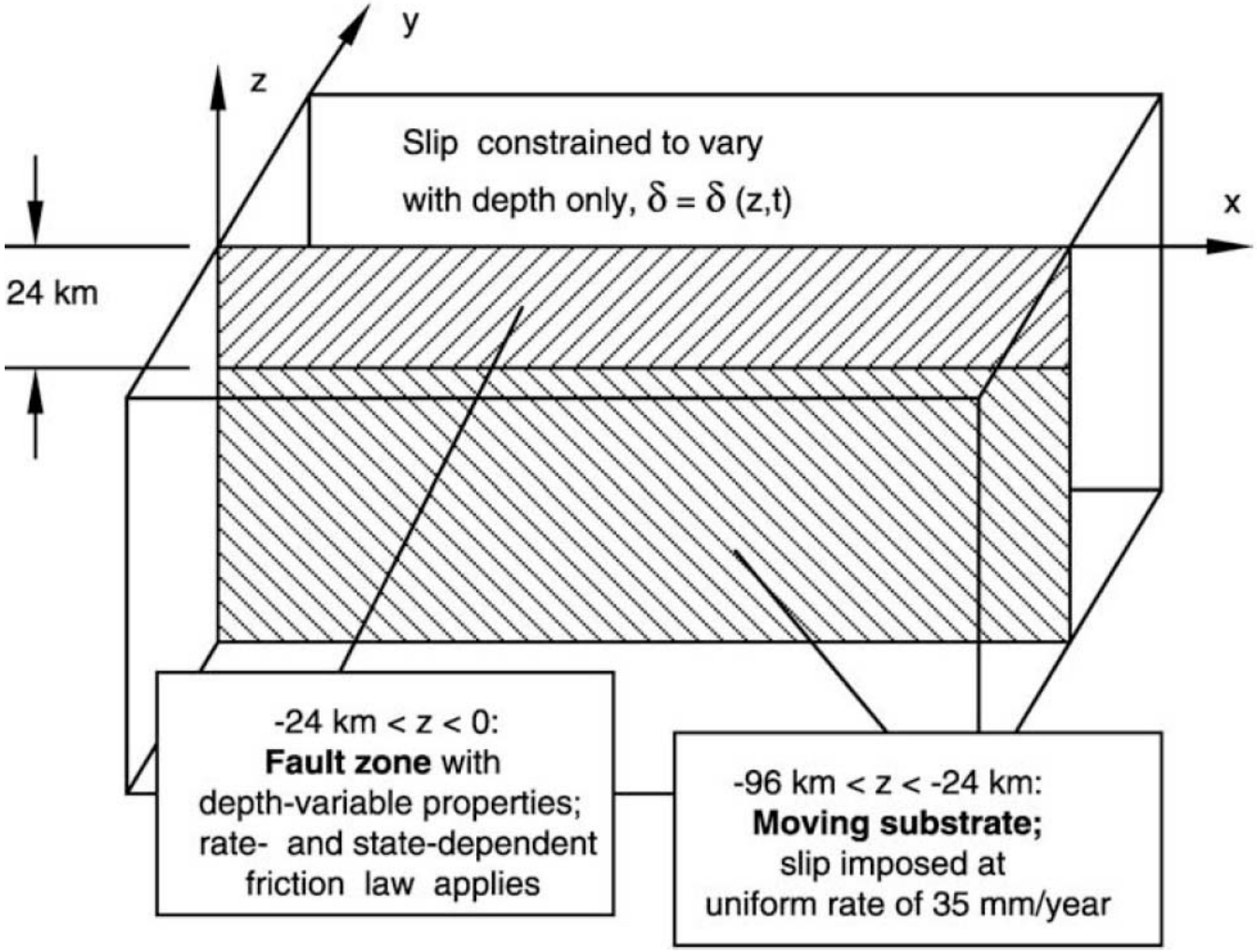

A vertical strike-slip fault in an elastic half-space.

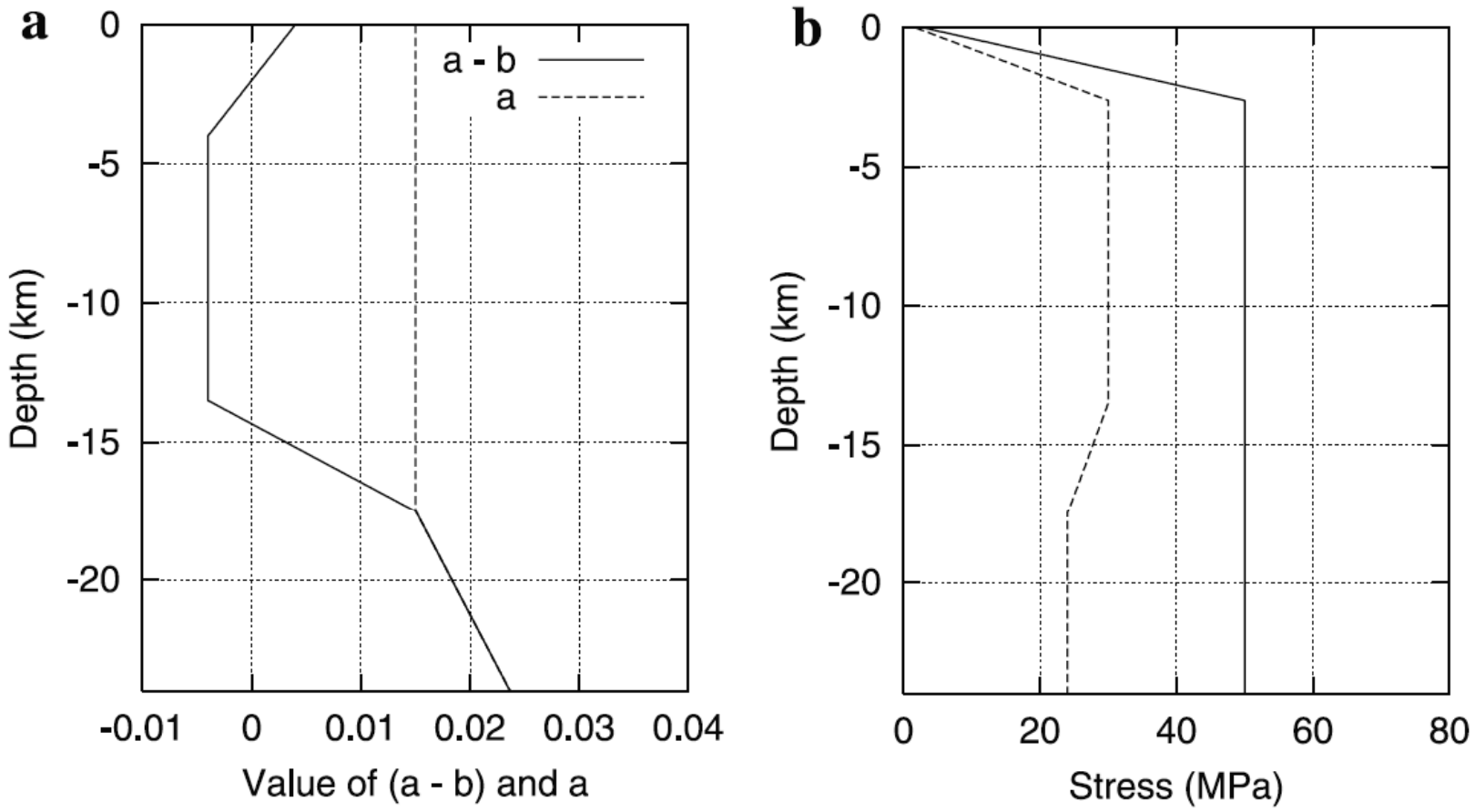

Figure 2. (a) Depth-variable distribution of frictional parameters ($a - b$) and a, the former from *Blanpied et al.* [1991, 1995] as adapted by *Rice* [1993] for granite gouge under hydrothermal conditions. (b) Depth-variable distribution of the effective normal stress $\bar{\sigma}$ (solid line) and initial shear stress $\tau^o(z)$ (dashed line). From *Lapusta et al.* [2000].

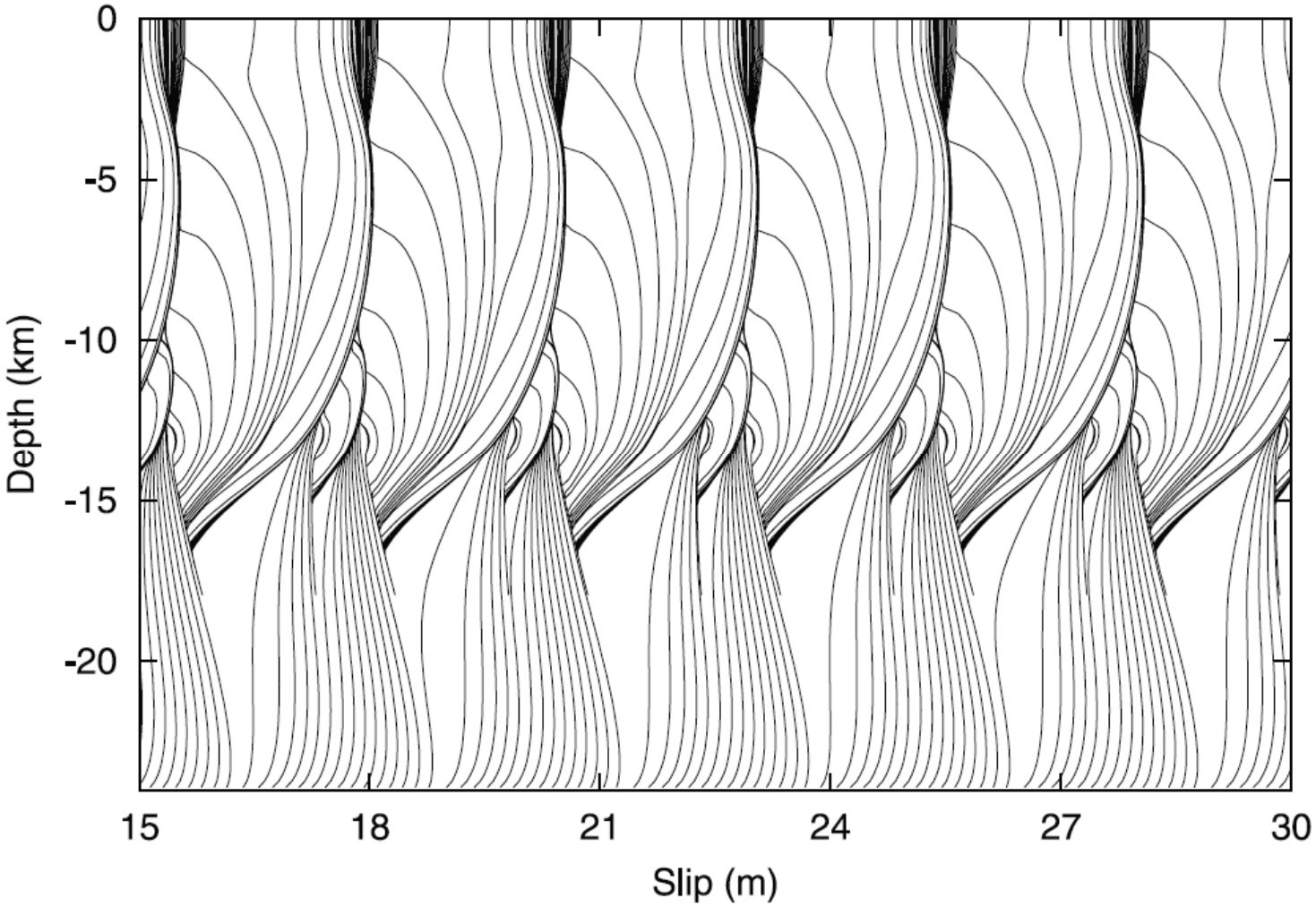

Slip accumulation for L = 2 mm with (top) all dynamic effects included.

Each line represents the profile of slip at a certain time:

- Solid lines show slip accumulation every 5 years.
- Dashed lines, which capture model earthquakes, are plotted every 1 second when maximum slip velocity on the fault is > 1 mm/s.

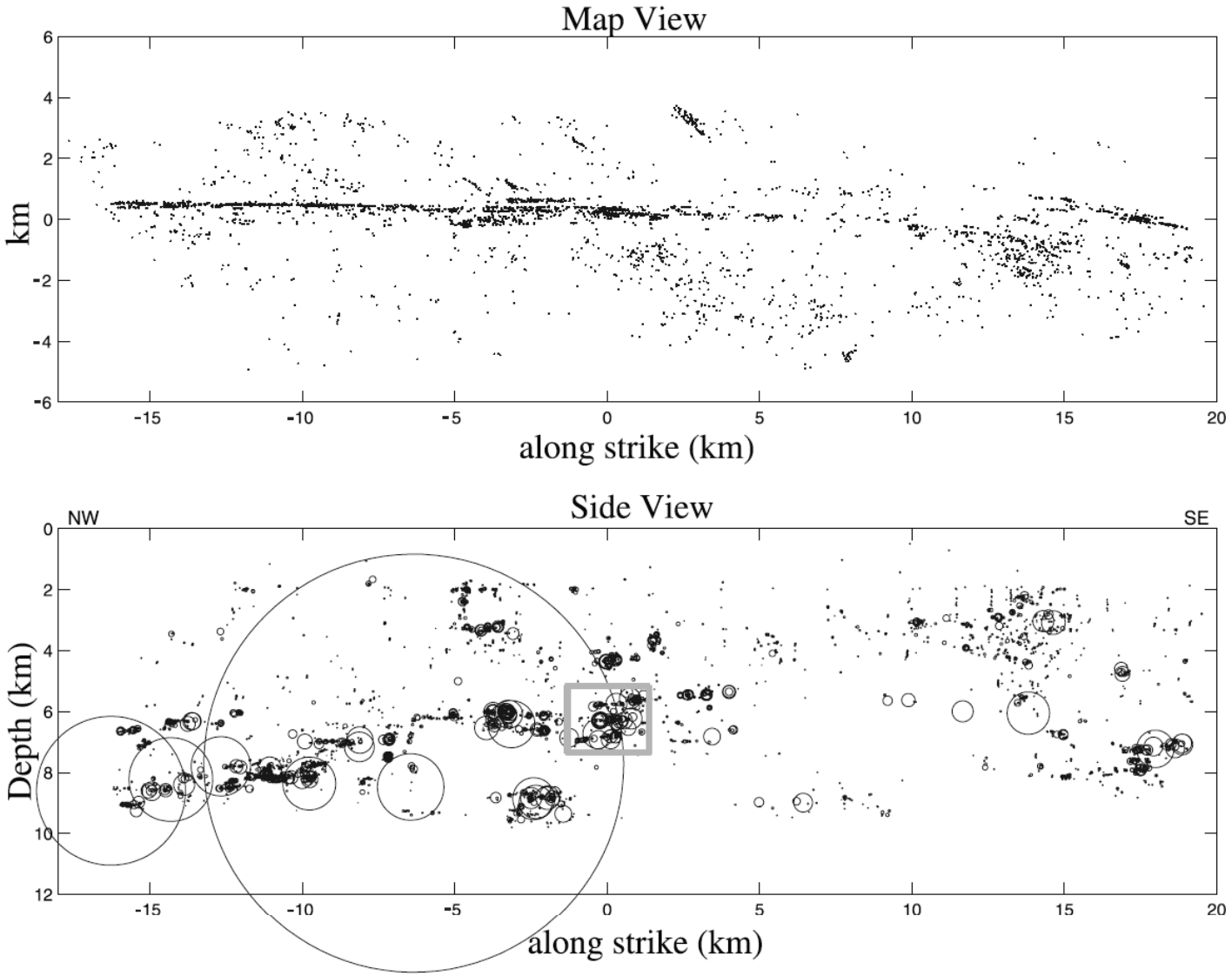

Figure 8. From *Schaff et al.* [2002], courtesy of D. P. Schaff. Earthquake locations for the Calaveras fault from 1984 until present, comprising 7857 events. (top) Map view of events along the Calaveras fault. (bottom) Fault plane side view displaying only on-fault earthquakes with estimated source sizes based on circular crack model using a 3 MPa stress drop. The largest event is the *M* 6.2 Morgan Hill 1984 main shock. The hole in microseismicity, outlined by small events, is located starting from about 4 km along strike and farther to the right. This was also the area of the largest slip during the Morgan Hill event.

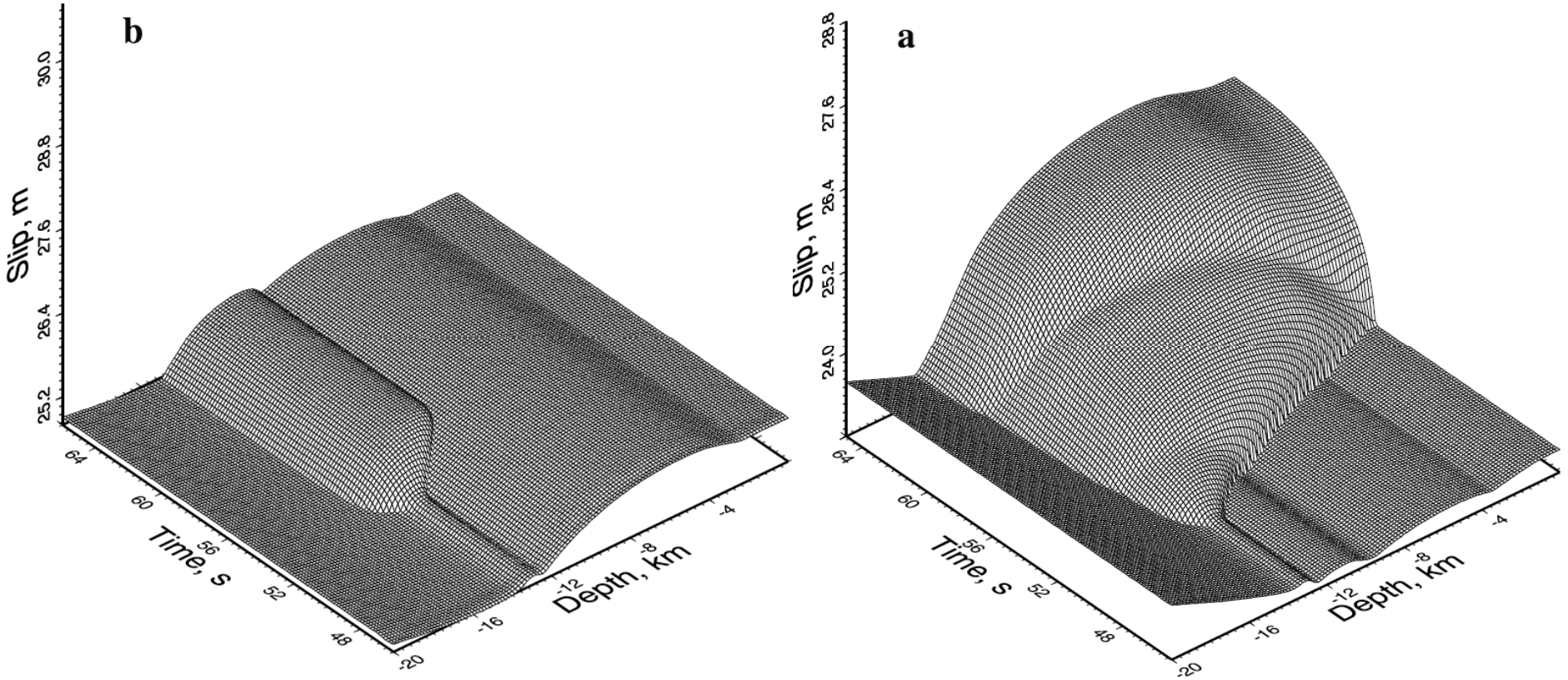

Comparison of moment rate (for slip distribution projected to a circular rupture), as function of time, for the large and small events.

The signal from the beginning of the two events is very similar.

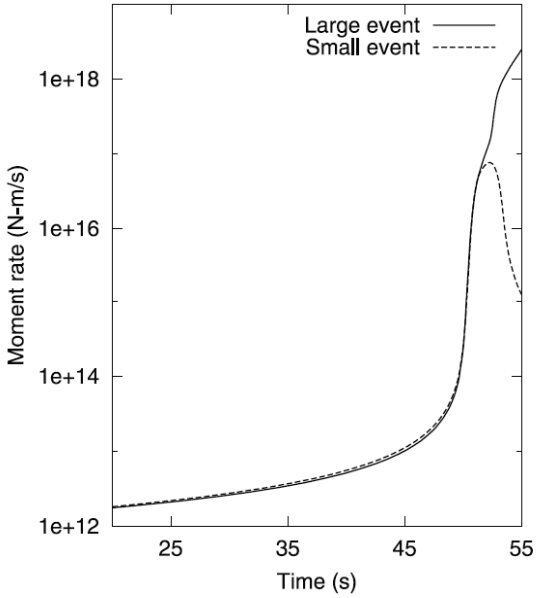

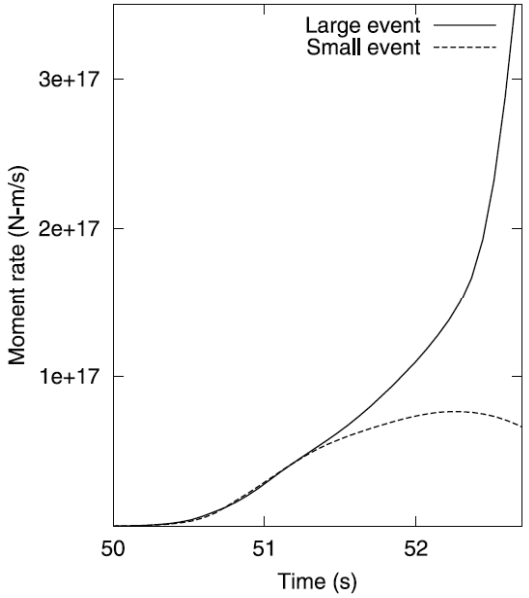

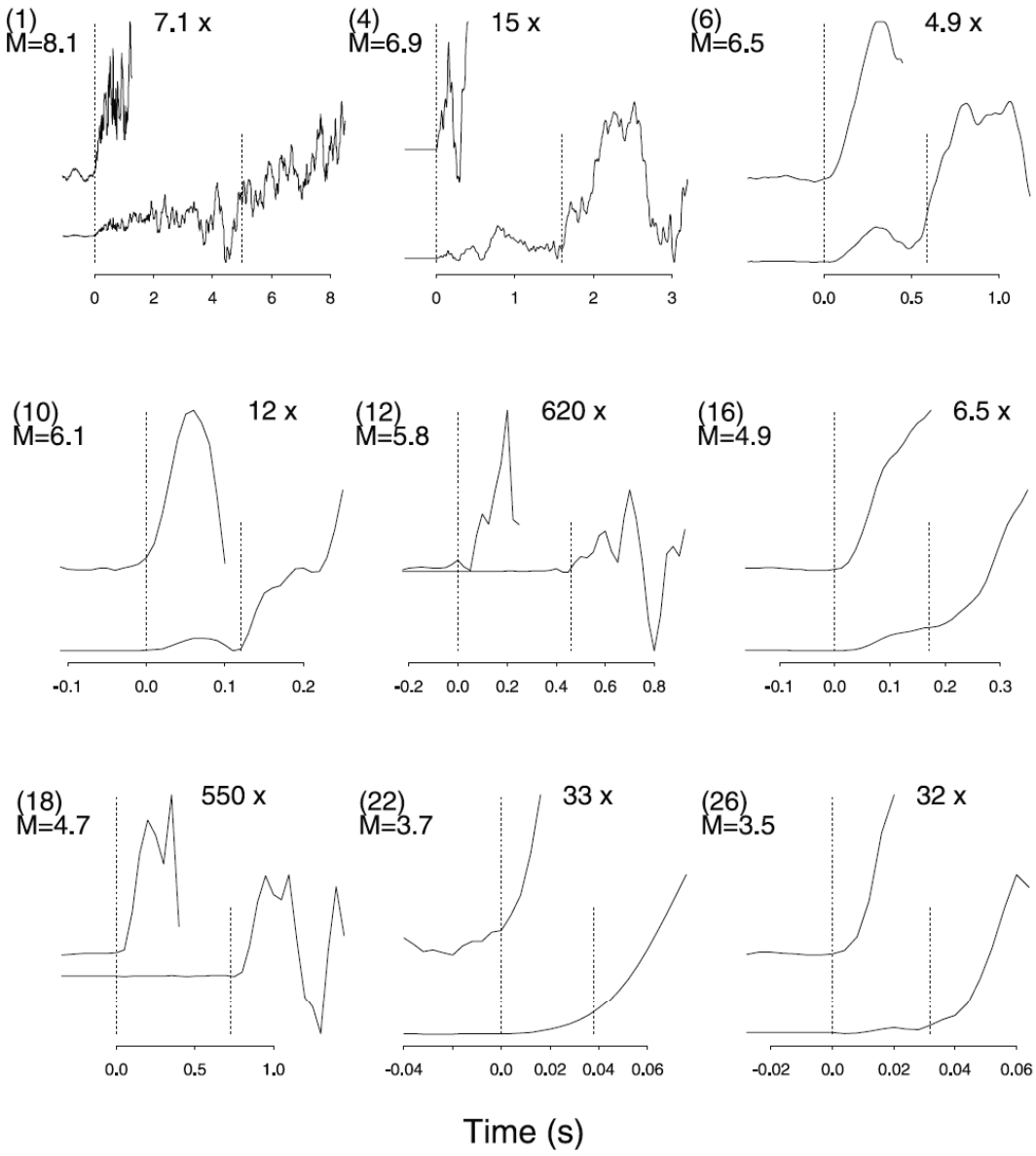

Figure 11. Broadband velocity seismograms are shown at two amplitude scales to display the character of the first arrival and the subsequent strong arrivals. Time increases from left to right and is at different scale for each seismogram. Note slowdowns and speedups in the initial phases, similar to model earthquakes in Figure 13. Reprinted with permission from *Ellsworth and Beroza* [1995] (copyright 1995 American Association for the Advancement of Science), courtesy of G. C. Beroza.

Cascadia
"Aseismic" Deformation Transients and Non-Volcanic Seismic Tremor

[Dragert, Wang & James, 2001]:

[Rogers & Dragert, 2003]:

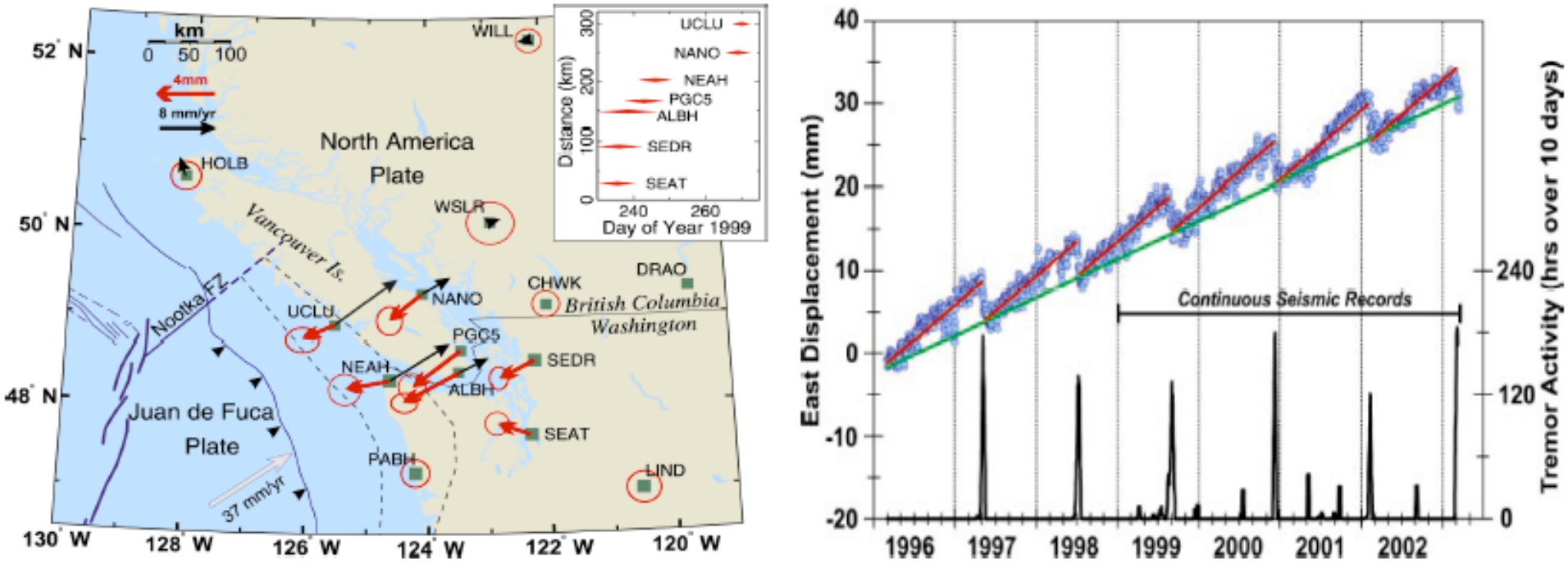

(a) (b)

Fig. 4. (a) Locations of continuous GPS sites (from Dragert et al., 2001). Bold red arrows show displacement, with respect to station DRAO, due to the aseismic slip event. Thin black arrows show 3 to 6-year average GPS motions with respect to DRAO. Two dashed lines delineate the nominal down-dip limits of the locked and transition zone (Peacock and Wang, 1995). (b) Comparison of slip and tremor activity observed for the Victoria area (from Rogers and Dragert, 2003).

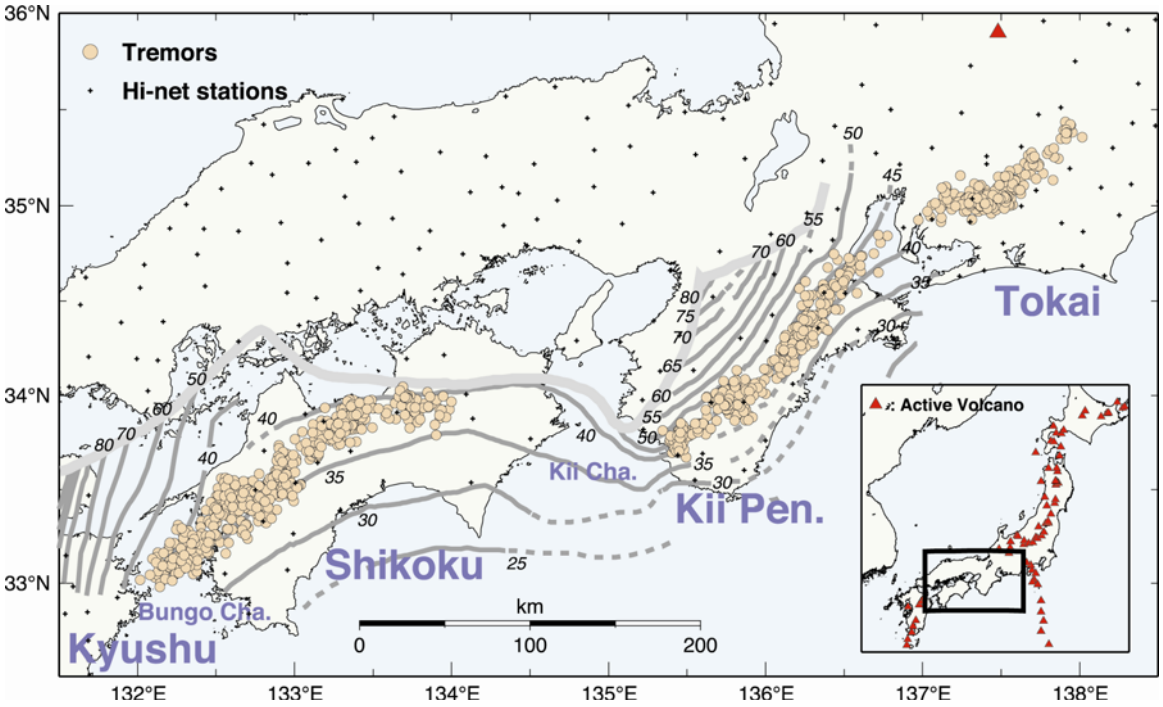

Non-volcanic tremors in SW Japan
[Obara, 2002]

Correlation with tilt transients
[Obara et al., 2004]

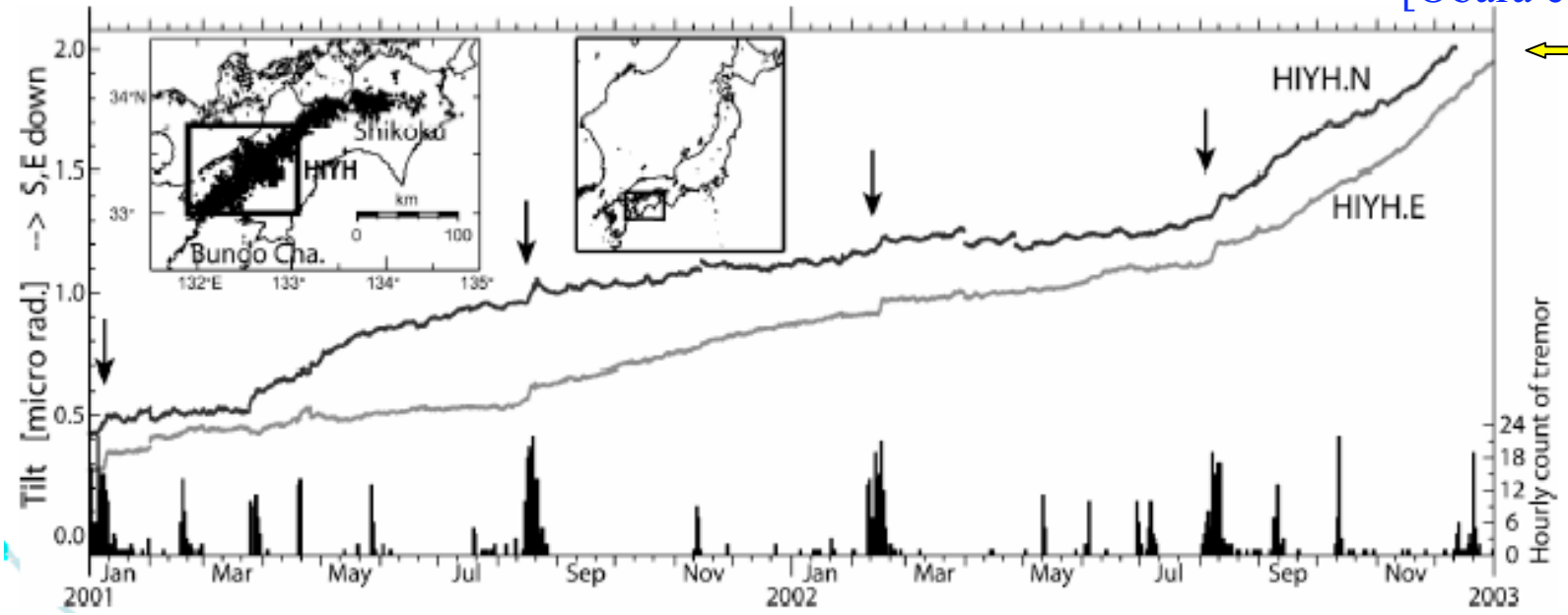

[Lowry, Larson, Kostoglodov & Sanchez, *GJI,* 2005]:

Aseismic deformation transients along the Middle American Trench, Guerrero, Mexico, region.

Note the large transient from October 2001 to April 2002, and other significant event in 1998.

(Later, another comparably large transient from March to December 2006.)

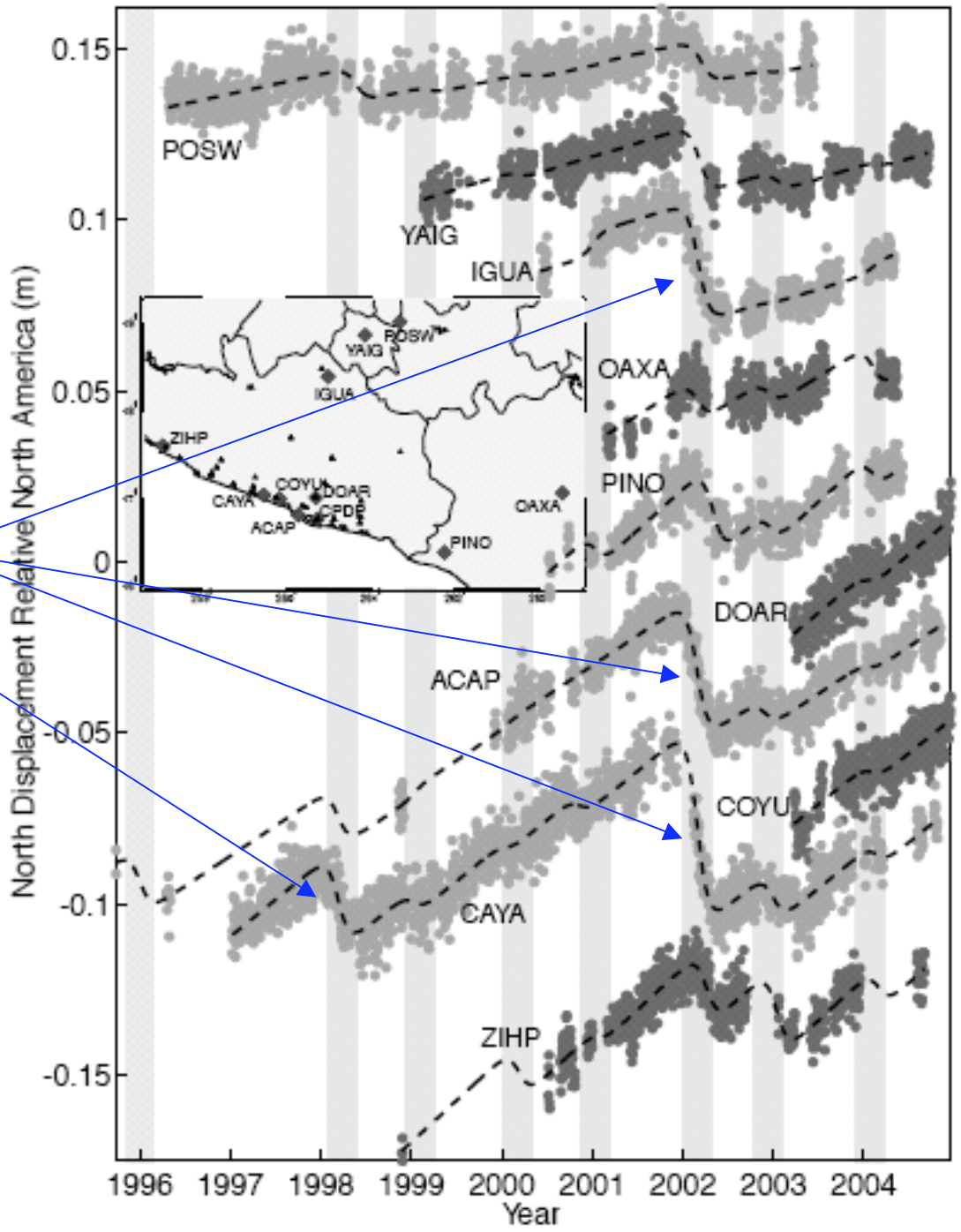

Liu et al. [*EPSL*, 2007]

Such transients may be the source of the *shifts of seismically active locations* discovered [Dmowska et al., *JGR*, 1988] elsewhere along the Middle American Trench.

Active areas shift in time from landward locations, where known mechanisms are extensional (N), to locations towards the trench where known mechanisms are compressional (T).

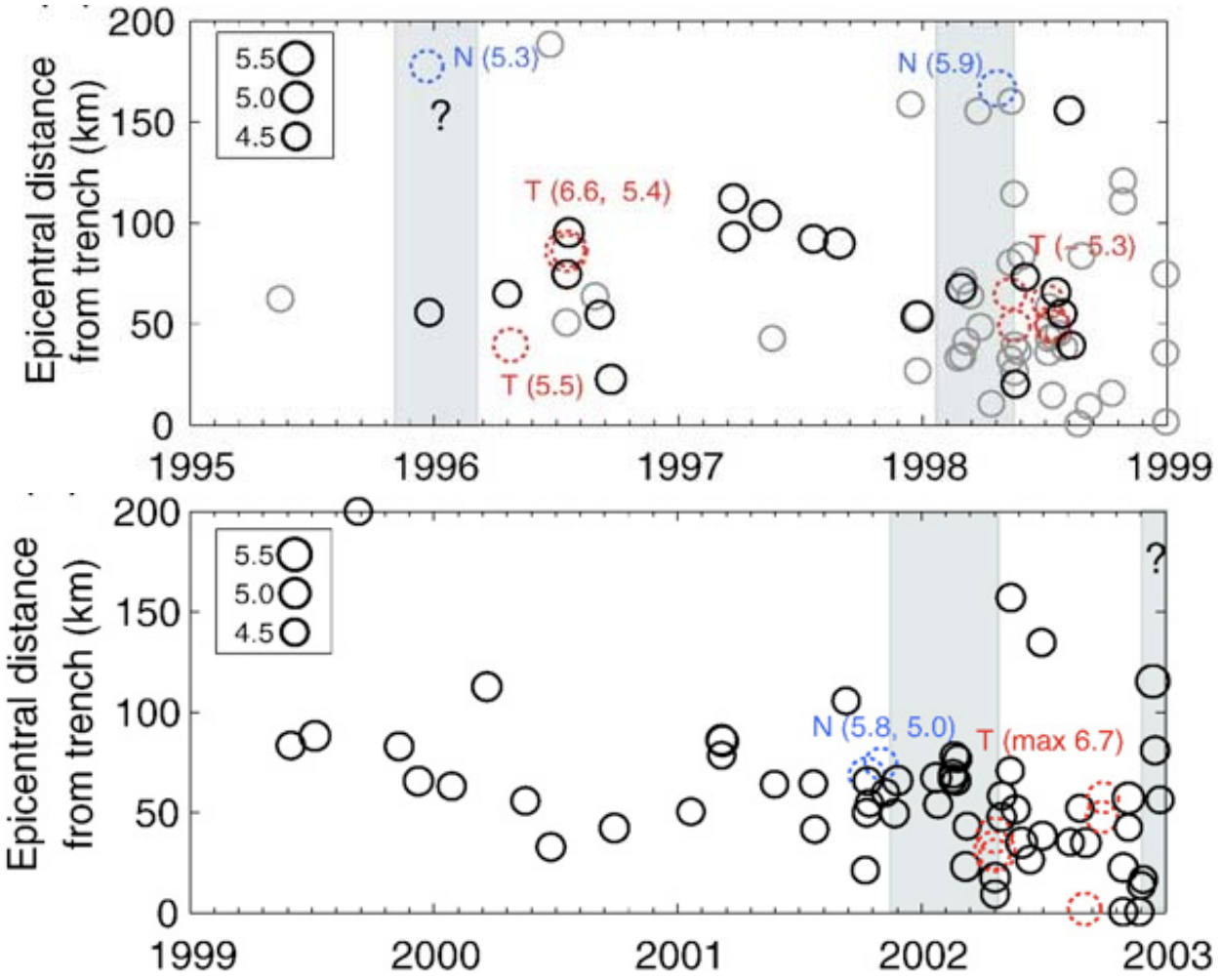

NEIC events with magnitude greater than 4.2, within the region of the network (see Liu et al. [*EPSL*, 2007]). Circle size is proportional to event magnitude. Dashed-line circles are NEIC events that have GCMT solutions: normal-faulting (N) and thrust faulting (T) marked. Numbers in parenthesis are moment magnitudes M_w from GCMT; only an average M_w is marked for a cluster of earthquakes, e.g., ~5.3 for the five T events after the 1998 transient. Gray circles represent events below Mc=4.5, but greater than 4.2.

2D Subduction Earthquake Model

[Liu & Rice, *JGR* 2007]

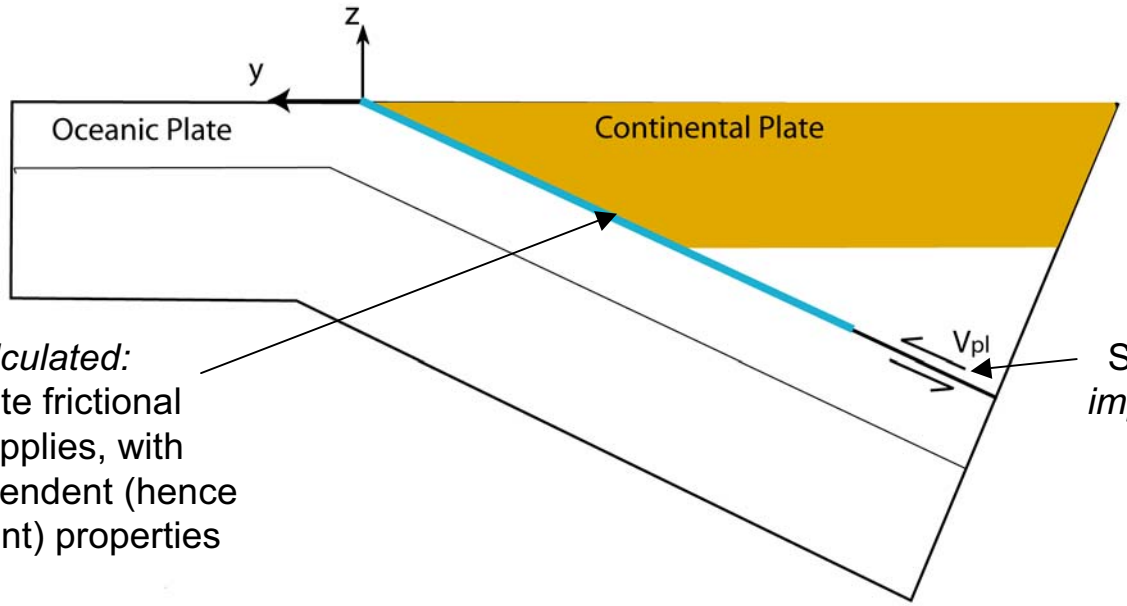

Slip is *calculated:*
Rate and state frictional description applies, with temperature-dependent (hence depth-dependent) properties

Slip is *imposed*

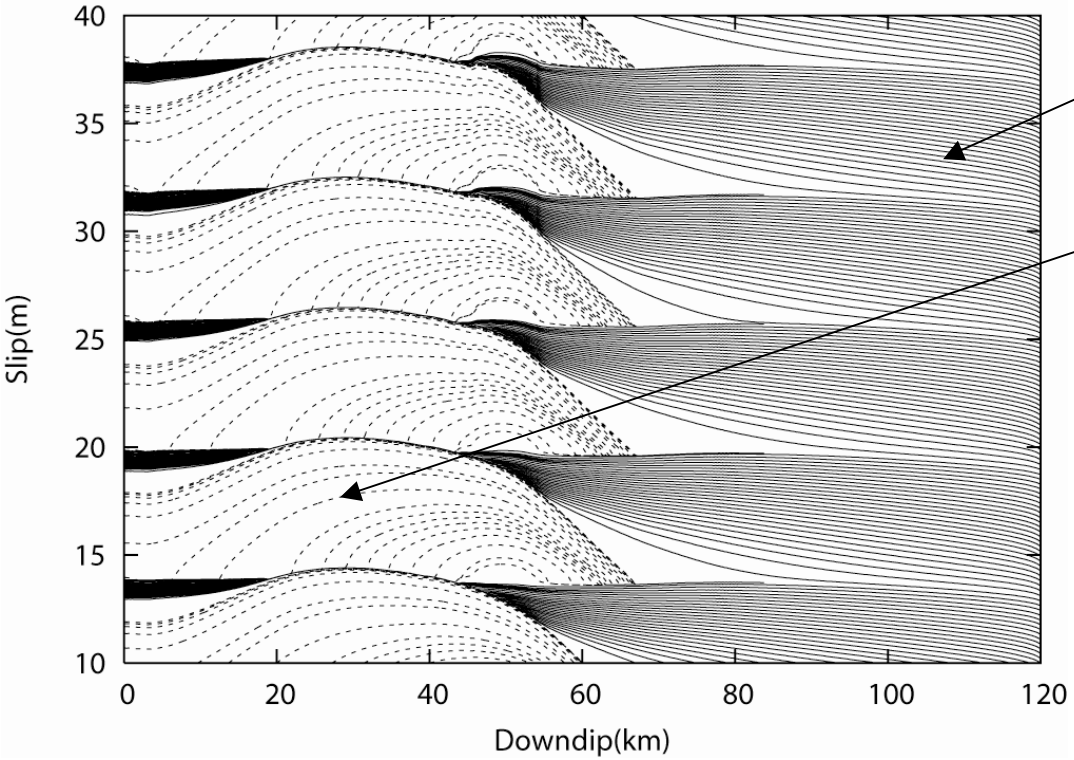

Interseismic slip plotted every 5 yrs

Coseismic slip plotted every 10 sec.

(Low rupture propagation and slip speeds, by factor of order 1/100, due to use, in this case, of radiation damping approximation to full elastodynamics)

Dehydration reactions should lead to near-lithostatic pore pressure at temperatures around ~450-550ºC

P-T phase diagram for rocks of oceanic crust

Superposed depth (~P) vs. T from thermal models of subduction zones

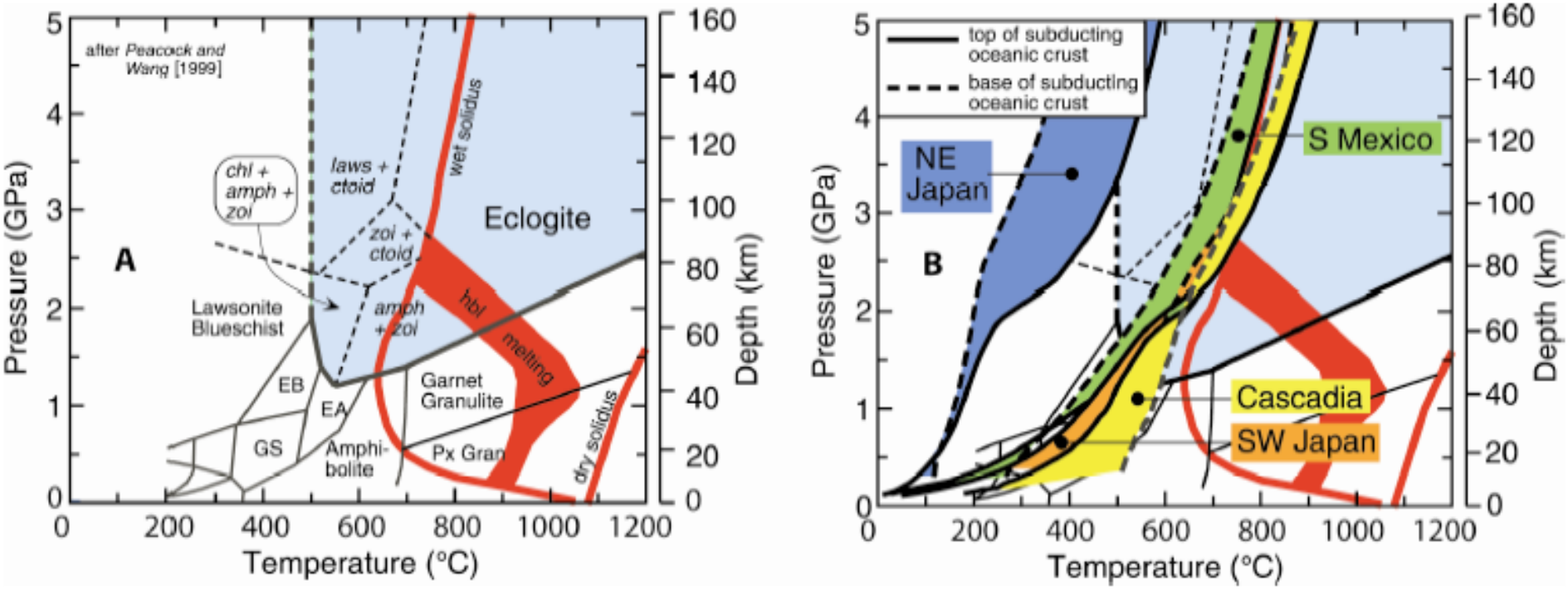

[Peacock et al., 2002]

Shelley, Beroza, Ide & Nakamula, *Nature,* 2006

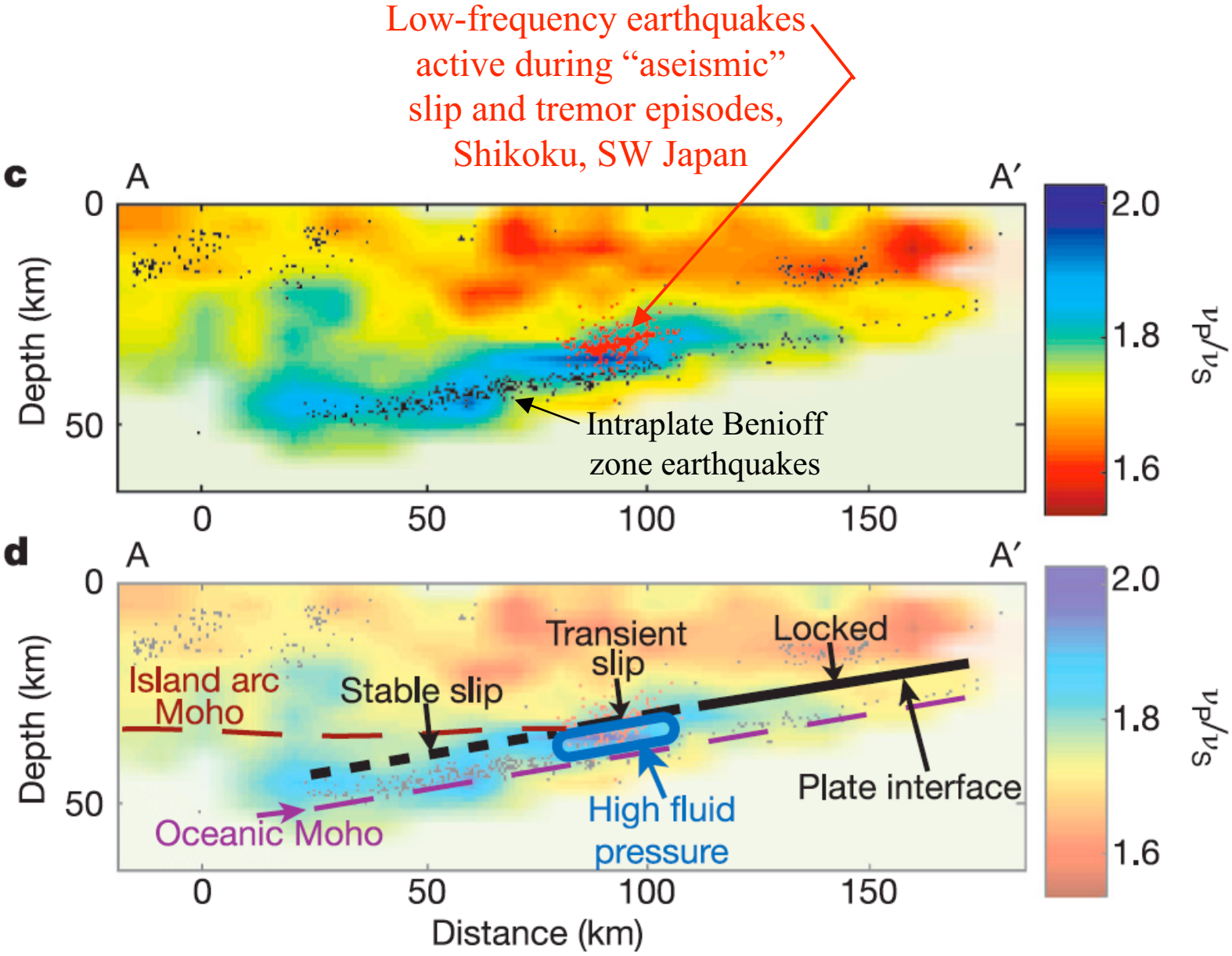

Liu & Rice
[*JGR*, 2009]

Estimate of zone of near-lithostatic pore pressure for N. Cascadia based on thermal models and inferred (from v_p / v_s) similar near-lithostatic zone in SW Japan.

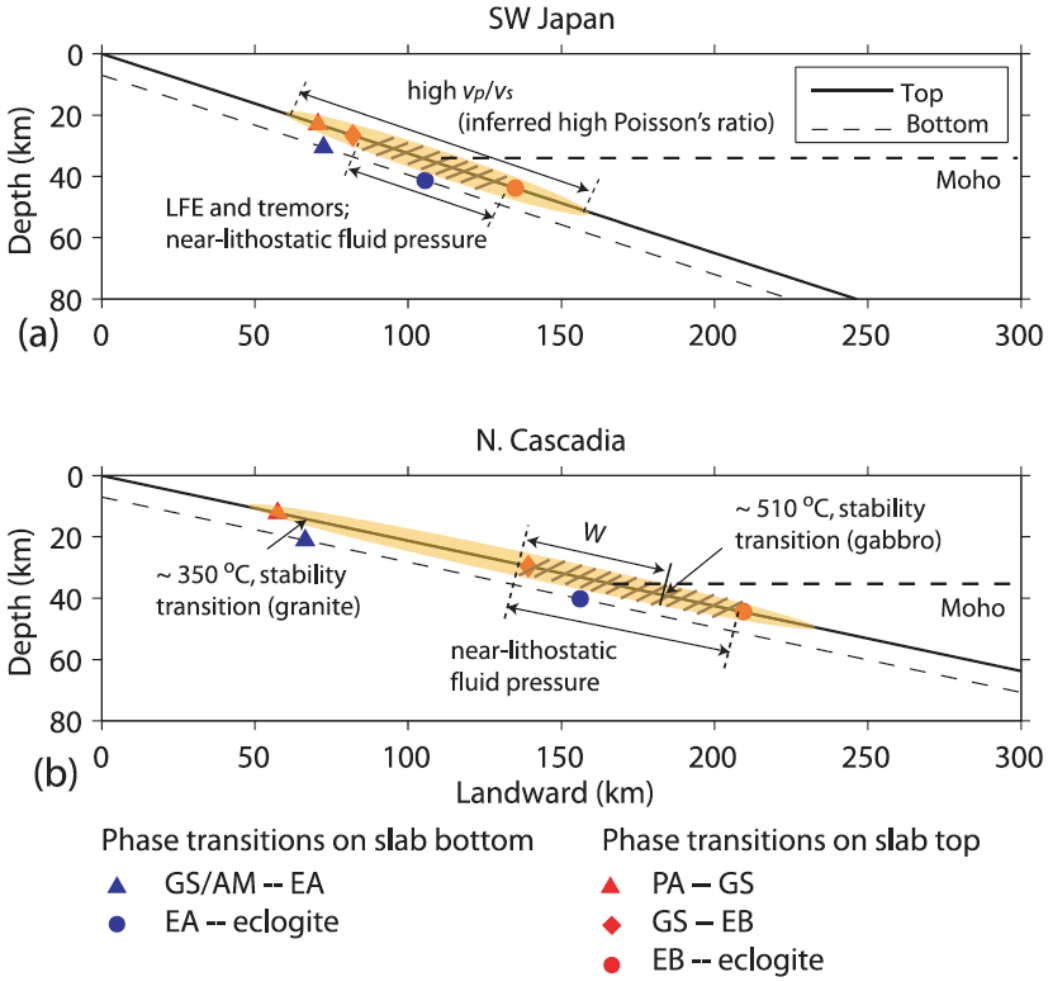

Figure 4. Schematic fluid pressure distribution on the subduction interface for SW Japan and northern Cascadia, based on petrological and thermal models of *Peacock et al.* [2002] and seismological observations of *Kodaira et al.* [2004], *Shelly et al.* [2006], and *Audet et al.* [2009]. Red and blue symbols represent major water-releasing phase transitions encountered by the top (solid) and bottom (dashed) of the subducting slab, respectively. See Table 1 for metamorphic facies abbreviations. Shaded yellow region represents generally high (overhydrostatic) fluid pressure p, and hatched lines represent depths of near-lithostatic p. In SW Japan, they correspond to the depth ranges of high v_p/v_s (and inferred high Poisson's ratio) and LFE/tremor locations, respectively. W is the distance updip from friction stability transition. The 510°C friction stability transition for gabbro gouge lies within the near-lithostatic p zone, while the 350°C transition for granite is much further updip.

Dry and wet granite gouge

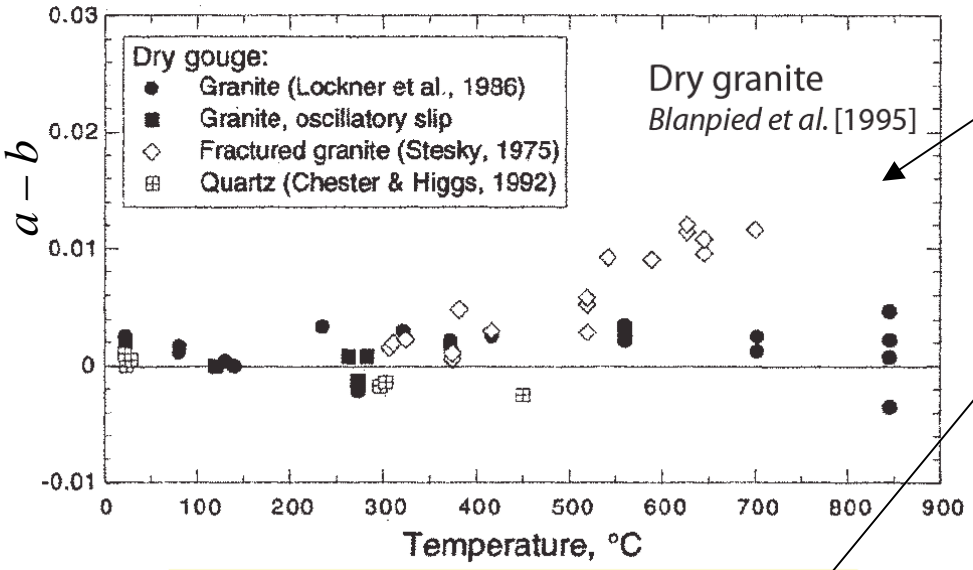

Lab measurements of *a-b* show large variations at temperatures around and above stability transition (granite, ~ 350°C; gabbro, ~ 510°C)

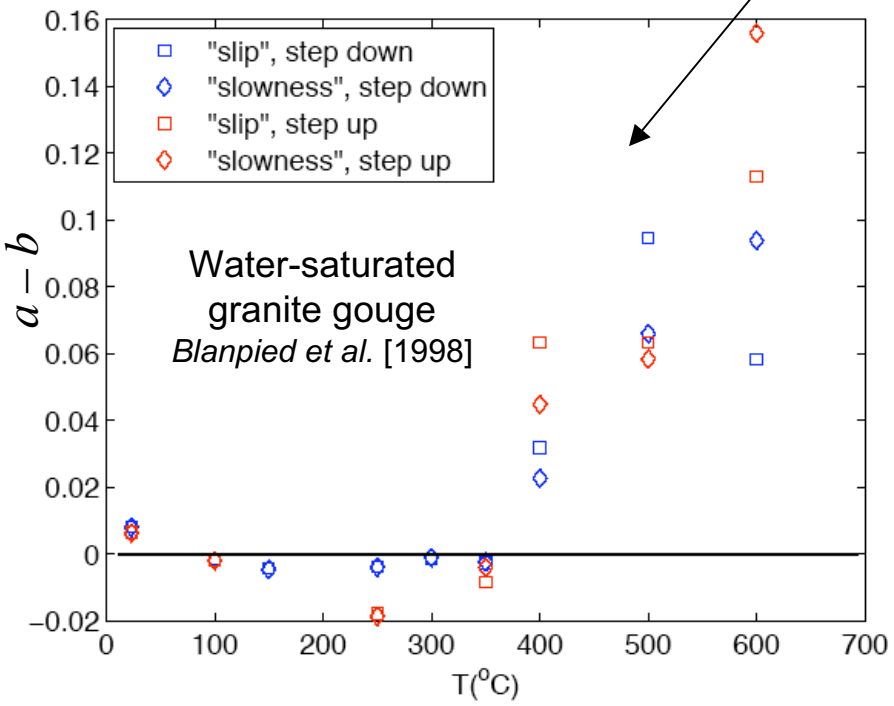

Over the stability transition, wet granite data show much more stabilizing effect (*a-b* ~0.1 at ~600°C) than the dry granite data (*a-b* ~0.01 at ~600°C). High positive values of *a-b* strongly prohibit the downdip propagation of aseismic slip.

Gabbro gouge

Lab measurements of *a-b* show large variations at temperatures around and above stability transition (granite, ~ 350°C; gabbro, ~ 450-500°C)

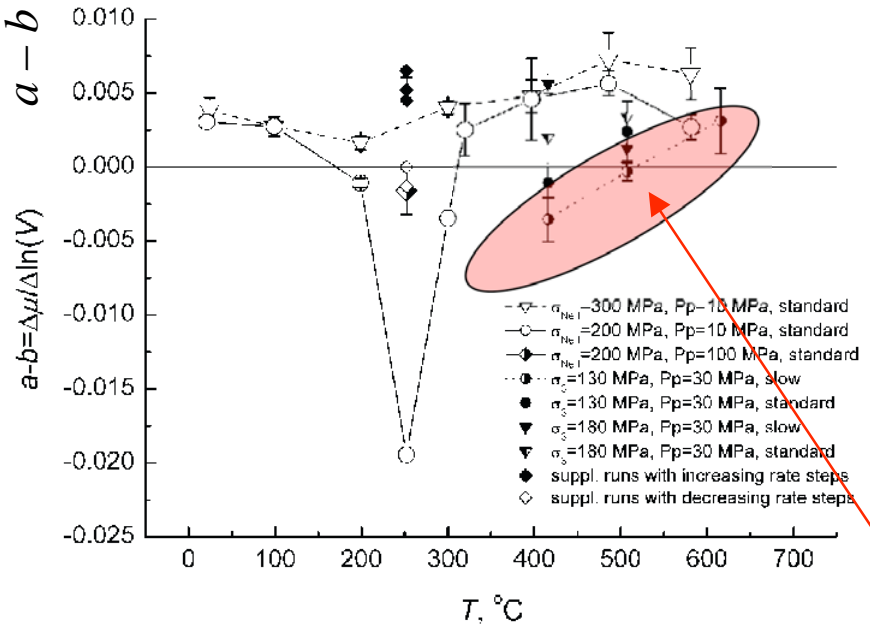

Gabbro is a better proxy for oceanic crust. Under supercritical water conditions (critical point: p_{H2O}=22 MPa, T=374°C), the velocity-weakening to strengthening stability transition takes place around 450-500°C. And at higher temperatures (up to ~600°C), *a-b* is smaller than 0.01. [Experimental data from He et al., 2006, 2007.]

Liu & Rice [2009]: Response in region of assumed near-lithostatic p zone near stability transition based on ***Wet Granite gouge*** data case: W=20 km, $\bar{\sigma}$ = 0.67 MPa, L ~ 0.4 mm, recurrence interval ~ 14 months, aseismic slip per event ~ 2 cm.

[Location of these events is *far too shallow*, giving poor fit to GPS data (next page).]

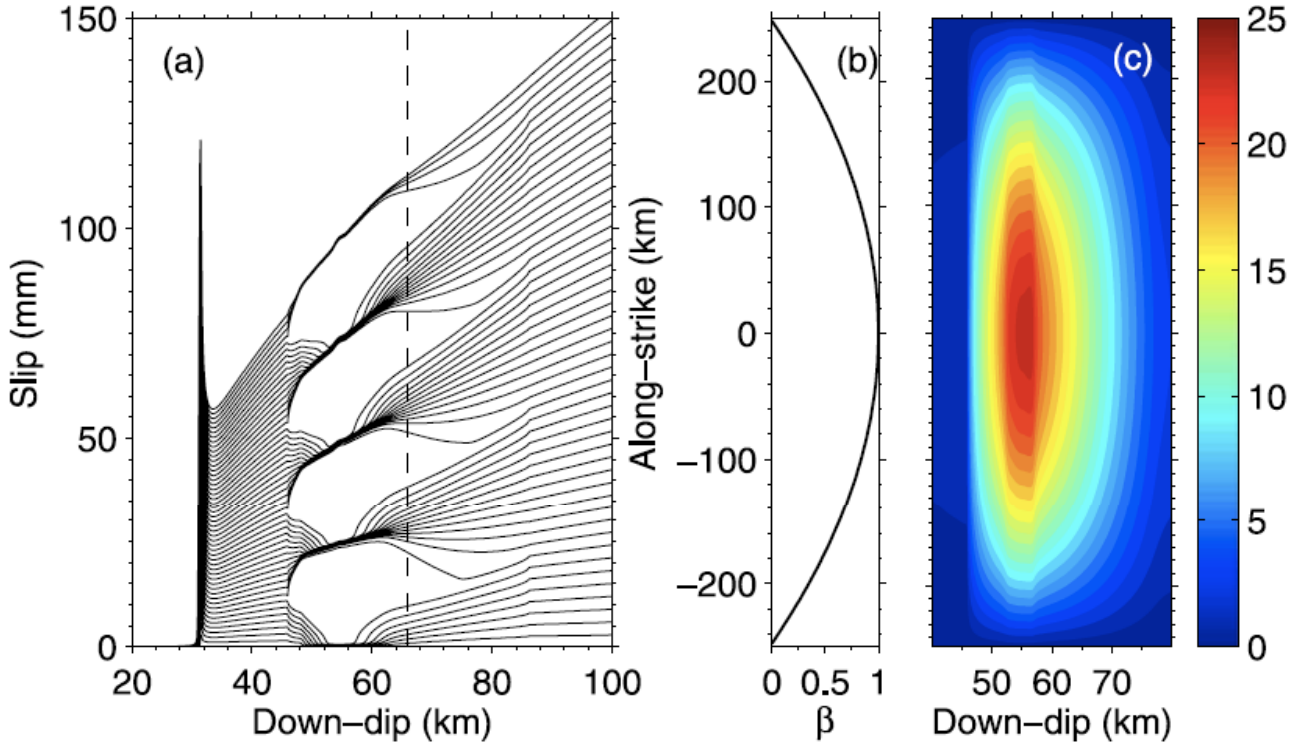

Figure 9. (a) Cumulative slip in a 5-year window, including four episodes of SSEs, using wet granite friction. Slip lines are plotted every 0.1 year. Vertical dashed line denotes the friction stability transition. During each SSE, maximum slip of about 23 mm is released in the velocity-weakening low $\bar{\sigma}$ zone, with much smaller slip in the downdip velocity-strengthening zone. Peak at ~30 km corresponds to the nucleation front for the next megathrust earthquake.

Liu & Rice [2009]:

Model based on ***Wet Granite Gouge*** friction properties in a near-lithostatic p zone, which is assumed to overlap the stability transition (necessary for the model to be able to predict aseismic slip transients).

Such models ***cannot fit GPS constraints***. This is because they put the near-lithostatic p zone at ***too shallow a depth*** compared to constraints of the thermal model and gabbroic phase diagram.

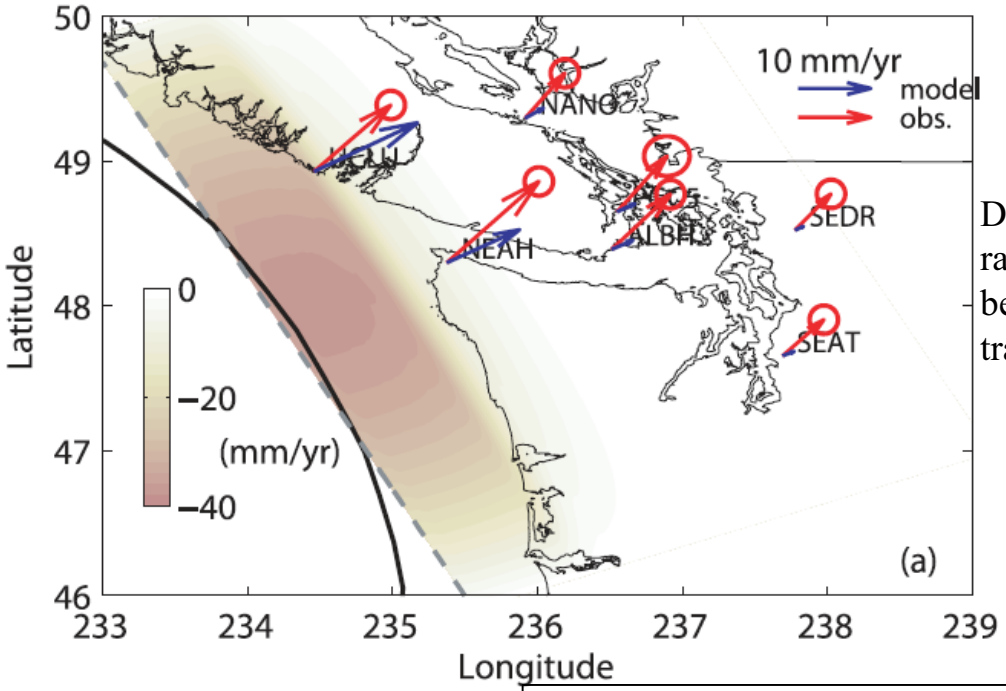

Displacement rates in period between transients

$W = 20$ km, $\bar{\sigma} = 0.67$ MPa, $L = 0.4$ mm

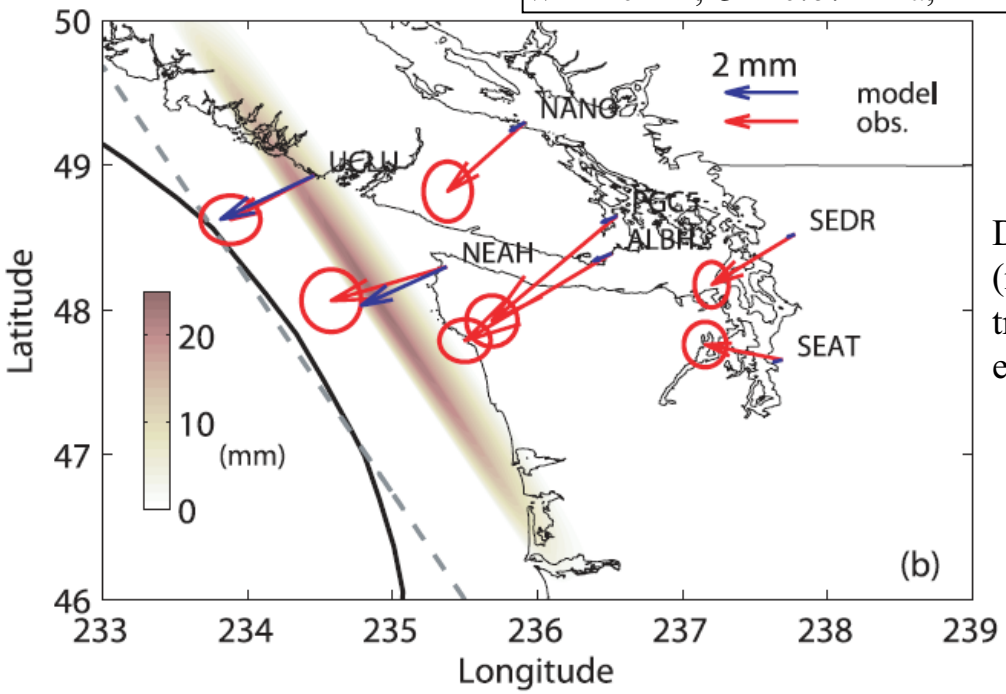

Displacement (net) during a transient episode

Liu & Rice [2009]:

Model based on ***Gabbro Gouge*** friction properties in a near-lithostatic p zone, with ***location based the thermal model for N. Cascadia and phase diagram*** for gabbroic ocean crust.

Such location ***overlaps the gabbro friction stability transition*** (necessary for the model to be able to predict aseismic slip transients)

Plausibly fits GPS constraints.

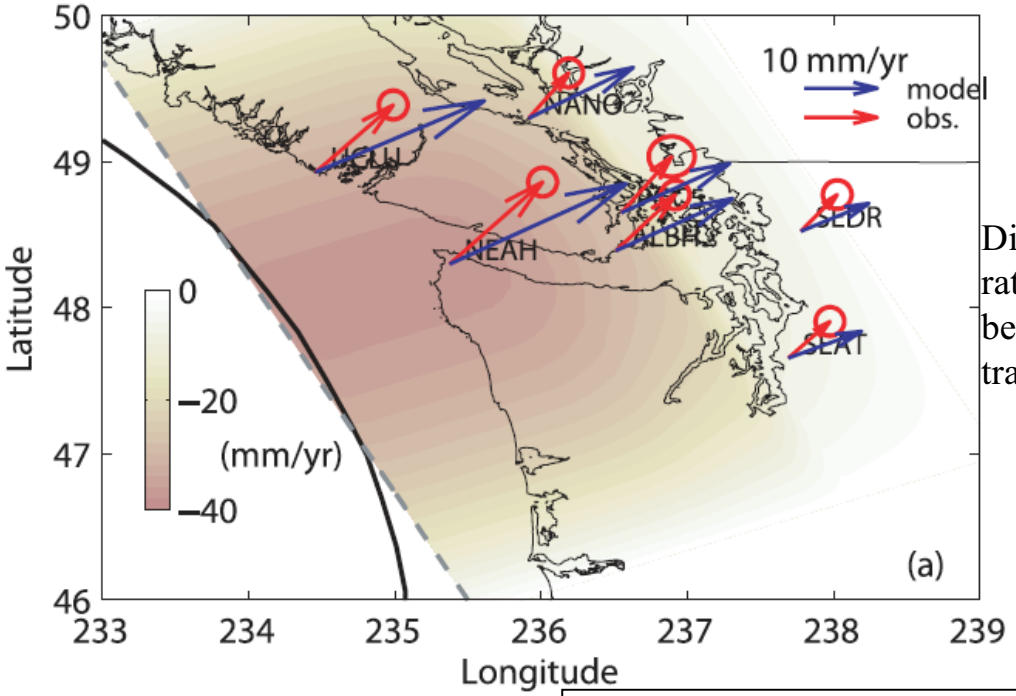

Displacement rates in period between transients

$W = 40$ km, $\bar{\sigma} = 1.15$ MPa, $L = 0.18$ mm

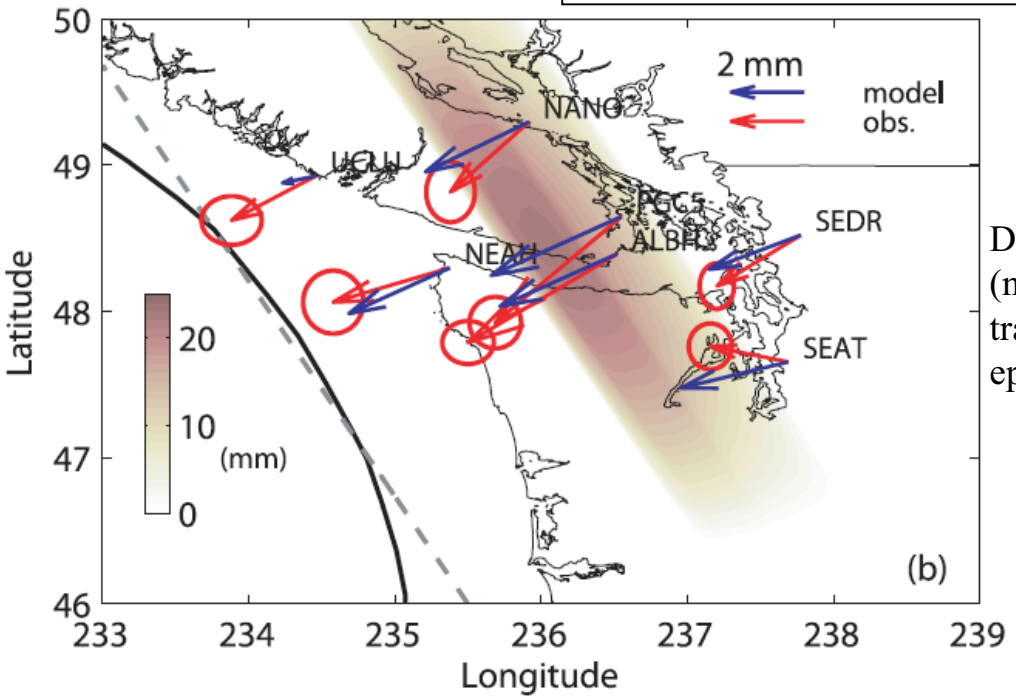

Displacement (net) during a transient episode

Dieterich [*JGR*, 1994]: Application of rate/state framework to a statistical array of independent fault segments (each modeled as a spring-slider). In absence of regional stress step, the array would produce failures at a uniform rate in time, the effect of which exactly balances the regional stressing rate $\dot{\tau}_r$.

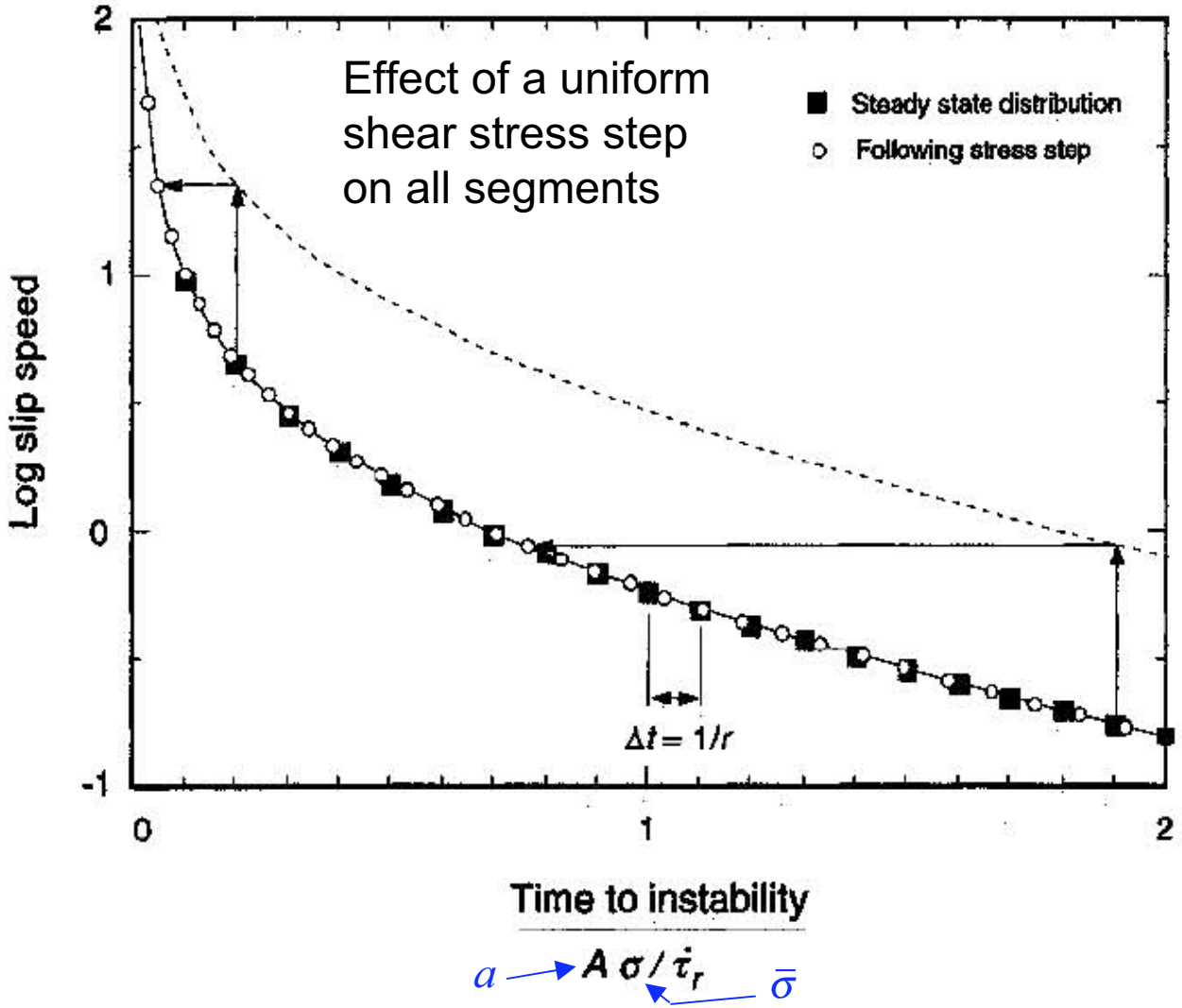

Omori Law:

$$R = \frac{r}{\exp\left(\frac{-\Delta\tau}{A\sigma}\right) + t\dot{\tau}_r / A\sigma}$$

r = steady background seismicity rate

R = seismicity rate after stress step

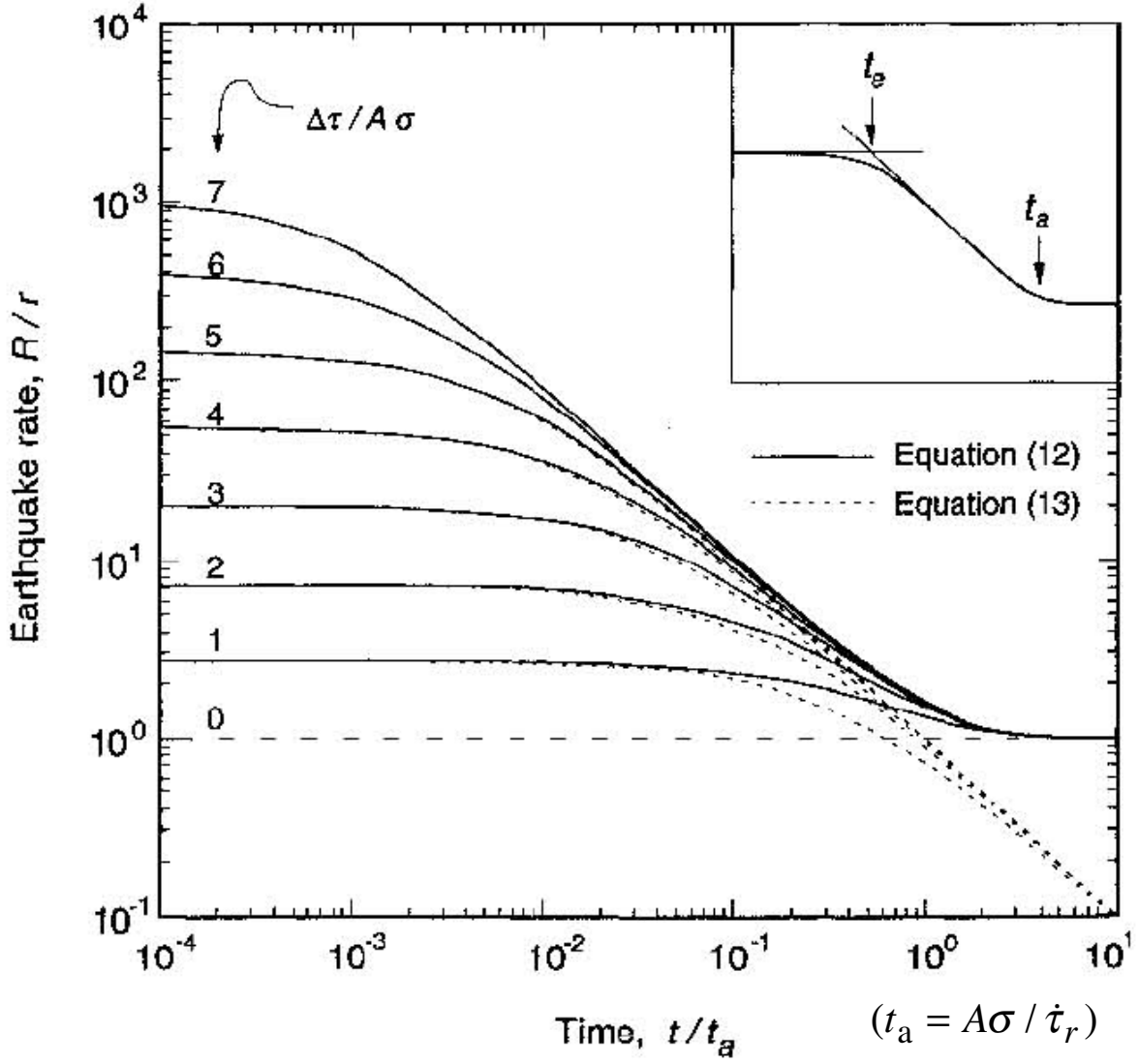

($t_a = A\sigma / \dot{\tau}_r$)

Resolving a quandary in seismology: Major faults operate under low overall driving stress, in a manner that generates negligible heat outflow -- what thermo-hydro-mechanical processes cause that?

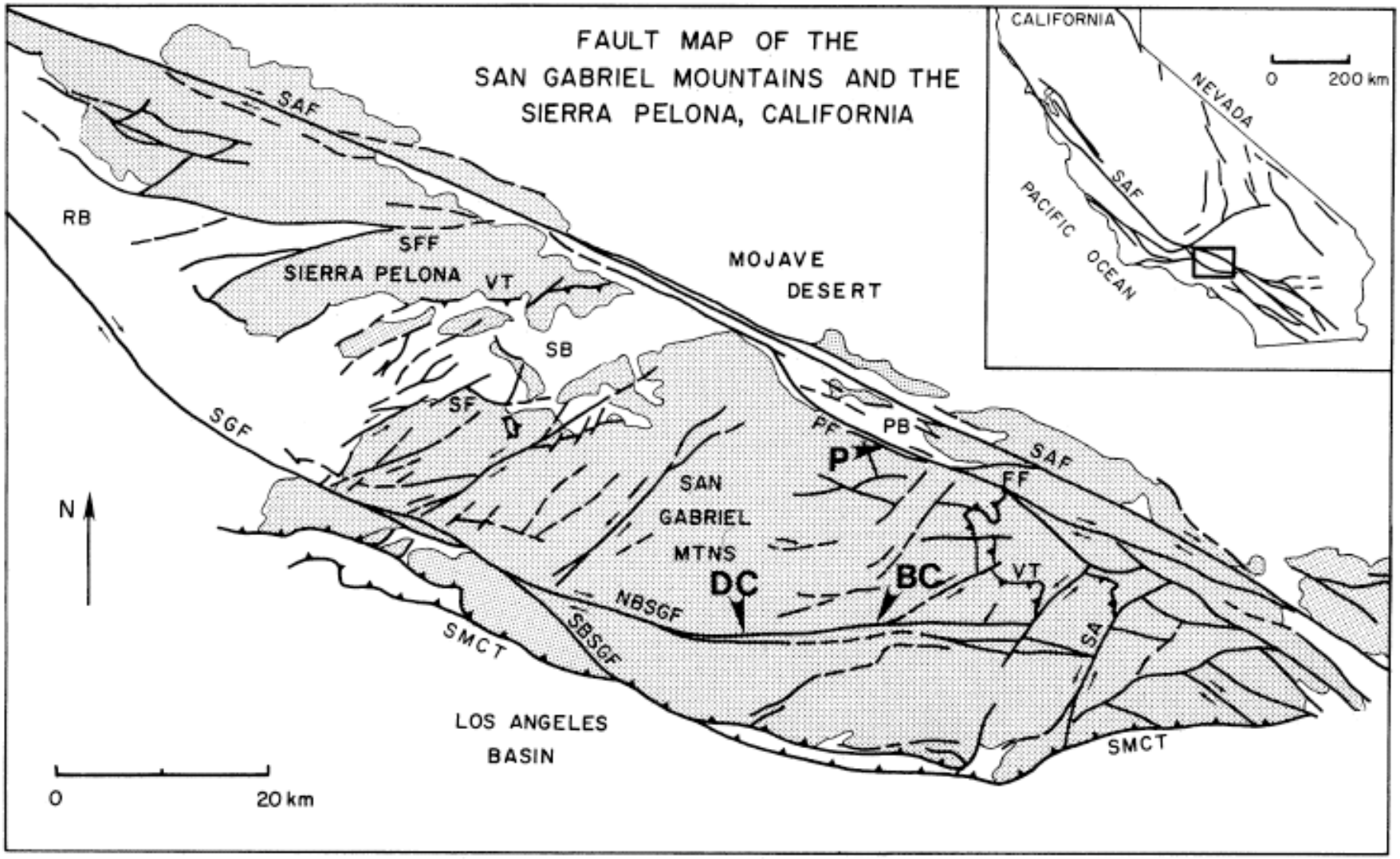

Fig. 1. Generalized geologic map of the San Gabriel Mountains and vicinity, southern California. Stippled pattern represents crystalline rocks. Bold arrows indicate the study localities discussed in the text: Devil's Canyon (DC), Bear Creek (BC), and Punchbowl (P). Key: active trace of the San Andreas fault (SAF), San Gabriel fault (SGF), North Branch San Gabriel fault (NBSGF), South Branch San Gabriel fault (SBSGF), Punchbowl fault (PF), Sierra Madre-Cucamonga thrust (SMCT), San Antonio fault (SA), Vincent thrust (VT), Fenner fault (FF), Soledad fault (SF), San Francisquito fault (SFF), Ridge basin (RB), Soledad basin (SB) and Punchbowl basin (PB).

Generic structure, mature fault zones:

F. Chester, J. Evans and R. Biegel, *J. Geoph. Res.,* **98** (B1), 771-786 (1993)

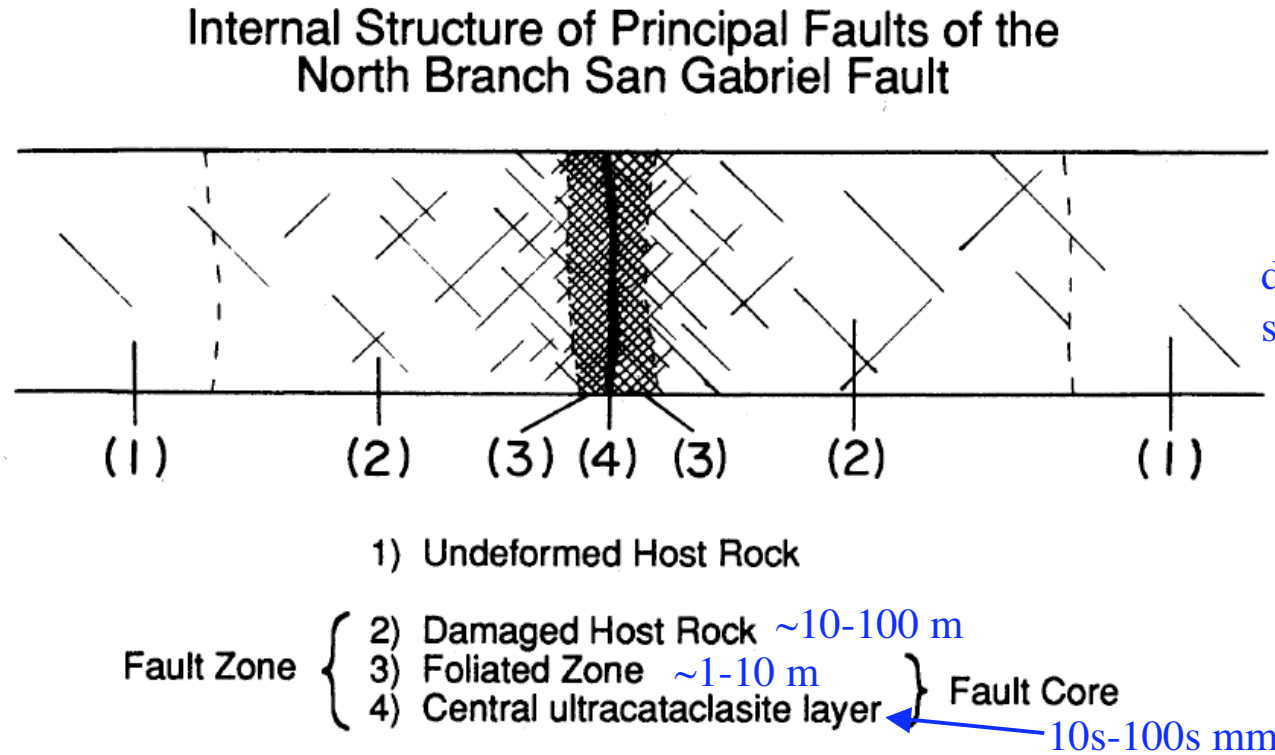

Damage may be dominantly on one side of fault core.

Fig. 2. Schematic section across the North Branch San Gabriel fault zone illustrating position of the structural zones of the fault. The diagram is not to scale.

Punchbowl PSS, composite based on Chester & Chester [*Tectonophys* '98] & Chester & Goldsby [*SCEC* '03]

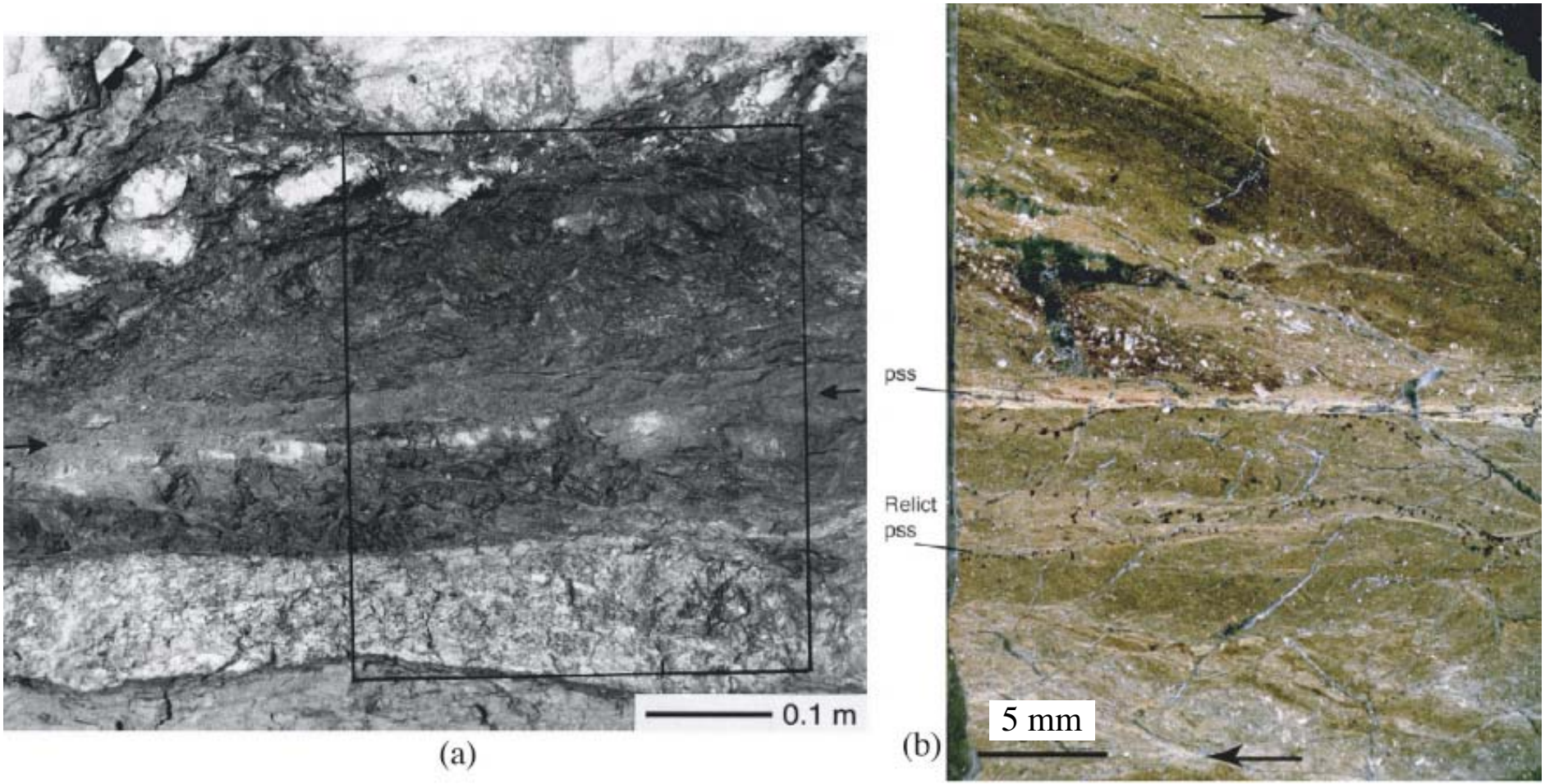

Figure 1. Principal slip surface (PSS) along the Punchbowl fault. (a) From *Chester and Chester* [1998]: Ultracataclasite zone with PSS marked by black arrows; note 100 mm scale bar. (b) From Chester et al. (manuscript in preparation, 2005) [also *Chester et al.*, 2003; *Chester and Goldsby*, 2003]: Thin section; note 5 mm scale bar and ~1 mm localization zone (bright strip when viewed in crossed polarizers due to preferred orientation), with microshear localization of most intense straining to ~100–300 μm thickness.

[Rice, *JGR* 2006]

[Heermance, Shipton & Evans, *BSSA*, 2003]

Core retrieved across the Chelungpu fault, which hosted the 1999 Mw 7.6 Chi-Chi, Taiwan, earthquake.

Suggests slip accommodated within a zone ~ 50–300 μm thick.

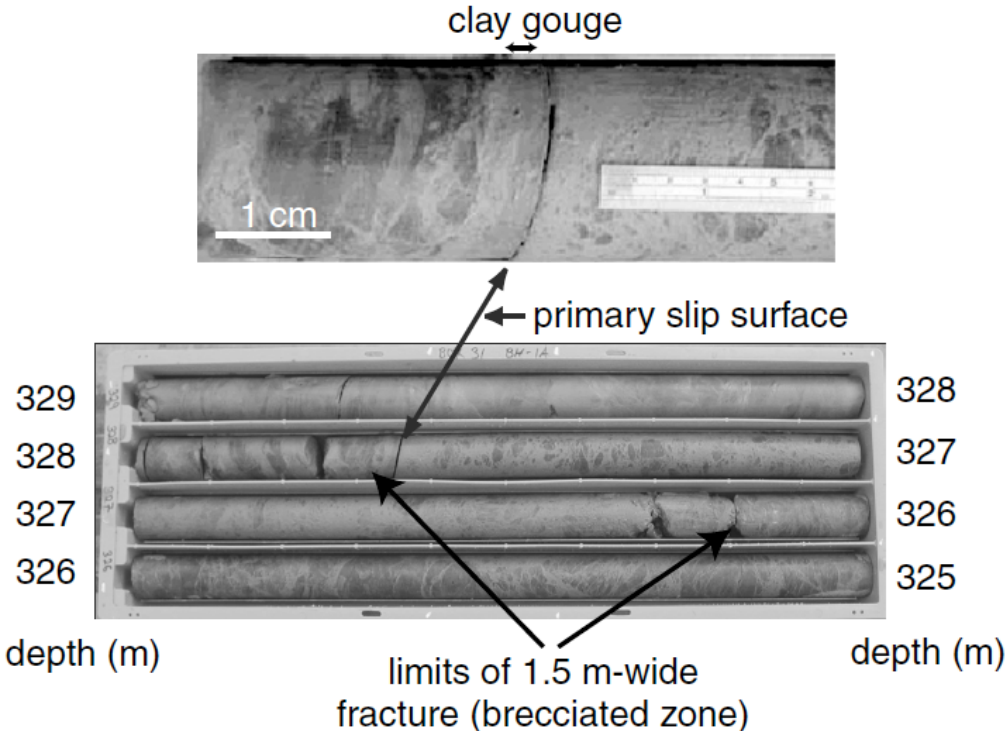

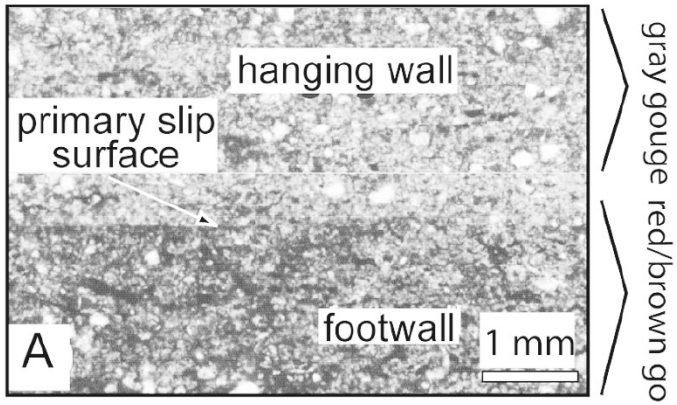

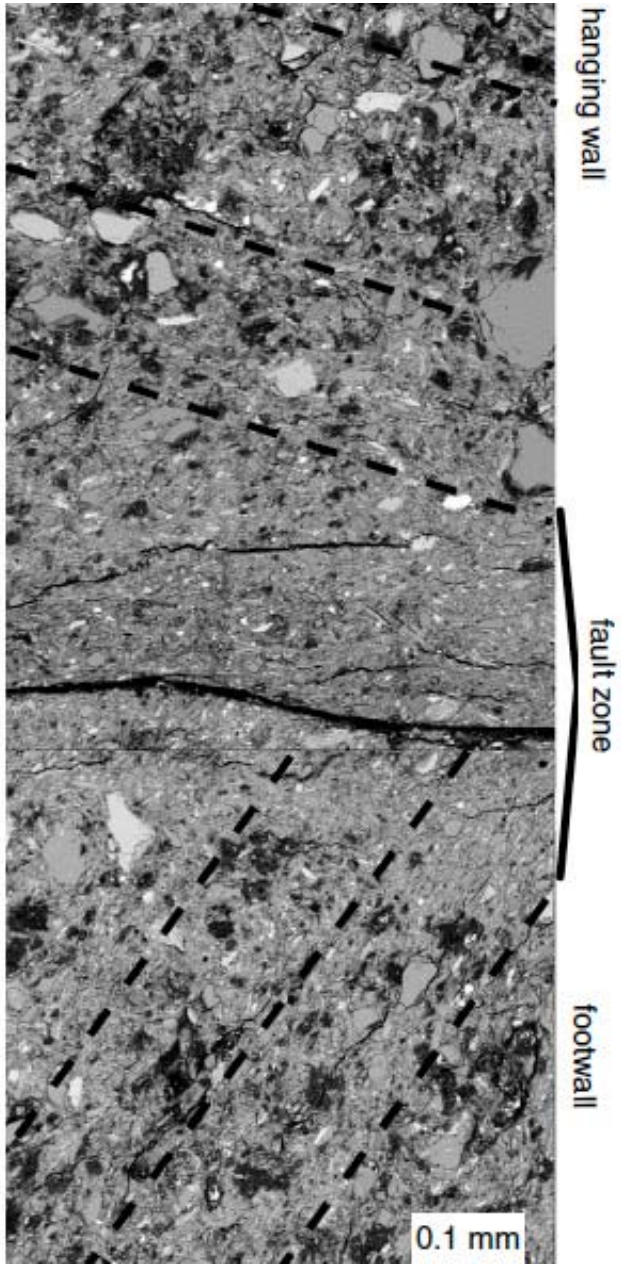

Median Tectonic Line Fault, Japan

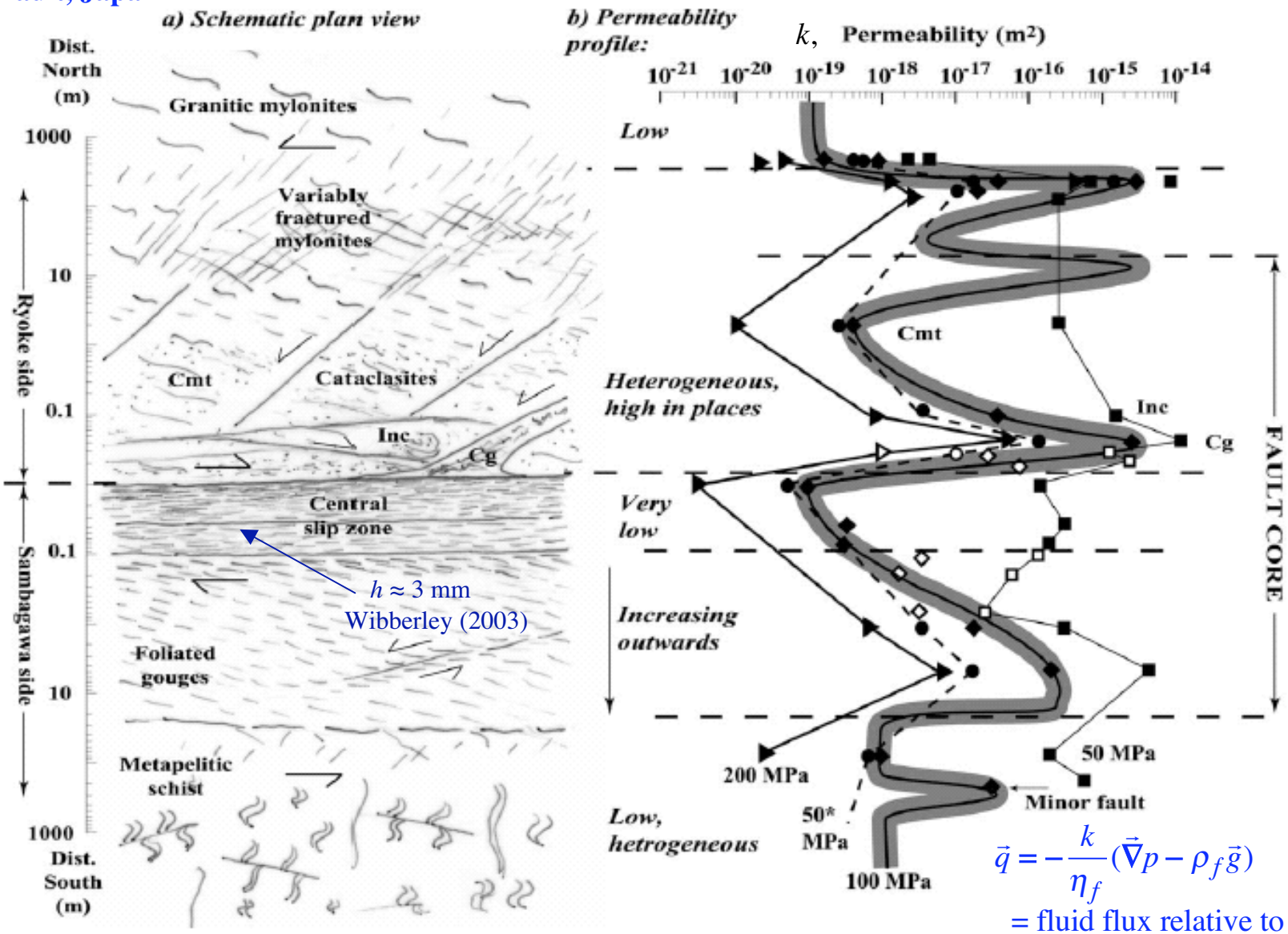

Fig. 11. Sketch summary of the main elements of permeability structure across the Median Tectonic Line. (a) Summary of the structural zones; (b) summary permeability data distribution for different confining pressures (stated at the base, with * denoting data from the deconfining path), for 20 MPa pore pressure, given the mapped distribution of fault rocks shown in Figs. 1–3. Note that the distance axis is logarithmic in both directions away from the Ryoke/Sambagawa contact. 'Cmt' and 'Inc' denote cemented and incohesive foliated cataclasites, respectively, and 'Cg' denotes crenulated gouge.

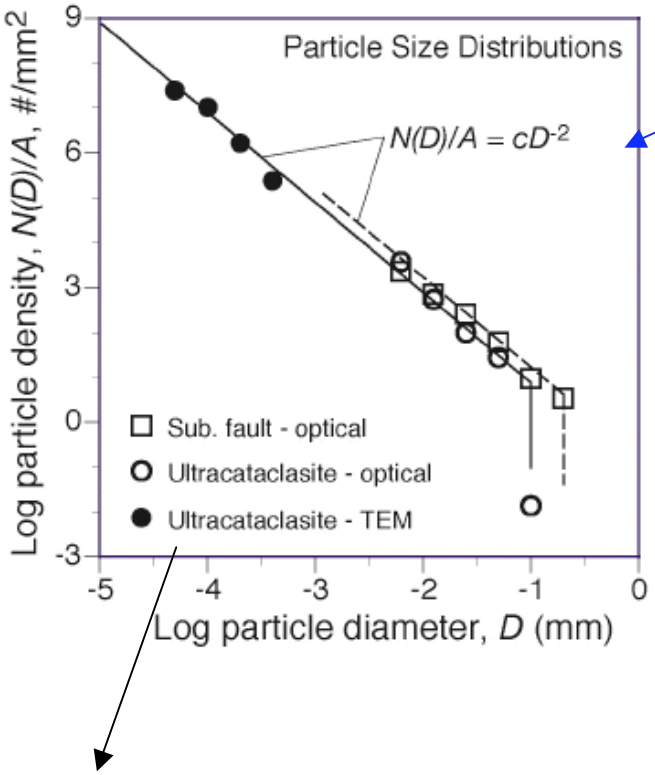

Particle size distribution for ultracataclasite hosting the Punchbowl pss

[J. Chester et al., *Nature*, 2005]

- $N(D)/A =$ number of particles per unit sample area with $2D/3 <$ diameter $< 4D/3$.

$N(D)/A \approx c/D^2$ for ~10-30 nm $< D <$ ~70 μm.

- D_{50} (= size such that 50% by wt. is larger) ~ 1 μm.

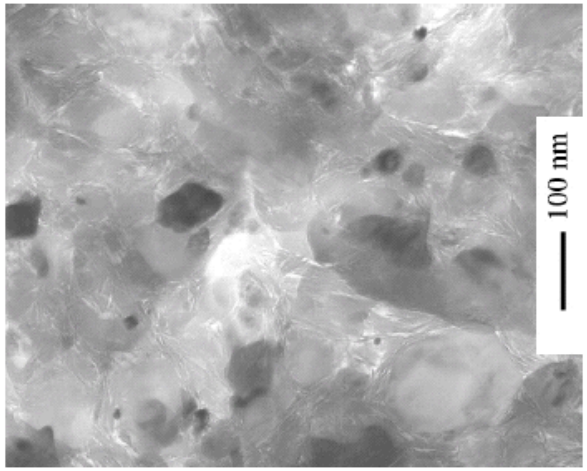

What's the right picture :

A miniature version of beach sand particles?

Clumping of small cohesive - sized particles, maybe like a fine - grained polycrystal with defect - ridden g.b.'s?

Compare, faults with > 5,000 large-slip earthquakes on previous slides vs. a fault with 1 earthquake (a fresh rupture) here

Fresh rupture in a M=3.7 earthquake at 2 km depth, 1997, due to mining operations in the Hartebeestfontein gold mine, South Africa.

Formed the *Bosman* fault within otherwise unfaulted quartzitic layers.

[Wilson, Dewers, Reches & Brune, *Nature*, 2005]

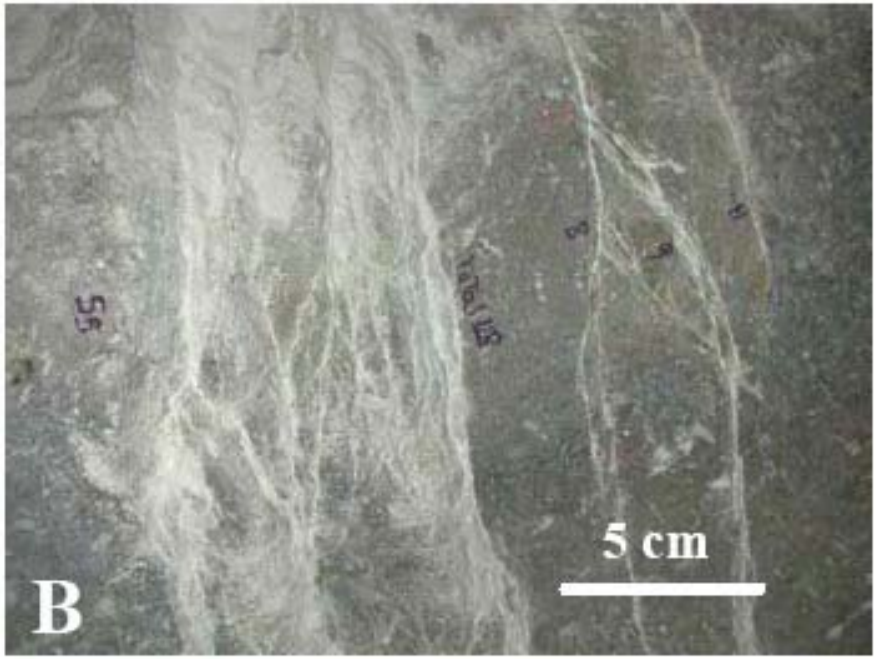

• 100 m long. • At least 5 m wide. • 0.4 m maximum slip.
• Contains 4-6 large, subparallel segments with hundreds of secondary, small fractures.

Quandary in seismology:

- Lab estimates of rock friction coefficient f usually high, $f \sim 0.6$-0.8.

  Shear strength $\tau = f \times (\sigma_n - p)$, where:

  σ_n = normal stress clamping the fault shut
  p = pore pressure in infiltrating fluid phase (groundwater)

- Fault slip zones are thin.

==> If those f prevail during seismic slip, we should find

- ***measurable heat outflow*** near major faults, and
- ***extensive melting*** along exhumed faults.

Neither effect is <u>generally</u> found.

One line of explanation: <u>Weak faults</u>:

$$\tau = f \times (\sigma_n - p)$$

- Fault core materials are different, have very low *f*.
- *f* isn't low, but pore pressure *p* is high over much of the fault.

Another line: <u>Statically strong</u> but <u>dynamically weak</u> faults, e.g., due to thermal weakening in rapid, large slip:

- *Processes expected to be important from start of seismic slip:*
  - Flash heating of asperity contacts, reduces *f* in rapid slip.
  - Thermal pressurization of pore fluid, reduces effective stress.
- *Other processes that may set in at large enough slip or rise in T*:
  - Thermal decomposition, fluid product phase at high pressure (*e.g.*, CO_2 from carbonates; H_2O from clays or serpentines).
  - Gel(?) formation at large slip in wet silica-rich faults.
  - Melting at large slip, *if* above set has not limited increase of *T*.

One line of explanation: <u>Weak faults</u>:

$$\tau = f \times (\sigma_n - p)$$

- **Fault core materials are different, have very low *f*.**
- *f* isn't low, but pore pressure *p* is high over much of the fault.

Another line: <u>Statically strong</u> but <u>dynamically weak</u> faults, e.g., due to thermal weakening in rapid, large slip:

- *Processes expected to be important from start of seismic slip:*
  - Flash heating of asperity contacts, reduces *f* in rapid slip.
  - Thermal pressurization of pore fluid, reduces effective stress.
- *Other processes that may set in at large enough slip or rise in T*:
  - Thermal decomposition, fluid product phase at high pressure (*e.g.*, CO_2 from carbonates; H_2O from clays or serpentines).
  - Gel(?) formation at large slip in wet silica-rich faults.
  - Melting at large slip, *if* above set has not limited increase of *T*.

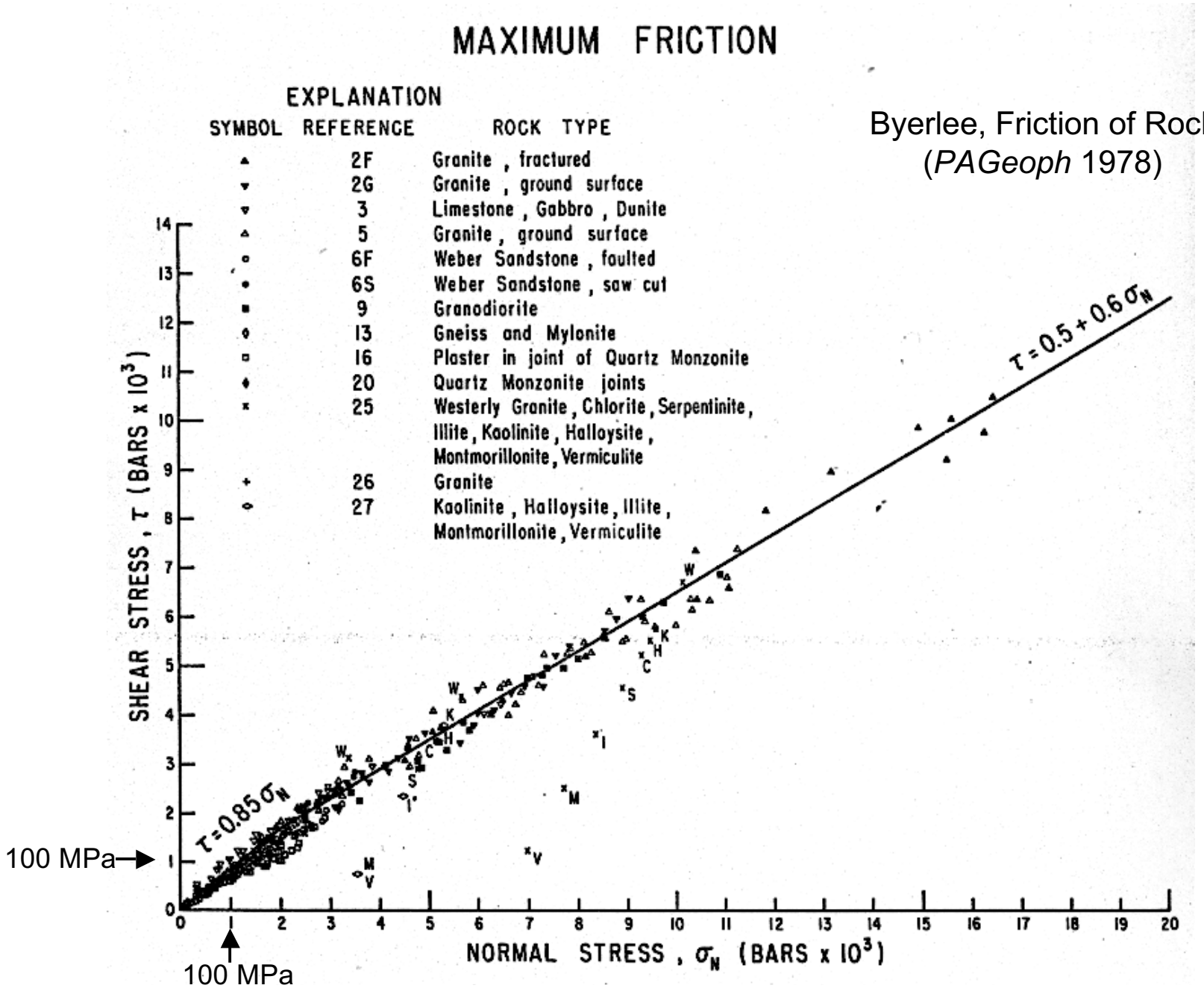

Byerlee, Friction of Rocks,
(*PAGeoph* 1978)

One line of explanation: <u>Weak faults</u>:

$$\tau = f \times (\sigma_n - p)$$

- Fault core materials are different, have very low *f*.
- ***f* isn't low, but pore pressure *p* is high over much of the fault.**

Another line: <u>Statically strong</u> but <u>dynamically weak</u> faults, e.g., due to thermal weakening in rapid, large slip:

- *Processes expected to be important from start of seismic slip:*
  - Flash heating of asperity contacts, reduces *f* in rapid slip.
  - Thermal pressurization of pore fluid, reduces effective stress.
- *Other processes that may set in at large enough slip or rise in T*:
  - Thermal decomposition, fluid product phase at high pressure (*e.g.*, CO_2 from carbonates; H_2O from clays or serpentines).
  - Gel(?) formation at large slip in wet silica-rich faults.
  - Melting at large slip, *if* above set has not limited increase of *T*.

Revil & Cathles, "Fluid transport by solitary waves along growing faults:
A field example from the South Eugene Island Basin, Gulf of Mexico", *EPSL,* 2002

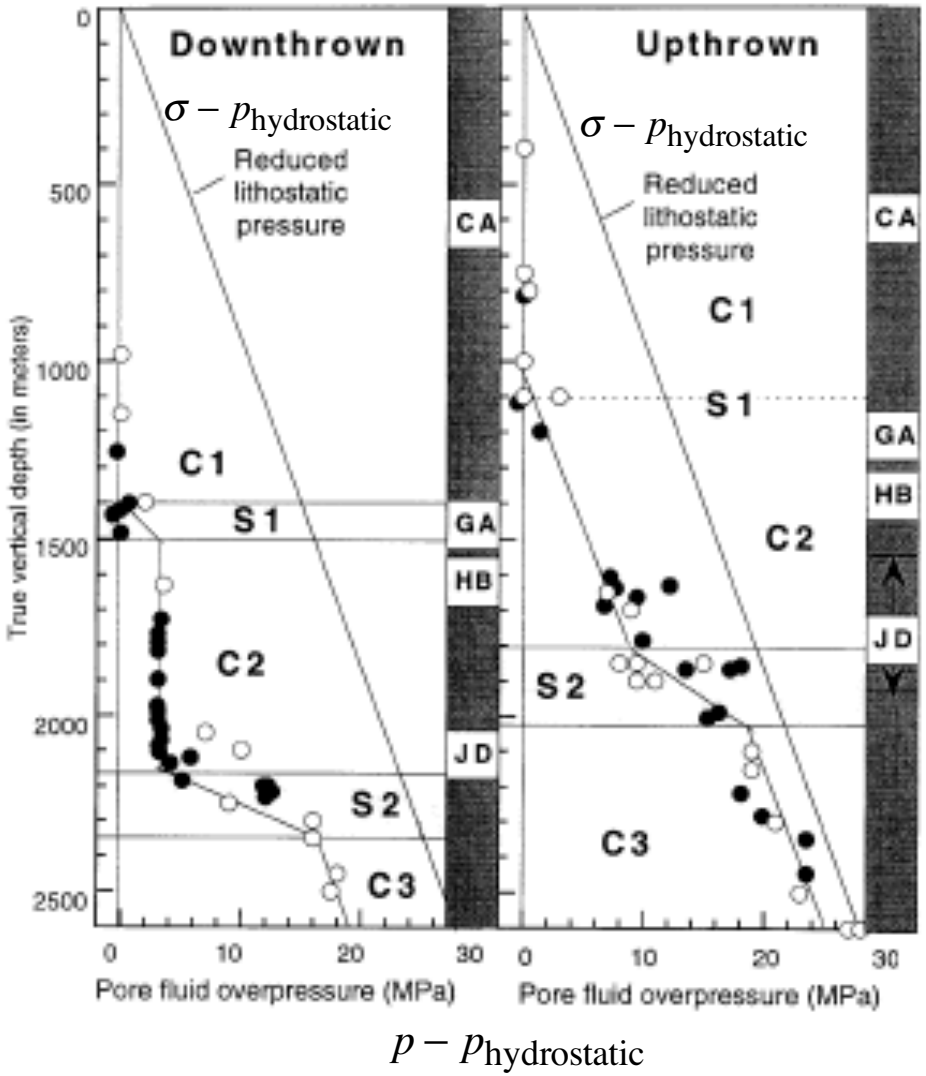

Fig. 3. Pore fluid overpressures (in MPa) in the downthrow and upthrow sides of the Red Fault system (Block 330). Three compartments can be observed on each side: C1 is the hydrostatic upper portion of the basin, C2 is a softly pressurized compartment, and C3 is a highly pressurized compartment. The boundaries S1 and S2 correspond to permeability barriers (shale and/or capillary barriers). Note the correlation between the location of S2 and the presence of the JD sand (the arrows surrounding the location of the JD sand on the upthrow side correspond to the shallowest and deepest depth of location of this sand). The filled circles correspond to direct pressure measurements made in the boreholes. The open circles represent mud weight data. The mud weight data correspond to the weight of the drilling mud used to drill the borehole and adjusted to compensate the fluid pressure of the formations in order to avoid any blow out of the borehole.

Trend: $dp/dz \rightarrow d\sigma/dz$ as depth increases.

(Similar examples in Berry, F. A. F., "High fluid potentials in California Coast Ranges and their tectonic significance", *Bull. Assoc. Petrol. Geol.* 57, pp. 1219-1249, 1973.)

Elementary model for $dp/dz \rightarrow d\sigma/dz$ [Rice, *Fault Mech. Transp. Prop. Rocks*, 1992]:

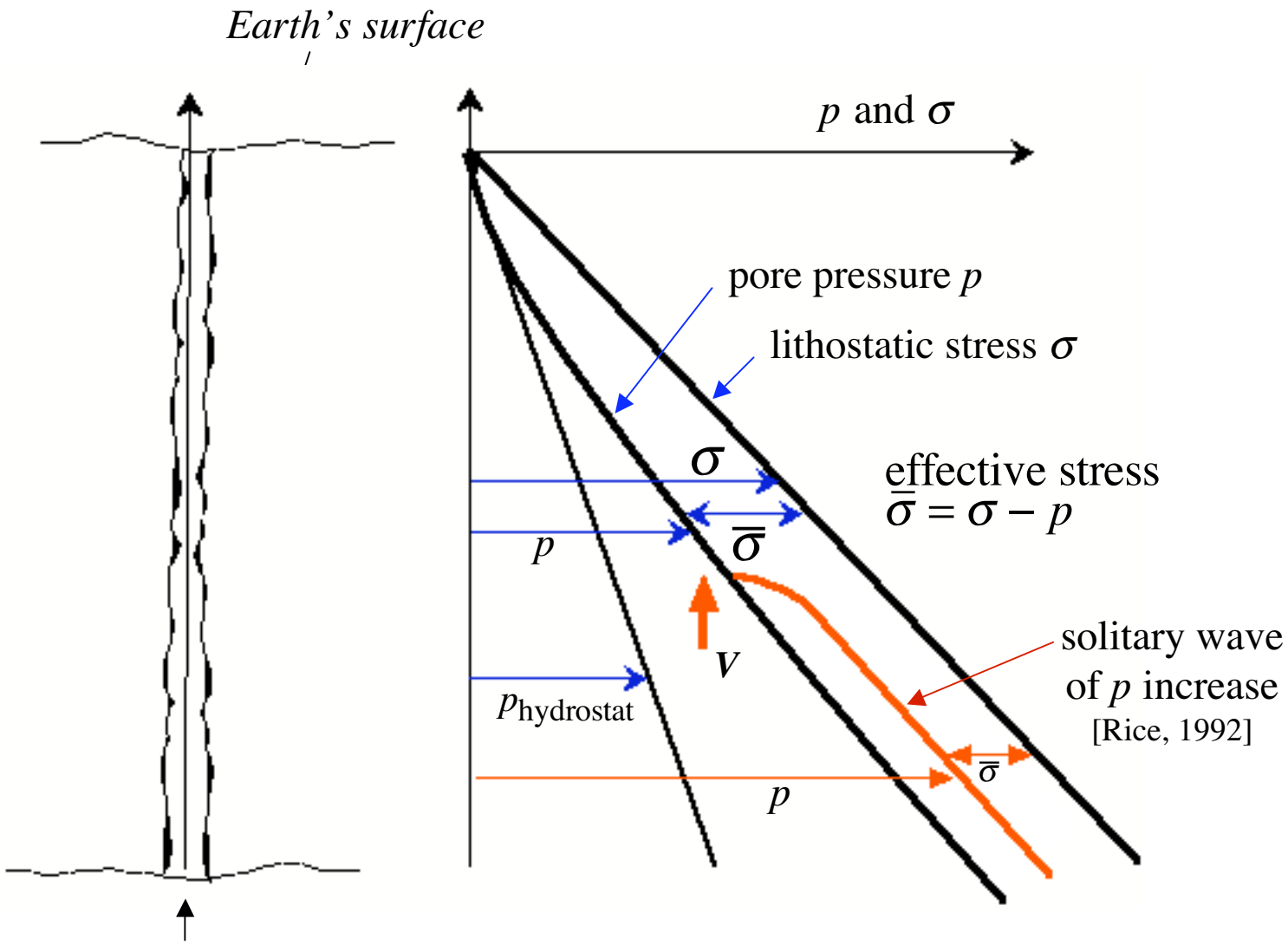

Conserved upflow rate from deep fluid source:
Assume permeability $k = k(\sigma - p)$ and const. flow width.
Then $dp/dz \rightarrow d\sigma/dz$ with increasing depth.

One line of explanation: <u>Weak faults</u>:

$$\tau = f \times (\sigma_n - p)$$

- Fault core materials are different, have very low *f*.
- *f* isn't low, but pore pressure *p* is high over much of the fault.

Another line: <u>Statically strong</u> but <u>dynamically weak</u> faults, e.g., due to thermal weakening in rapid, large slip:

- ***Processes expected to be important from start of seismic slip:***
  - **Flash heating of asperity contacts, reduces *f* in rapid slip.**
  - Thermal pressurization of pore fluid, reduces effective stress.
- *Other processes that may set in at large enough slip or rise in T*:
  - Thermal decomposition, fluid product phase at high pressure (*e.g.*, CO_2 from carbonates; H_2O from clays or serpentines).
  - Gel(?) formation at large slip in wet silica-rich faults.
  - Melting at large slip, *if* above set has not limited increase of *T*.

Flash heating of microscopic frictional asperity contacts

[Rice, *EOS* 1999; *JGR* 2006; Beeler and Tullis, *EOS* 2003, Beeler et al. *JGR* 2008]

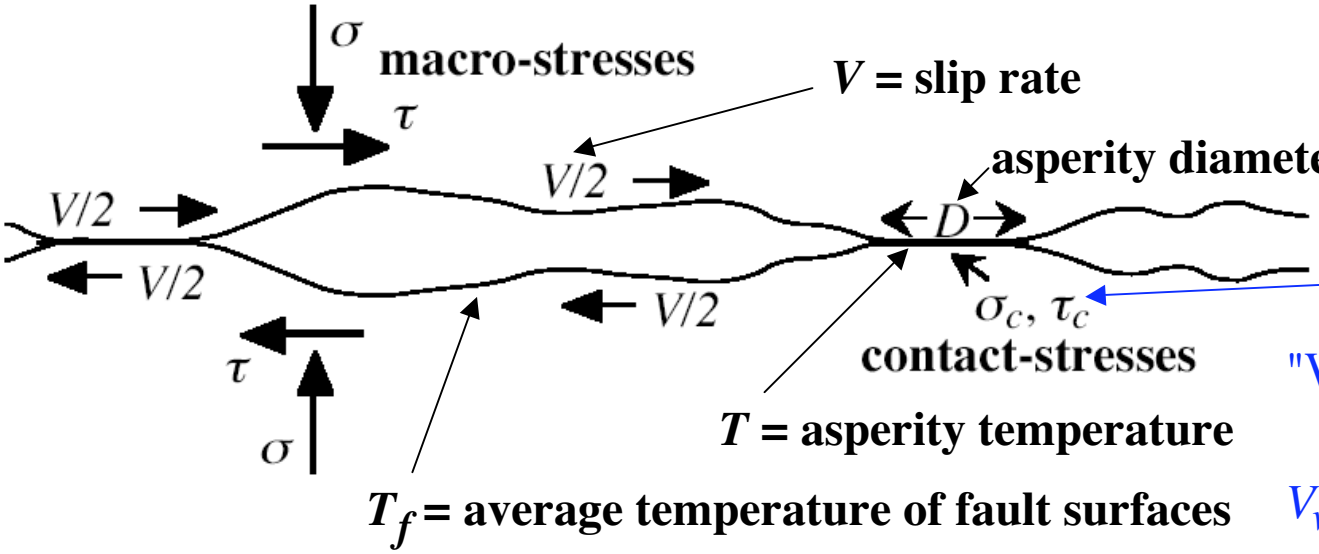

~ 0.1 μ

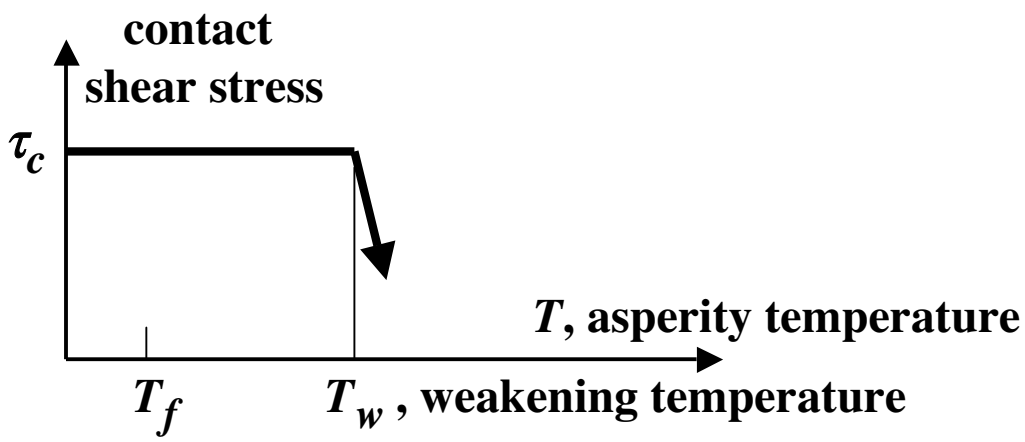

"Weakening" slip rate:

$$V_w = \pi \frac{\alpha_{th}}{D} \left(\frac{T_w - T_f}{\tau_c / \rho c} \right)^2$$

When $V > V_w$, asperity is weak for some of its life; suggests friction coef

$$f \approx f_{slow} \frac{V_w}{V} + f_{weak} \left(1 - \frac{V_w}{V} \right)$$

$$= f_{weak} + (f_{slow} - f_{weak}) \frac{V_w}{V}$$

when $V > V_w$.

[Tullis & Goldsby, *SCEC*, 2003; *EOS*, 2003]

Arkansas novaculite (~100% ***quartzite***)

Rotary Shear Apparatus

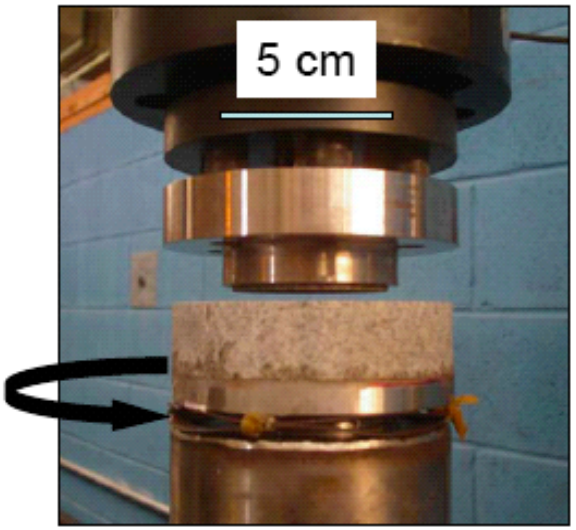

High speed $V \leq 0.36$ m/s

$\sigma_n = 5$ MPa

Rotary shear, 1.2 mm pre-slip at ~10 μm/s, followed by rapid slip for remaining 43 mm.

At low V, $f \approx 0.65$

At $V > 0.3$ m/s, $f \approx 0.30$

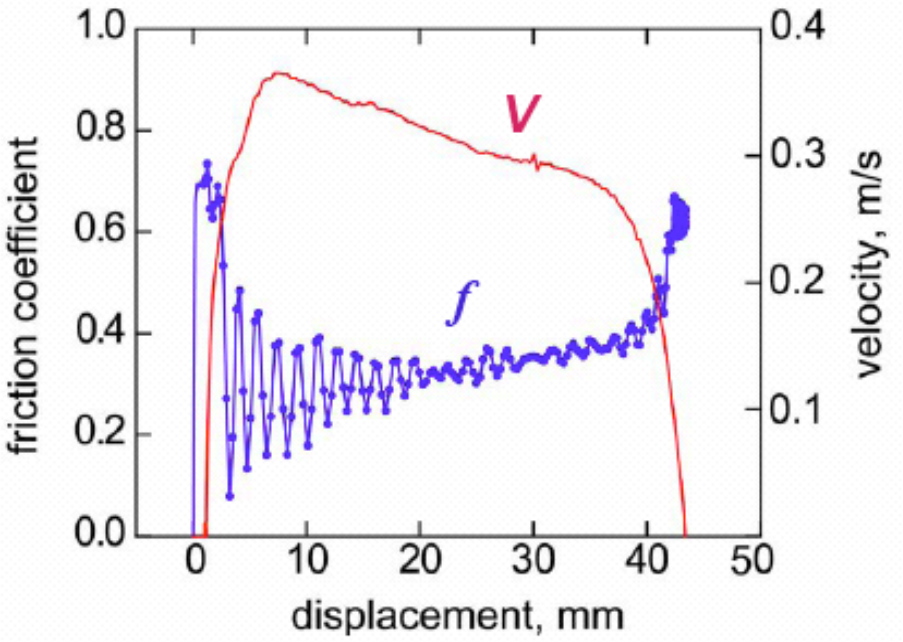

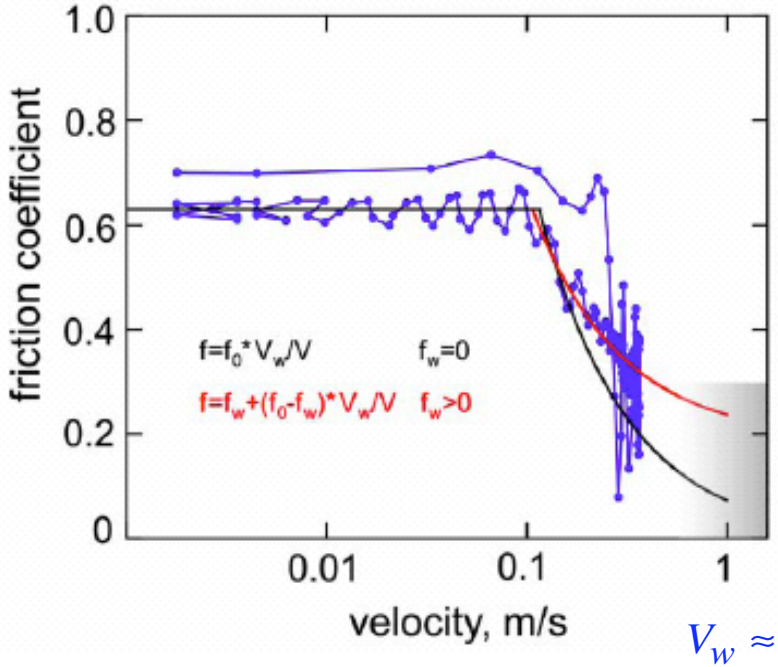

$V_w \approx 0.14$ m/s

Torsional Kolsky bar apparatus

[Yuan & Prakash, *Int. J. Solids & Structures*, 2008]

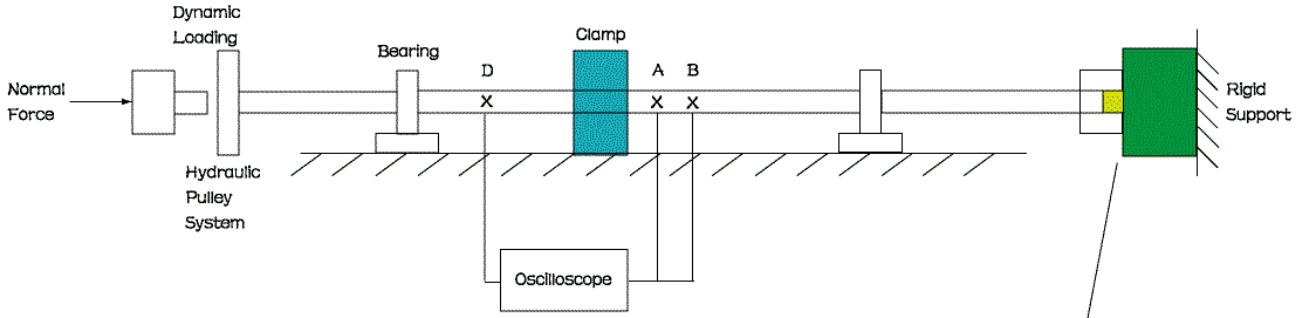

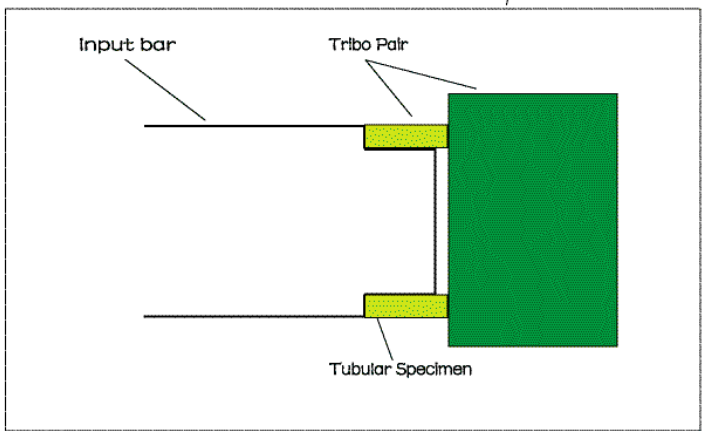

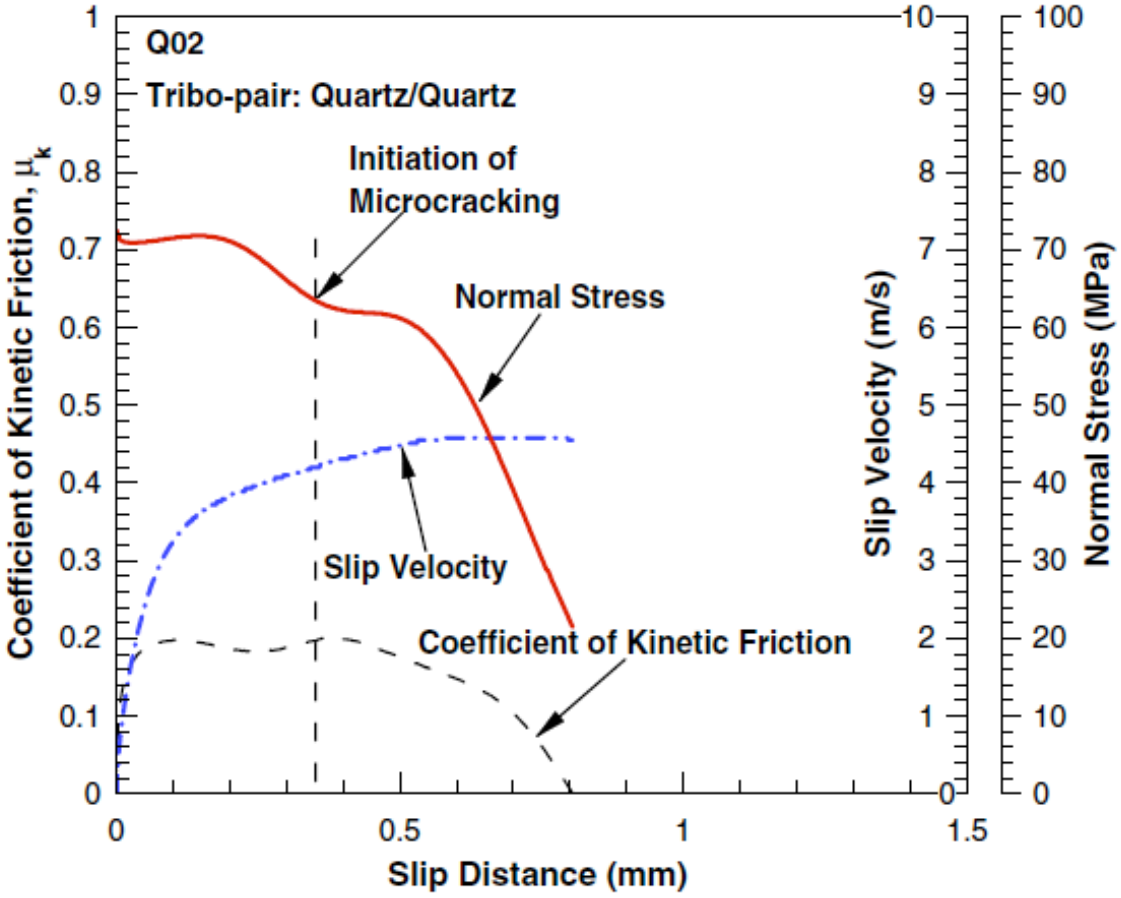

Arkansas novaculite (quartzite)

(Experiment becomes uninterpretable after small slip, marked, due to cracking in wall of specimen.)

Slip at $V \approx$ 2-4 m/s, resulting in $f \approx 0.20$.

[Noda, Dunham & Rice, *JGR* `09]

Based on Tullis and Goldsby [SCEC, `03] parameters f_o, f_w and V_w for granite; drawn for ~ 7 km depth (mid-seismogenic crustal depth) with hydrostatic p.

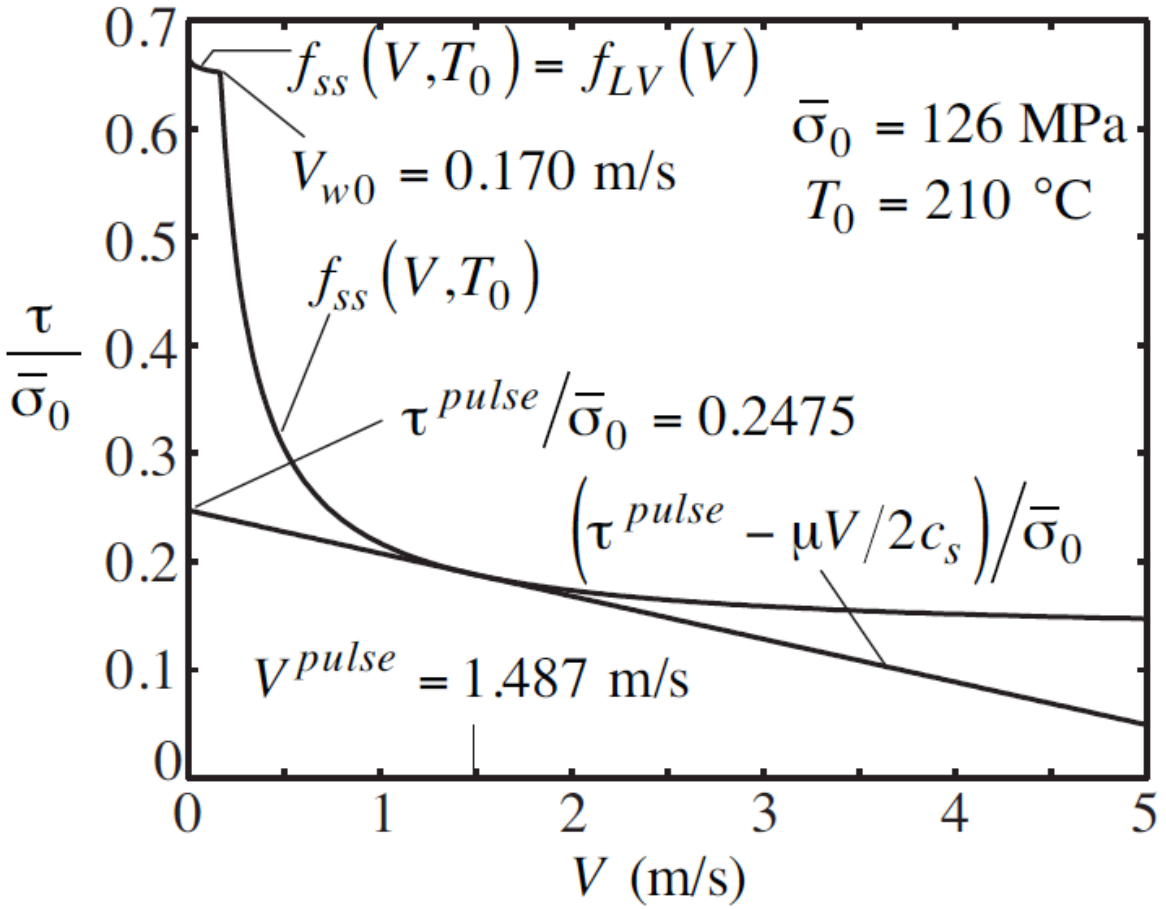

Figure 1. Steady state frictional shear stress, τ_{ss}, normalized by initial effective normal stress, $\overline{\sigma}_0$, as a function of slip velocity, V. τ^{pulse} is defined for the initial ambient conditions at 7 km depth ($T = 210$ °C, $\sigma = 196$ MPa, $p = 70$ MPa) by the radiation-damping line which fits tangentially to $\tau_{ss}(V)$ at $V = V^{pulse}$ (= 1.487 m/s). The weakening slip rate is $V_w = 0.170$ m/s. Due to extreme velocity weakening at elevated slip rates, τ^{pulse} is very small (0.2475 $\overline{\sigma}_0$).

One line of explanation: <u>Weak faults</u>:

$$\tau = f \times (\sigma_n - p)$$

- Fault core materials are different, have very low *f*.
- *f* isn't low, but pore pressure *p* is high over much of the fault.

Another line: <u>Statically strong</u> but <u>dynamically weak</u> faults, e.g., due to thermal weakening in rapid, large slip:

- ***Processes expected to be important from start of seismic slip:***
  - Flash heating of asperity contacts, reduces *f* in rapid slip.
  - **Thermal pressurization of pore fluid, reduces effective stress.**
- *Other processes that may set in at large enough slip or rise in T*:
  - Thermal decomposition, fluid product phase at high pressure (*e.g.*, CO_2 from carbonates; H_2O from clays or serpentines).
  - Gel(?) formation at large slip in wet silica-rich faults.
  - Melting at large slip, *if* above set has not limited increase of *T*.

[Rice, *JGR*, 2006]

Thermal pressurization of pore fluid

Governing equations, 1-space-dimension shearing field, constant normal stress σ_n:

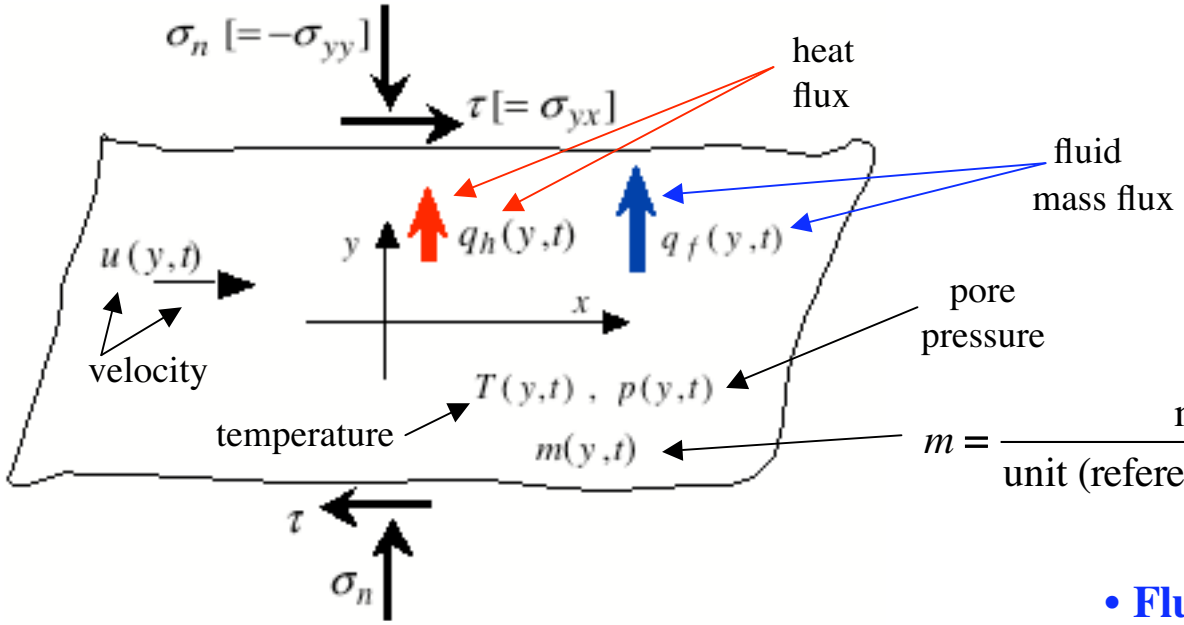

(Habib 67, 75, Sibson 73, Anderson 80, Lachenbruch 80, Voight & Faust 82, Mase & Smith 85, 87, Lee & Delaney 87, Vardoulakis 02, Andrews 04, many more in recent yrs.)

$$m = \frac{\text{mass of pore fluid}}{\text{unit (reference) vol. of porous medium}} = \rho_f n$$

• Energy equation :

$$\tau\dot{\gamma} = \rho c\frac{\partial T}{\partial t} + \frac{\partial q_h}{\partial y}\ ,\quad q_h = -K\frac{\partial T}{\partial y}\ ,$$

$$\dot{\gamma} = \partial u/\partial y \geq 0\ ,\quad \tau = f\times(\sigma_n - p) \text{ when } \dot{\gamma} > 0;$$

$$\Rightarrow f(\sigma_n - p)\dot{\gamma} = \rho c\frac{\partial T}{\partial t} - \frac{\partial}{\partial y}\left(\rho c\alpha_{th}\frac{\partial T}{\partial y}\right);$$

$$\rho c \approx 2.7 \text{ MPa/°C};\quad \alpha_{th} = \frac{K}{\rho c} \approx 0.7 \text{ mm}^2/\text{s}.$$

• Fluid mass conservation :

$$\frac{\partial m}{\partial t} + \frac{\partial q_f}{\partial y} = 0\ ,\quad q_f = -\frac{\rho_f k}{\eta_f}\frac{\partial p}{\partial y} \Rightarrow$$

$$\frac{\partial p}{\partial t} = \Lambda\frac{\partial T}{\partial t} - \frac{1}{\beta}\frac{\partial n^{pl}}{\partial t} + \frac{1}{\rho_f\beta}\frac{\partial}{\partial y}\left(\rho_f\beta\alpha_{hy}\frac{\partial p}{\partial y}\right),$$

$$\alpha_{hy} = k/\eta_f\beta\ ;$$

$\Lambda \approx 0.3\text{-}1.0$ (MPa/°C), $\beta \equiv n(\beta_f + \beta_n) \approx 5\text{-}30\times10^{-11}$/Pa;

β_f, β_n = fluid compressibility, pore space expansivity.

One line of explanation: Weak faults:

$$\tau = f \times (\sigma_n - p)$$

- Fault core materials are different, have very low *f*.
- *f* isn't low, but pore pressure *p* is high over much of the fault.

Another line: Statically strong but dynamically weak faults, e.g., due to thermal weakening in rapid, large slip:

- *Processes expected to be important from start of seismic slip:*
  - Flash heating of asperity contacts, reduces *f* in rapid slip.
  - Thermal pressurization of pore fluid, reduces effective stress.

- ***Other processes that may set in at large enough slip or T rise*:**
  - **Thermal decomposition, fluid product phase at high *p* (*e.g.*, CO_2 from carbonates; H_2O from clays or serpentines).**
  - **Gel(?) formation at large slip in wet silica-rich faults.**
  - **Melting at large slip, *if* above set has not limited rise of *T*.**

Han, Shimamoto, Hirose, Ree & Ando [*Sci.,* 2007]: Carbonate faults

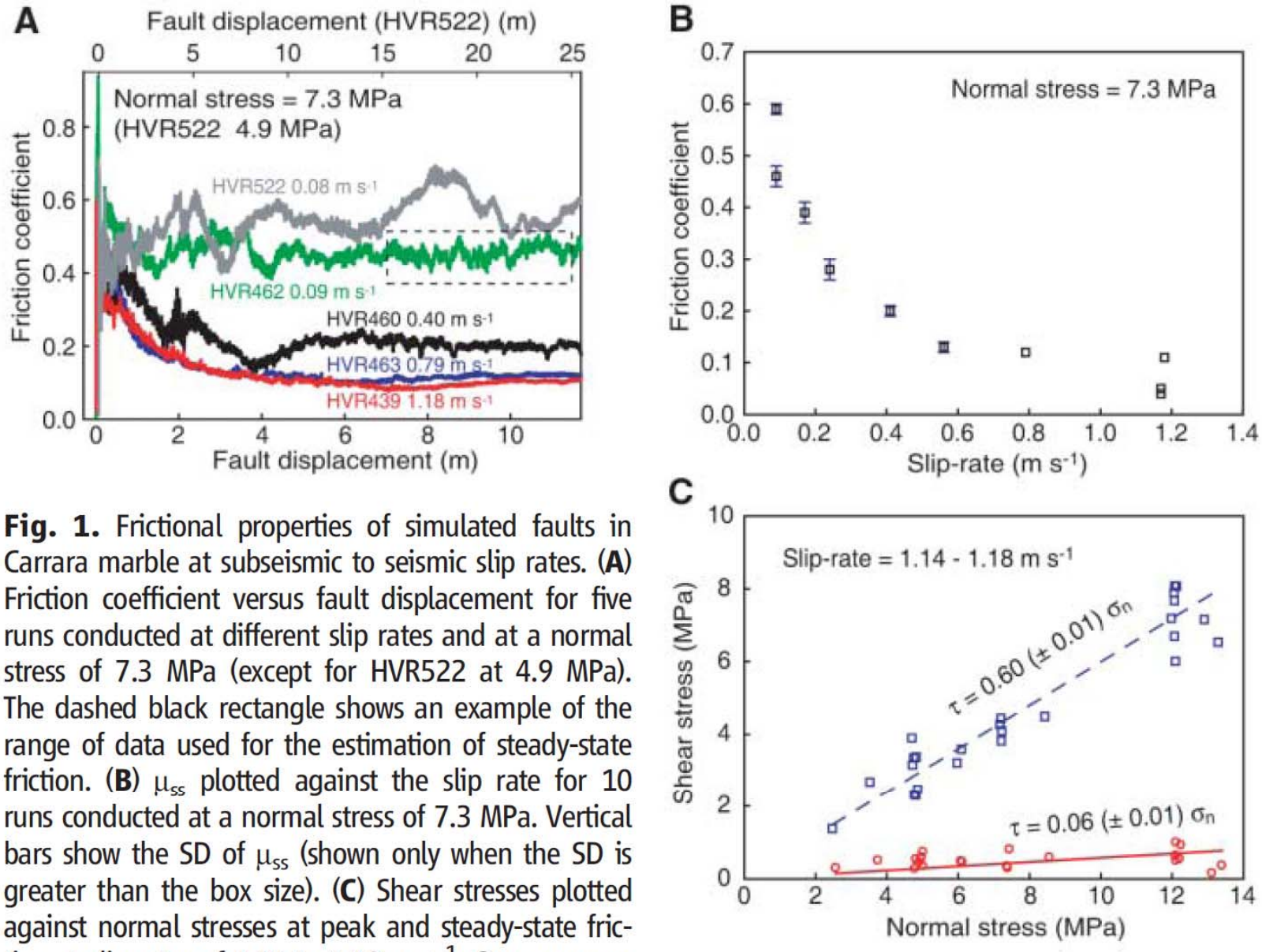

Fig. 1. Frictional properties of simulated faults in Carrara marble at subseismic to seismic slip rates. (**A**) Friction coefficient versus fault displacement for five runs conducted at different slip rates and at a normal stress of 7.3 MPa (except for HVR522 at 4.9 MPa). The dashed black rectangle shows an example of the range of data used for the estimation of steady-state friction. (**B**) μ_{ss} plotted against the slip rate for 10 runs conducted at a normal stress of 7.3 MPa. Vertical bars show the SD of μ_{ss} (shown only when the SD is greater than the box size). (**C**) Shear stresses plotted against normal stresses at peak and steady-state friction at slip rates of 1.14 to 1.18 m s^{-1}. Open squares and circles indicate initial peak friction and steady-state friction, respectively. The slopes of the lines give frictional coefficients at peak and steady-state friction. τ, shear stress; σ_n, normal stress.

Dynamic rupture simulations, incorporating flash heating of asperity contacts and thermal pressurization of pore fluid, with parameters constrained (to the extent possible) by laboratory observations

[Noda, Dunham & Rice, *JGR* 2009]

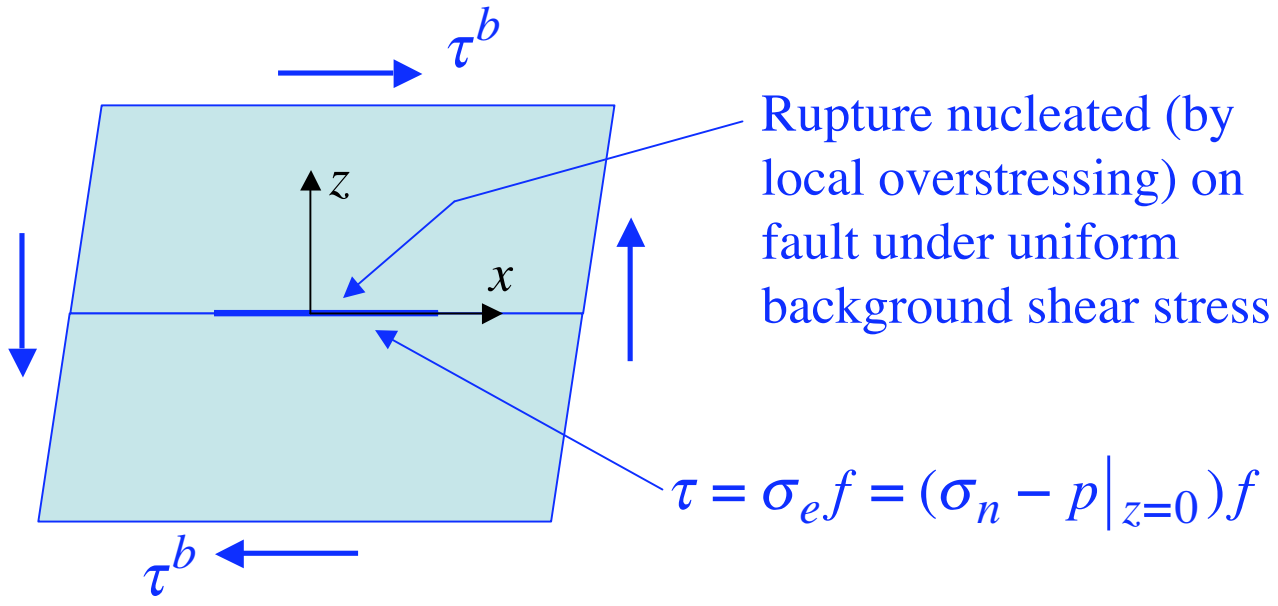

Flash heating *(in dynamic rupture simulations, Noda, Dunham & Rice, JGR 09)*

Effective stress law:

$$\tau = \sigma_e f = (\sigma_n - p|_{z=0})f$$

given, fixed compressive normal stress

friction coefficient

pore pressure on slip surface

Rate and state friction concepts, together with flash heating at microscopic contacts during rapid slip:

$$\frac{df}{dt} = \frac{a}{V}\frac{dV}{dt} - \frac{V}{L}\left[f - f_{ss}(V)\right]$$

- $$f_{ss}(V) = \begin{cases} f_{LV}(V), & V \le V_w, \\ f_w + \left(f_{LV}(V) - f_w\right)\dfrac{V_w}{V}, & V \ge V_w, \end{cases}$$

with $V_w = \pi \dfrac{\alpha_{th}}{D}\left(\dfrac{T_w - T}{\tau_c/\rho c}\right)^2$;

- $$f_{LV}(V) = f_o + (a-b)\ln\left(\frac{V}{V_o}\right)$$

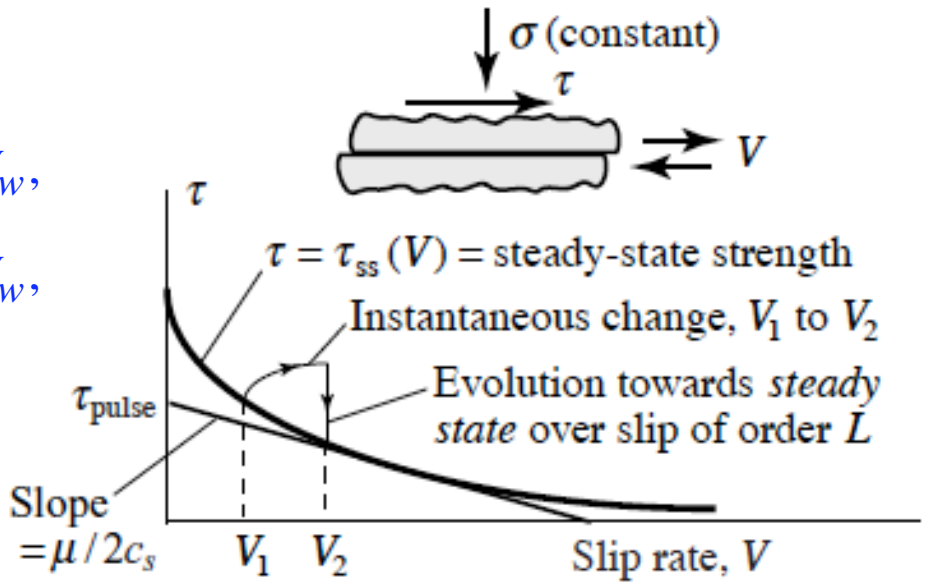

[Noda, Dunham & Rice, *JGR* `09]

Based on Tullis and Goldsby [SCEC, `03] parameters f_o, f_w and V_w for granite.

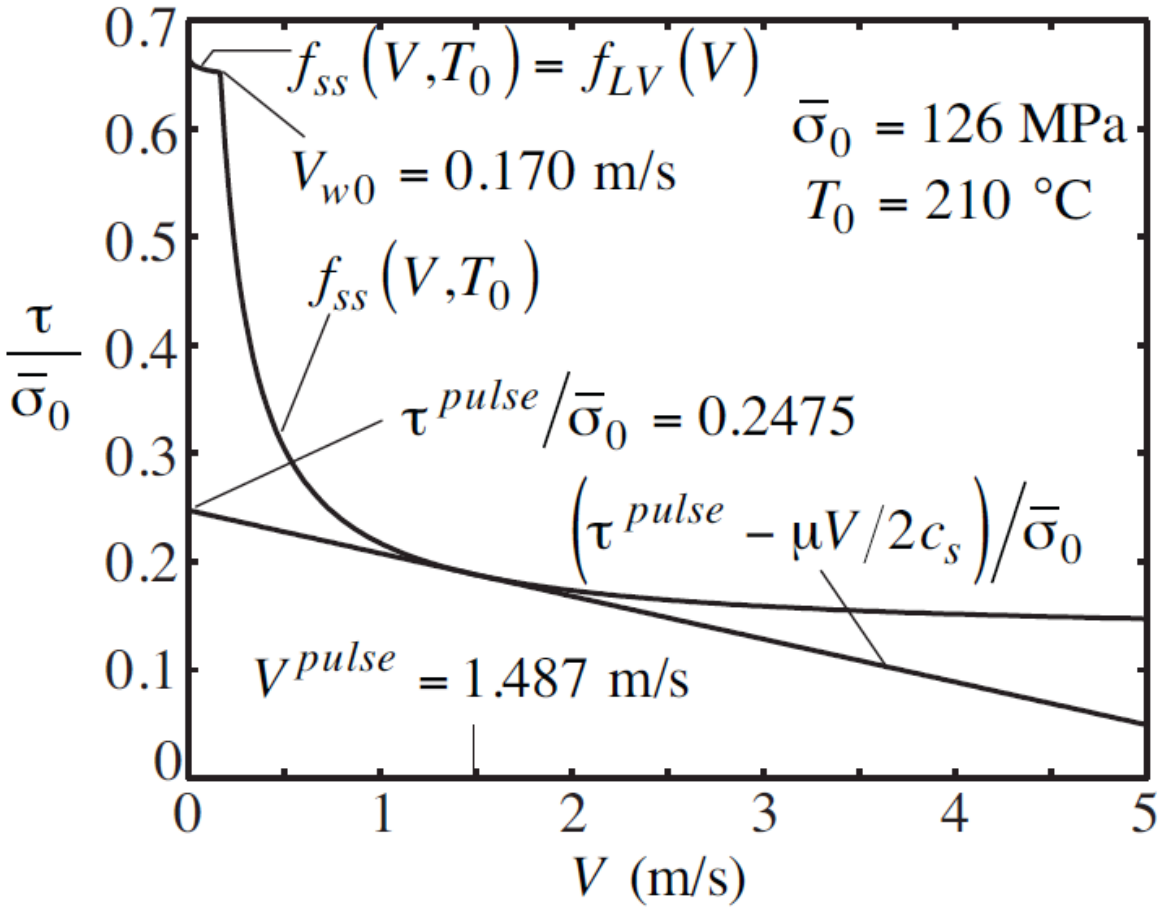

Figure 1. Steady state frictional shear stress, τ_{ss}, normalized by initial effective normal stress, $\overline{\sigma}_0$, as a function of slip velocity, V. τ^{pulse} is defined for the initial ambient conditions at 7 km depth ($T = 210$ °C, $\sigma = 196$ MPa, $p = 70$ MPa) by the radiation-damping line which fits tangentially to $\tau_{ss}(V)$ at $V = V^{pulse}$ ($= 1.487$ m/s). The weakening slip rate is $V_w = 0.170$ m/s. Due to extreme velocity weakening at elevated slip rates, τ^{pulse} is very small ($0.2475\ \overline{\sigma}_0$).

Thermal pressurization *(in dynamic rupture simulations, Noda, Dunham & Rice, JGR 09)*

Effective stress law:

$$\tau = \sigma_e f = (\sigma_n - p|_{z=0}) f$$

given, fixed compressive normal stress

friction coefficient

pore pressure on slip surface

Thermal pressurization, finite thickness of slipping zone, with Gaussian shear distribution having *r.m.s.* width w:

Conservation of energy
(first law of thermodynamics):

$$\frac{\partial T}{\partial t} = \alpha_{th} \frac{\partial^2 T}{\partial z^2} + \frac{\tau}{\rho c} \frac{V}{\sqrt{2\pi}\, w} \exp\left(-\frac{z^2}{2w^2} \right)$$

Conservation of fluid mass:

$$\frac{\partial p}{\partial t} = \alpha_{hy} \frac{\partial^2 p}{\partial z^2} + \Lambda \frac{\partial T}{\partial t}$$

$\alpha_{th} \sim 0.7$ mm^2/s; $\alpha_{hy} \sim 0.9$ - 6 mm^2/s at mid-seismogenic depths; $\rho c \sim 2.7$ MJ/m^{3}K; $\Lambda \sim 0.3$ - 1.0 MJ/m^{3}K (Rice [*JGR* 2006] & Rempel & Rice [*ibid*], based on Wibberley [*EPS* 2002, *priv comm* 2003] & Wibberley & Shimamoto [*JSG* 2003], and estimates of damage)

[Noda, Dunham & Rice, *2008.*]

Effect of hydrothermal properties

$\tau^{per} = 30\text{MPa}$
$D^{per} = 5\text{cm}$

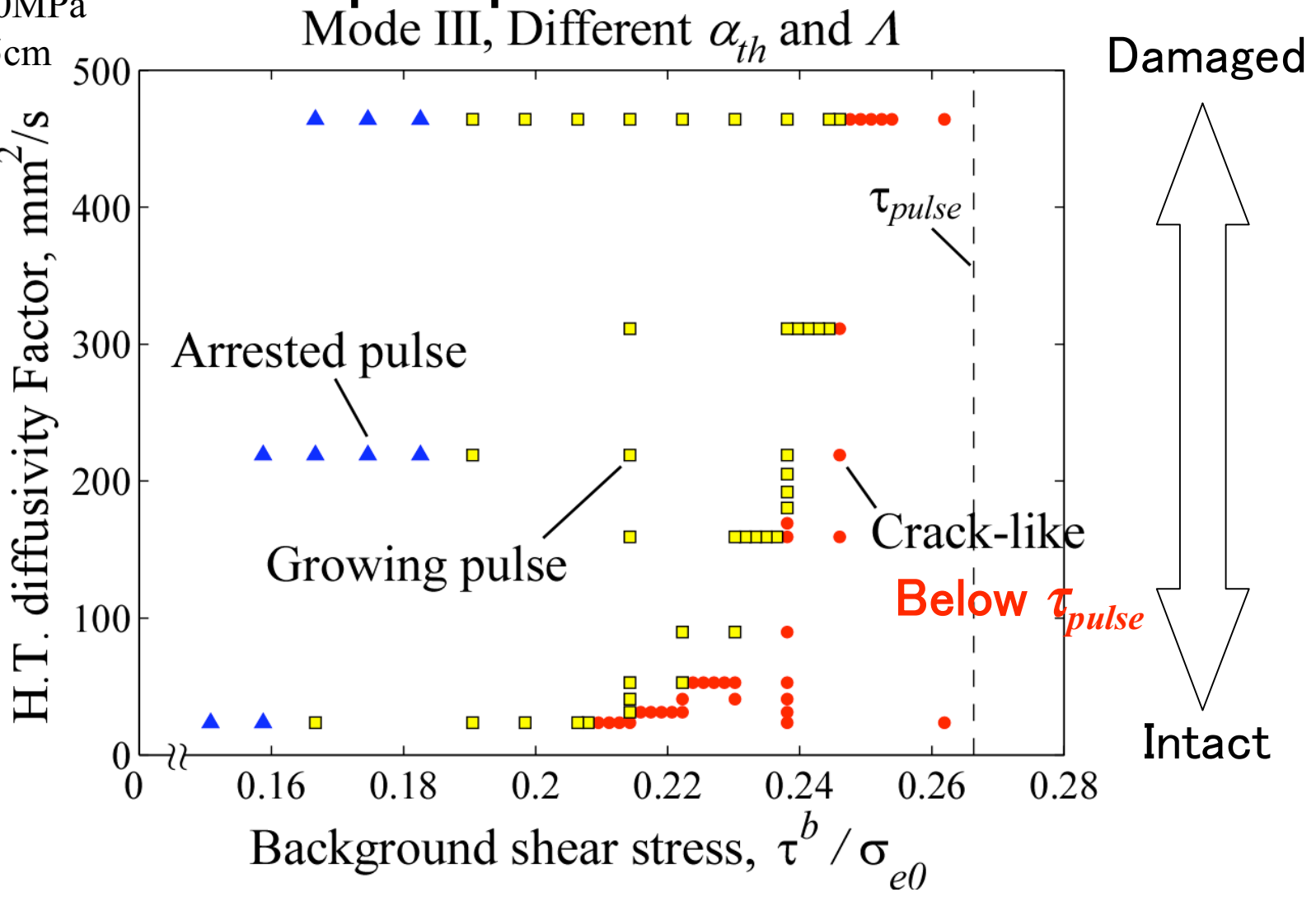

Shown:
The case $w = 0$, slip on a plane.

High τ^b favors crack-like solution, thermal pressurization does too.

[Noda, Dunham & Rice, *2008.*]

Effect of hydrothermal properties

$\tau^{per} = 30\text{MPa}$
$D^{per} = 5\text{cm}$

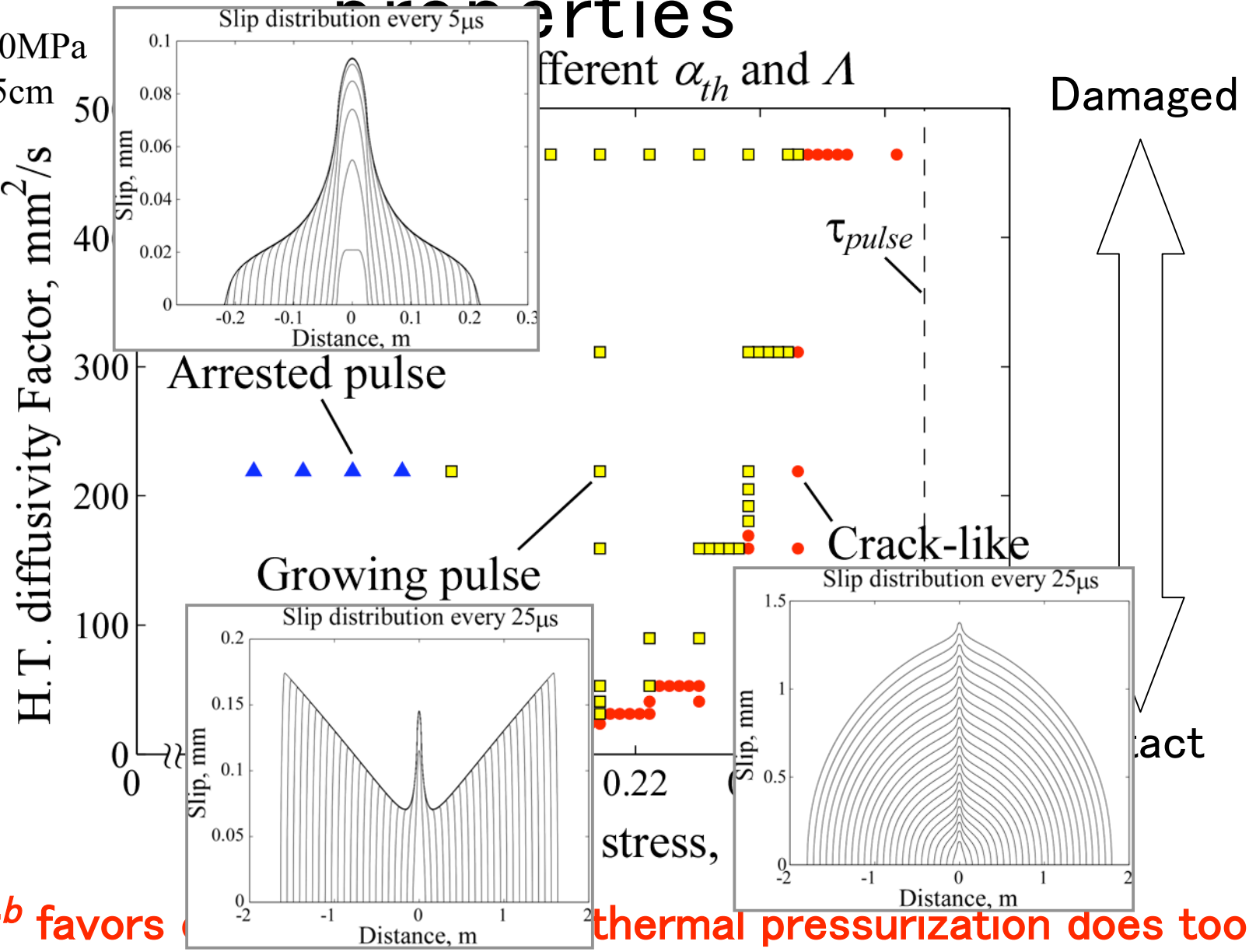

Shown:
The case $w = 0$, slip on a plane.

High τ^b favors (thermal pressurization does too.

[Noda, Dunham & Rice, *2008.*]

Effect of hydrothermal properties

$\tau^{per} = 30\text{MPa}$
$D^{per} = 5\text{cm}$

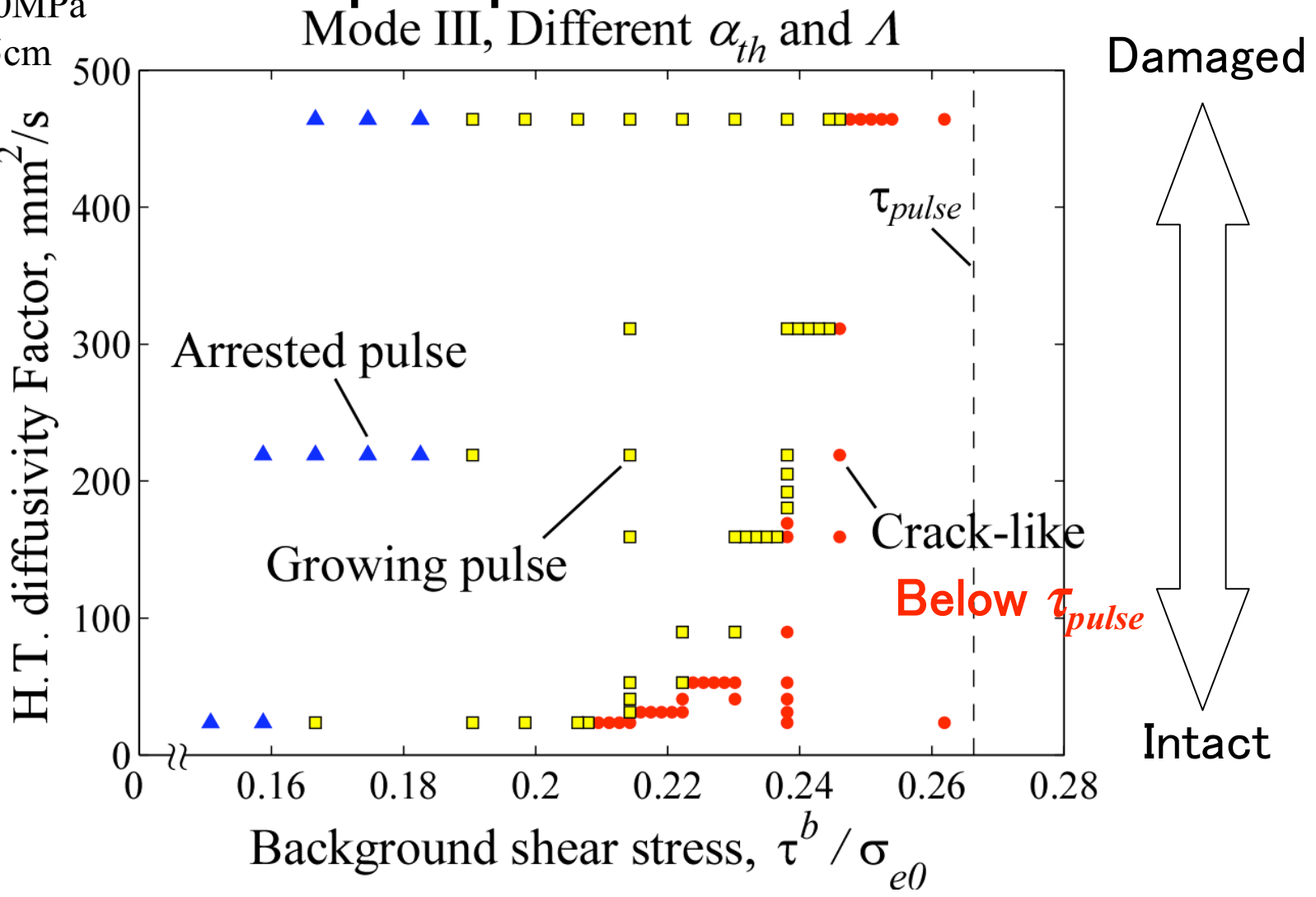

Shown:
The case $w = 0$, slip on a plane.

High τ^b favors crack-like solution, thermal pressurization does too.

Noda, Dunham & Rice [*JGR*, 2009]

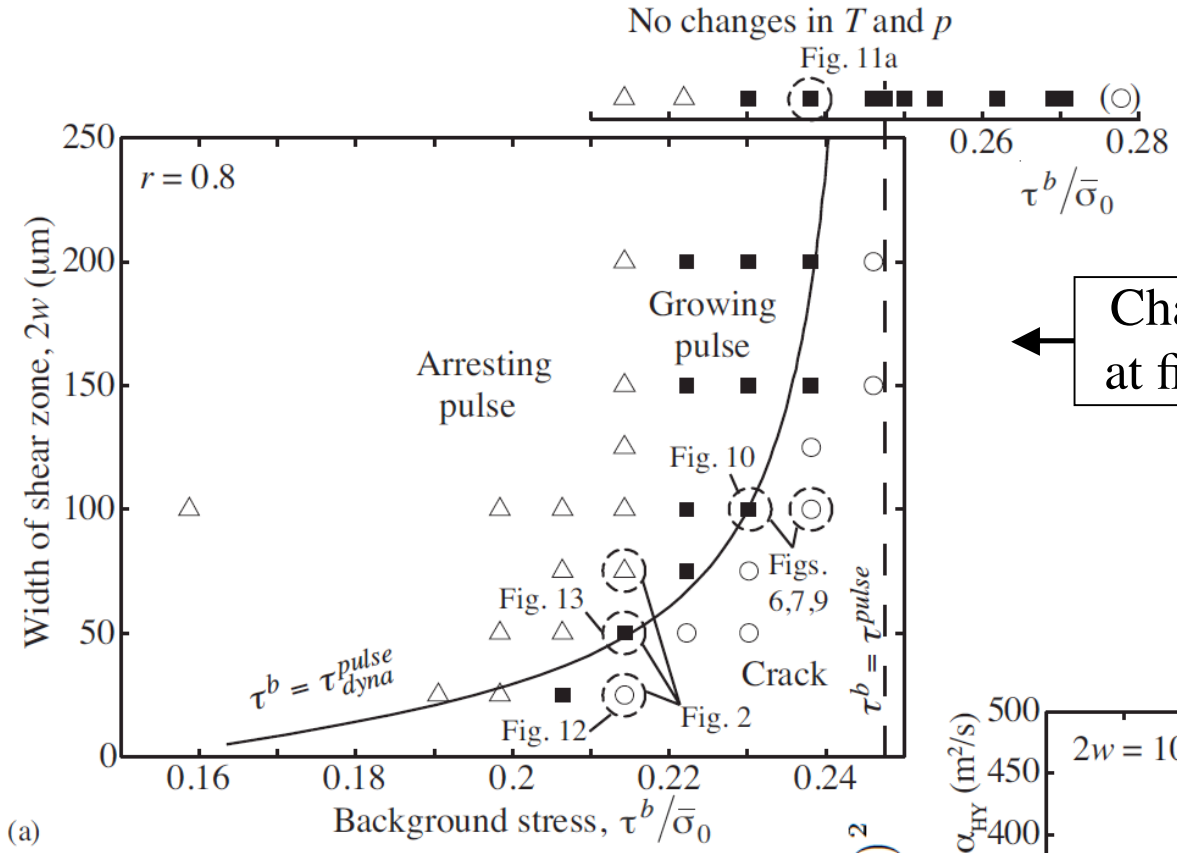

Changing width $2w$ of shear zone, at fixed damage intensity ($r = 0.8$).

Changing damage intensity (hence magnitude of hydro-thermal diffusivity factor), at fixed width $2w = 100$ μm of shear zone.

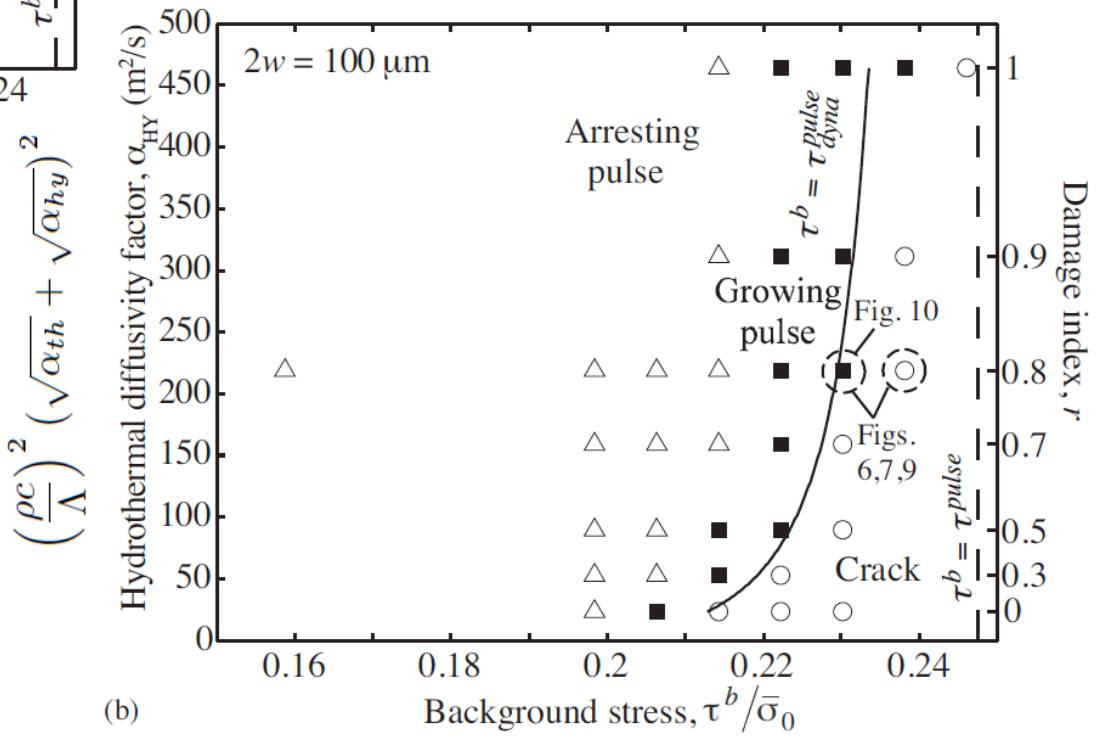

Noda, Dunham & Rice [*JGR, 2009*] longest simulation to date: ~30 m rupture length

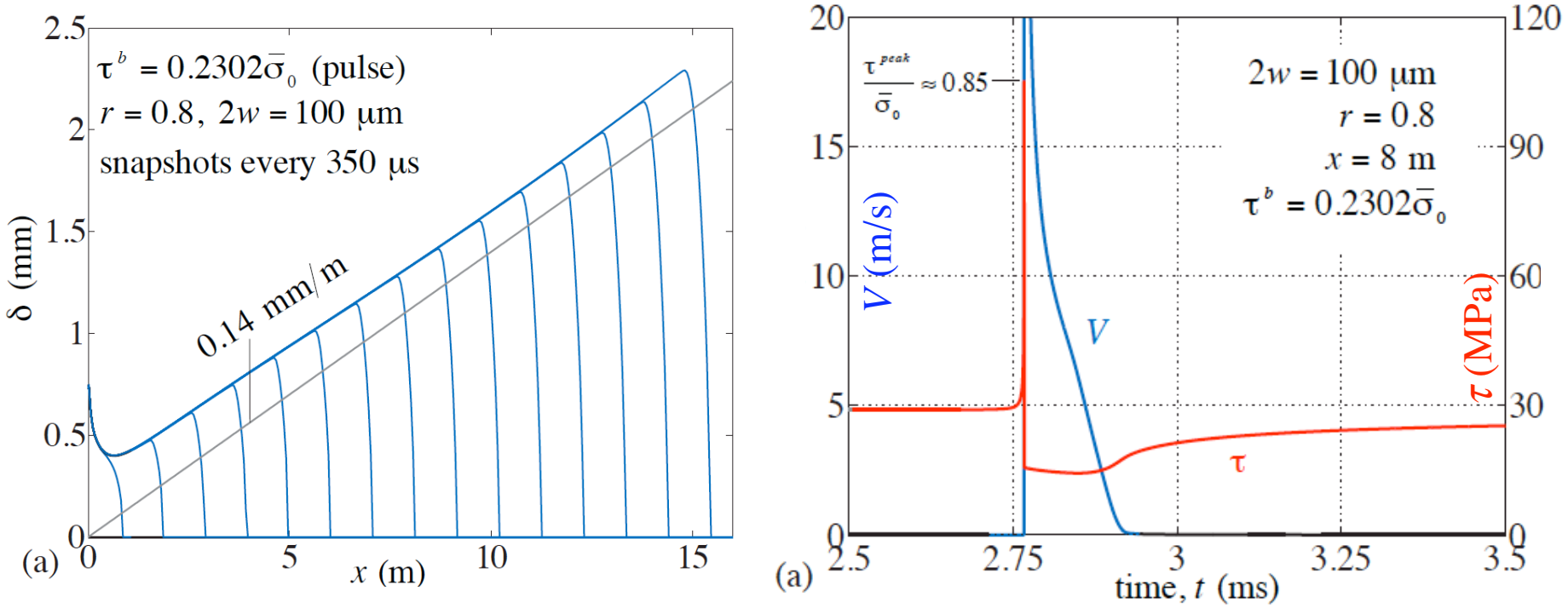

left: Distribution of slip δ showing a ~linear increase with x by 0.14 mm/m.

right: History of slip rate V and shear stress τ at $x = 8$ m:

- Peak V is extremely high (> 100 m/s).
- τ^b (= initial shear stress) ~ 29 MPa = 0.23 $(\sigma - p_o)$ $[\sigma - p_o = 126$ MPa$]$.
- τ^{peak} (= peak stress at rupture front) ~ 107 MPa = 0.85 $(\sigma - p_o)$
- $\tau^b - \tau^{final}$ (= seismic stress drop $\Delta\sigma$) ~ 3 MPa

Noda, Dunham & Rice [*JGR, 2009*]

Comparing a growing slip pulse at $\tau^b = 0.230\ (\sigma_0 - p_0)$ to an enlarging shear crack at $\tau^b = 0.238\ (\sigma_0 - p_0)$

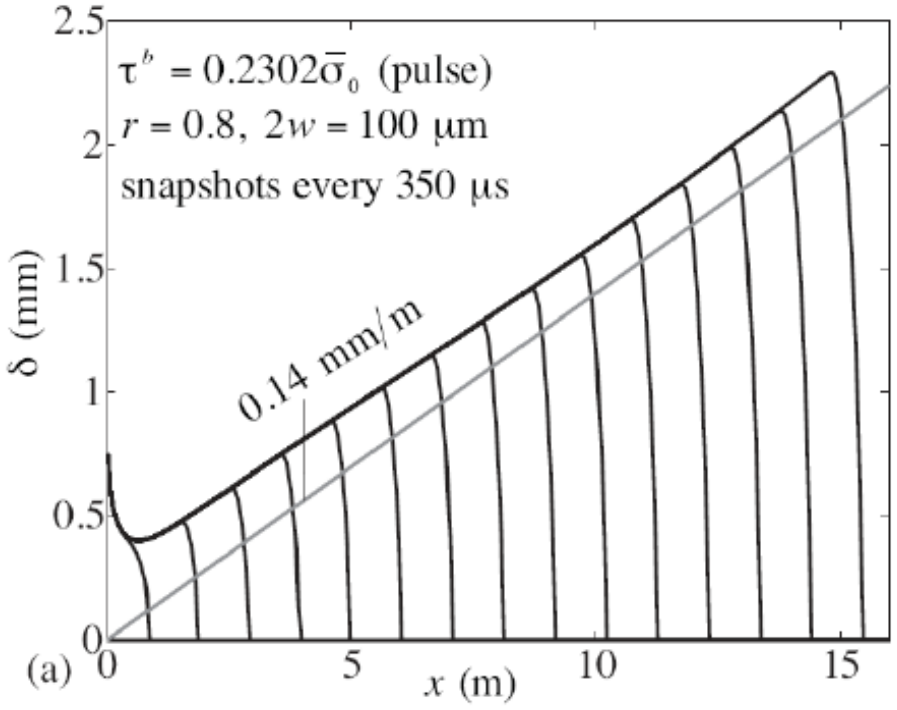

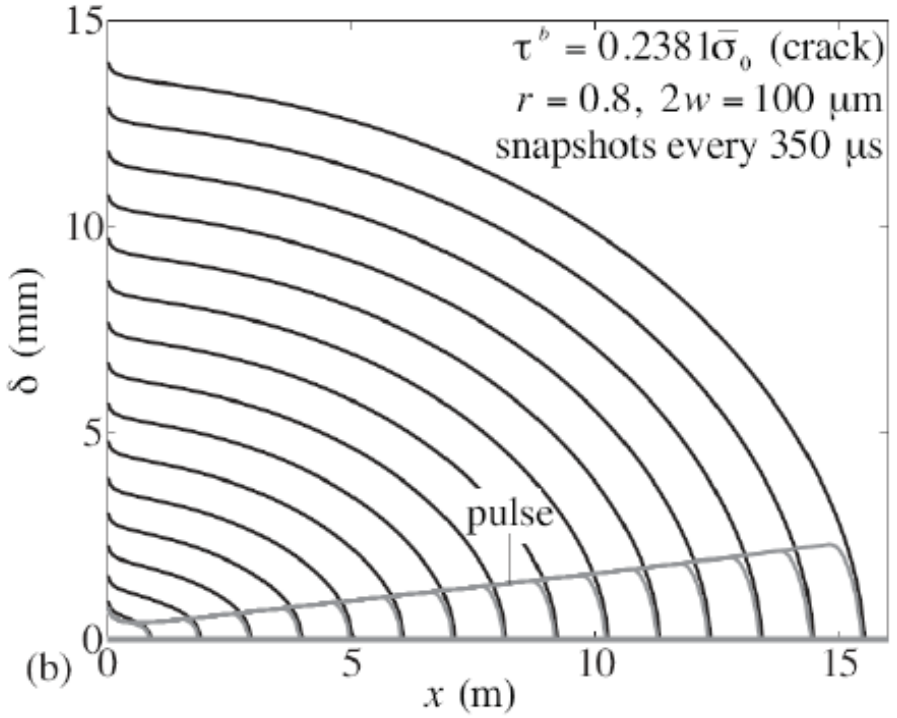

For ***self-healing slip pulse*** simulation, seismic stress drop $\tau^b - \tau^{final} \sim 3$ MPa.

For ***crack-like*** simulation, seismic stress drop $\tau^b - \tau^{final} \sim 19$ MPa.

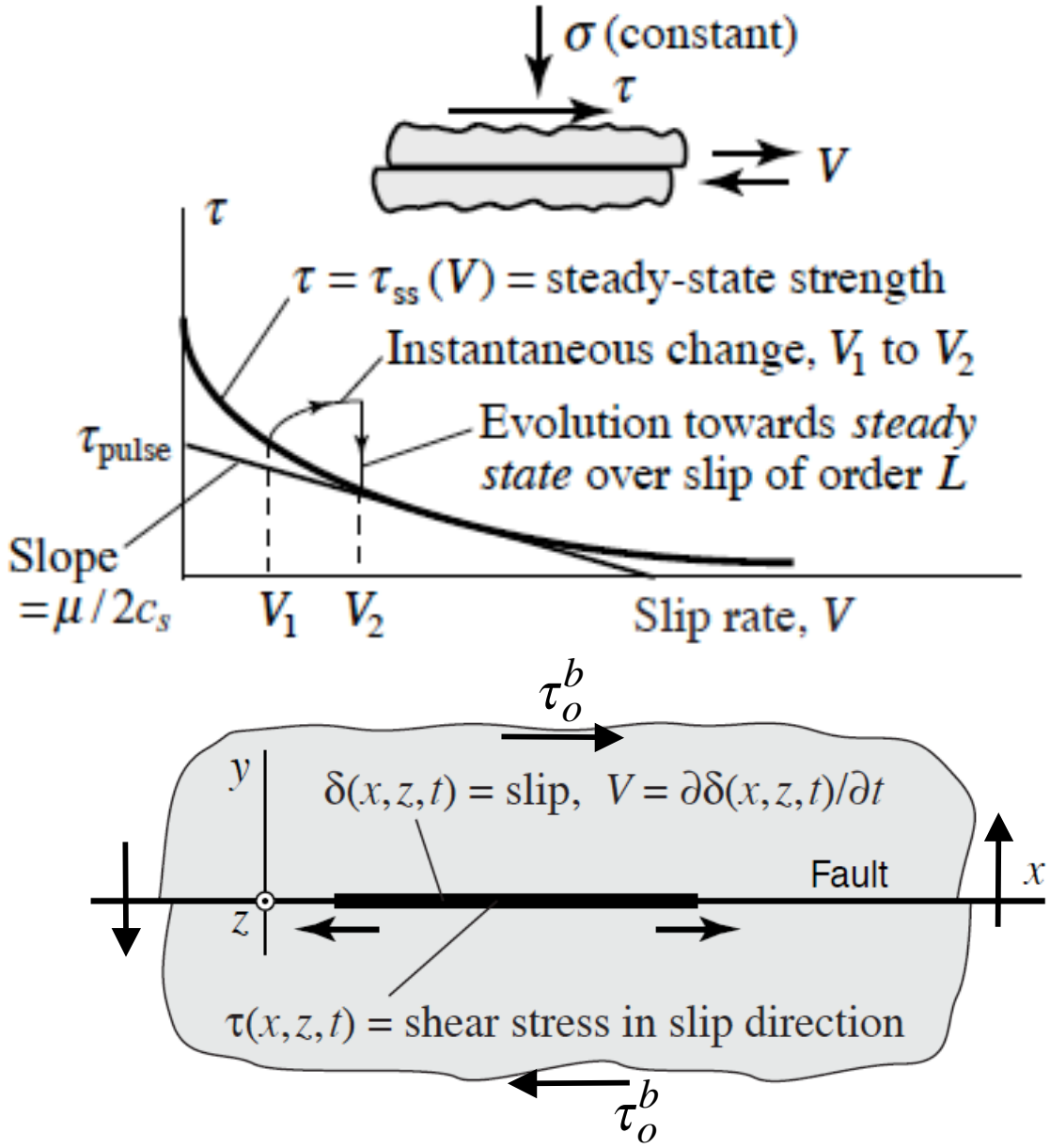

Zheng & Rice theorem [*BSSA* 1998]:

No crack-like rupture is possible if

$\tau_o^b < \tau_{pulse}$

Figure 6 Identical elastic half-spaces meeting on a fault plane $y = 0$; for discussion of crack-like versus self-healing rupture mode.

[Lykotrafitis, Rosakis & Ravichandran, *Sci.* 2006; Lu, Lapusta & Rosakis, *PNAS* 2007]

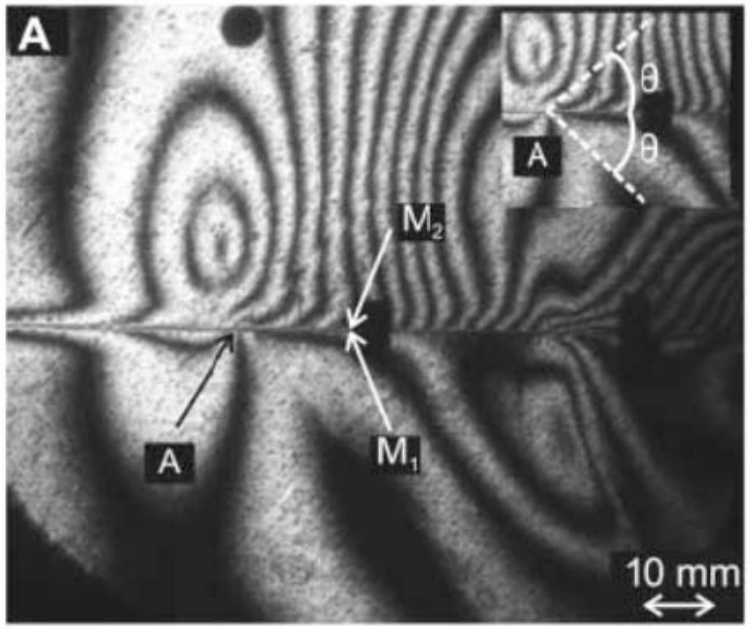

Theory Consistent with Laboratory Experiments

(transition from crack to pulse as shear/normal load decreases)

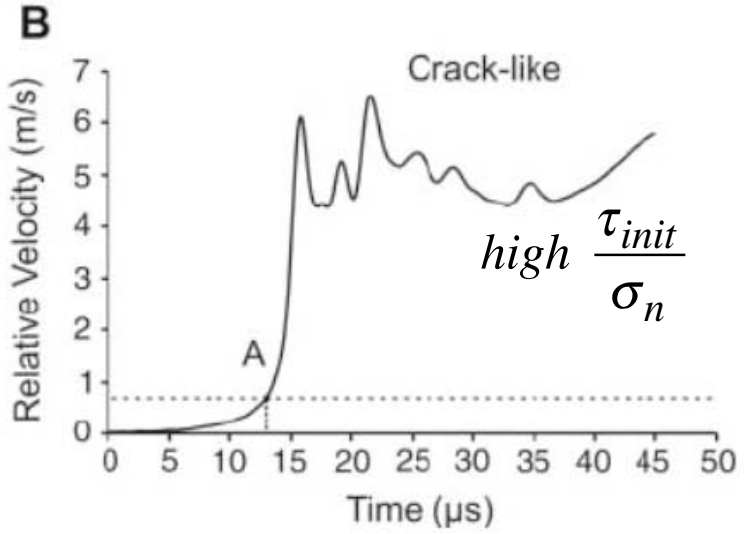

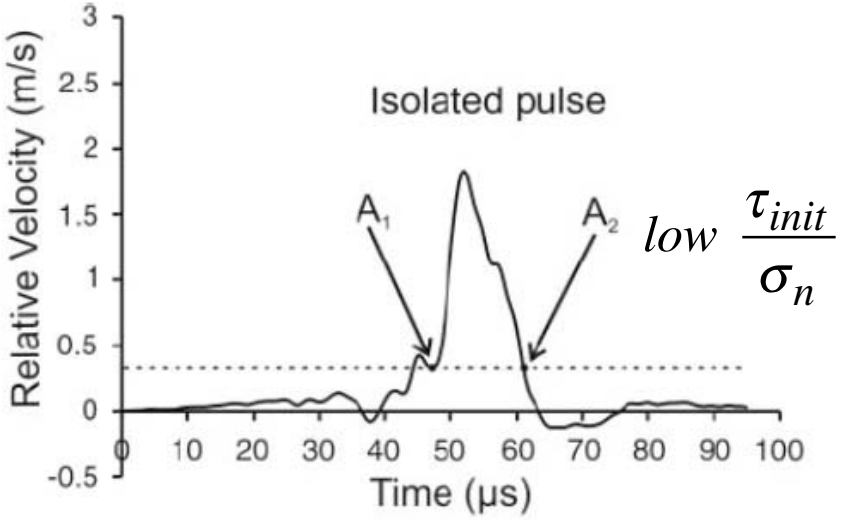

… and Seismic Slip Inversions for Natural Events Suggest Self-Healing!

Heaton [*PEPI*, 1990]

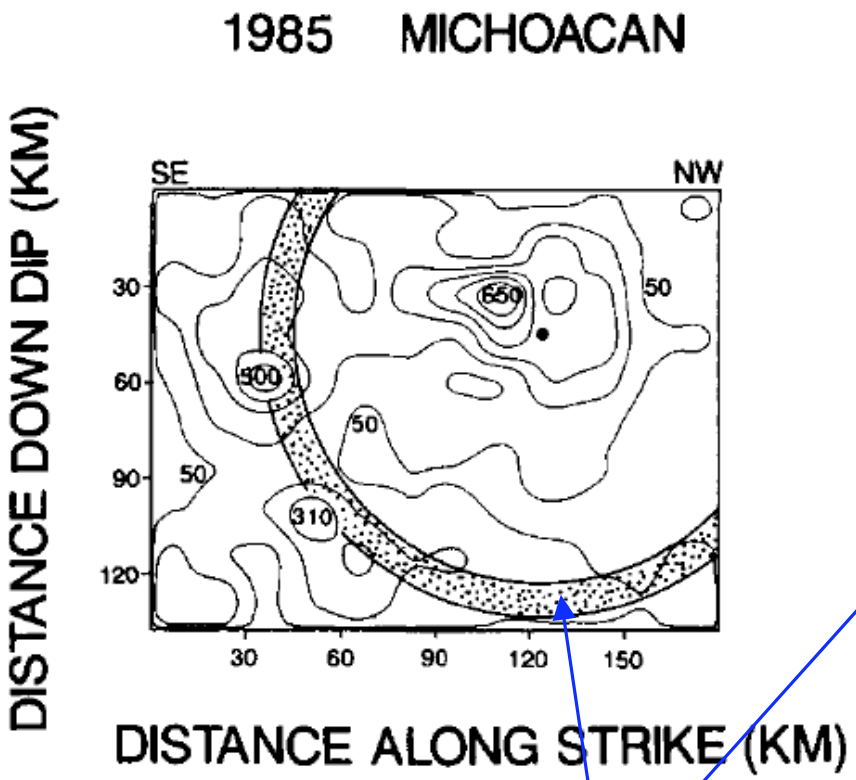

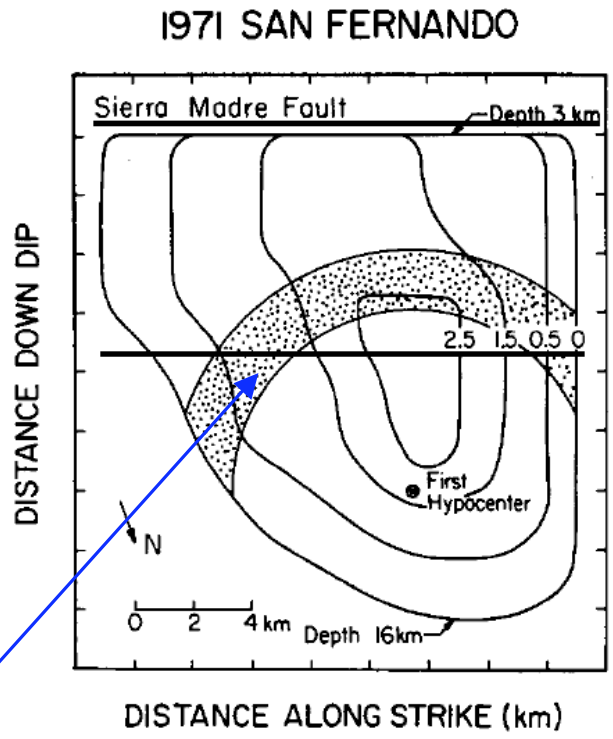

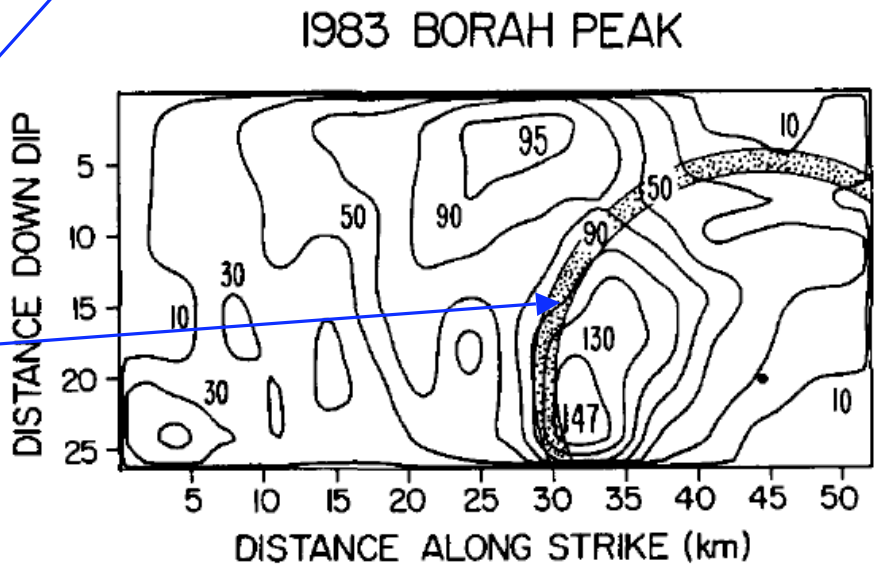

approximate region slipping at a particular moment in time

Heaton [*PEPI*, 1990]

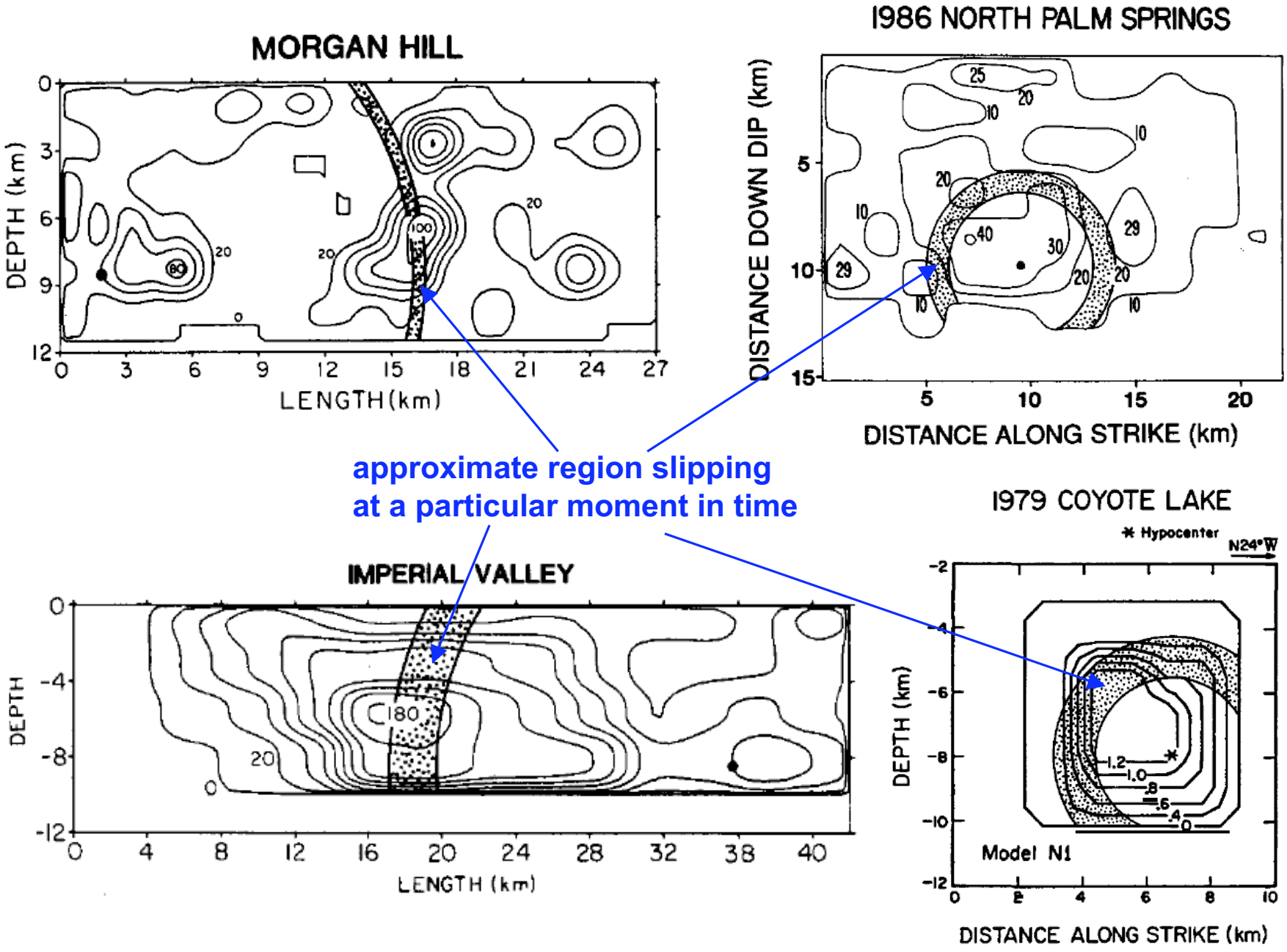

[Allmann & Shearer, "**Global variations of stress drop for moderate to large earthquakes**", *JGR*, 2009]

For ***self-healing pulse*** simulation shown, seismic stress drop $\tau^b - \tau^{final} \sim 3$ MPa.

For ***crack-like*** simulation shown, seismic stress drop $\tau^b - \tau^{final} \sim 19$ MPa.

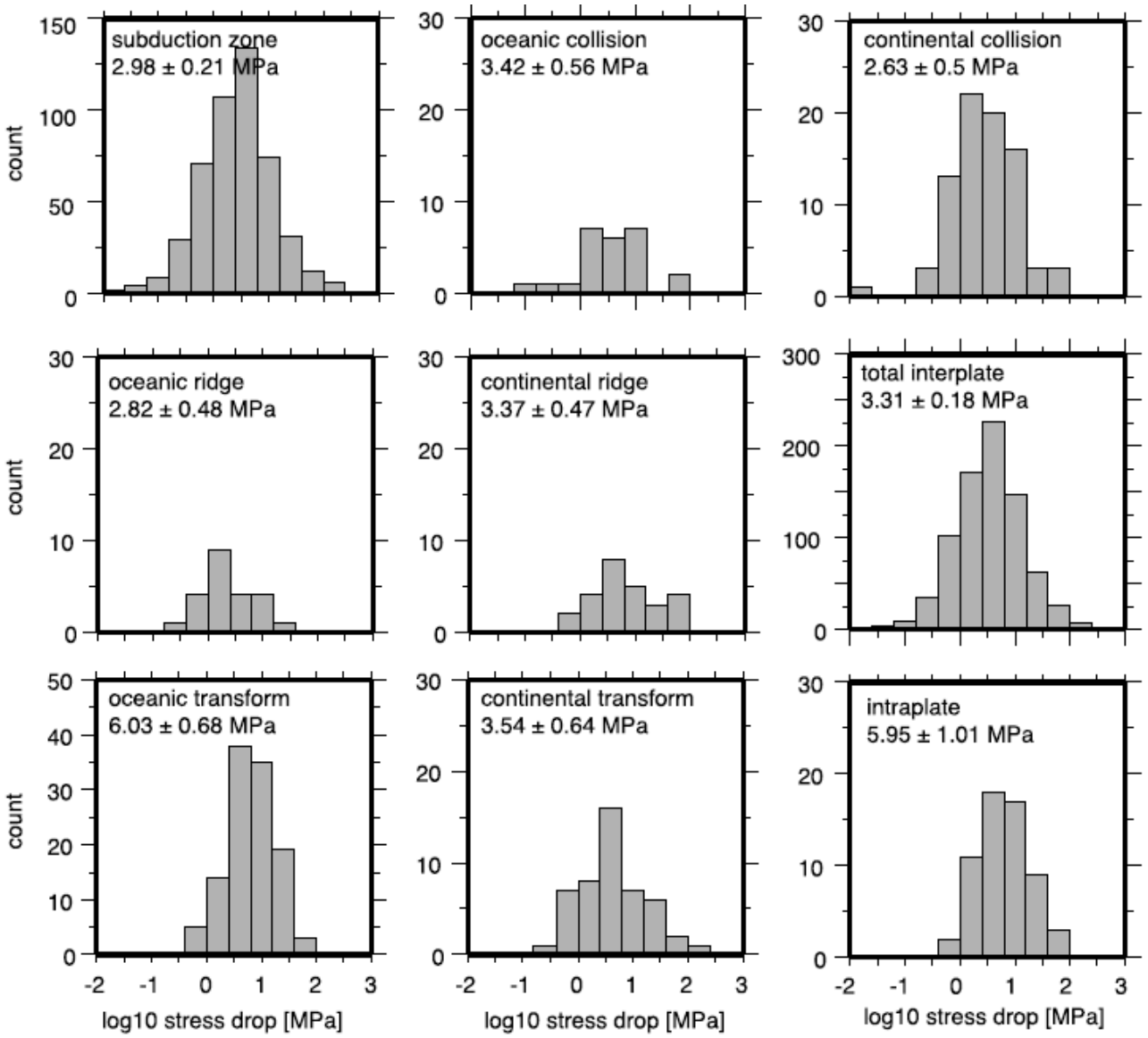

Figure 18. Histograms of stress drop distributions by tectonic region. See Table 1 for number of events in each class. The listed number denote the median stress drops together with their standard errors.

Noda, Dunham & Rice [*JGR, 2009*]

Comparing a growing slip pulse at $\tau^b = 0.230\,(\sigma_0 - p_0)$ to an enlarging shear crack at $\tau^b = 0.238\,(\sigma_0 - p_0)$

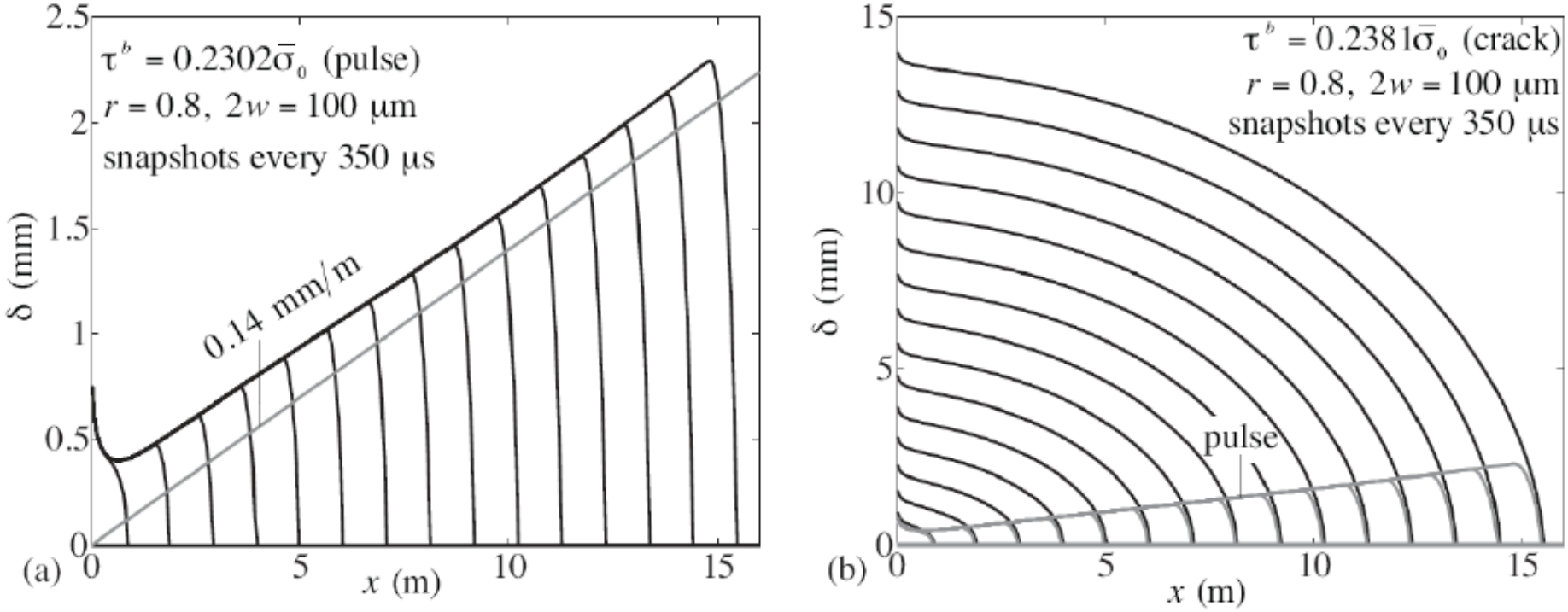

Both predict (if projected to circular fault) Seismic Moment M_o [Nm] $\approx \lambda \times 10^{17}\,(t$ [s]$)^3$;

$\lambda \approx 1.7$ for ***slip pulse***, $\lambda \simeq 10.5$ for ***crack***; compare, $\lambda \approx 2$ for Parkfield 2004 [Uchide]

[Using $\delta^{3D}/\delta^{2D} = 0.73$, μ=35 GPa, ρ=2800 kg/m^3 (c_s = 3.5 km/s), and $v_r = 0.8 c_s$]

Parkfield: San Andreas Fault Observatory at Depth

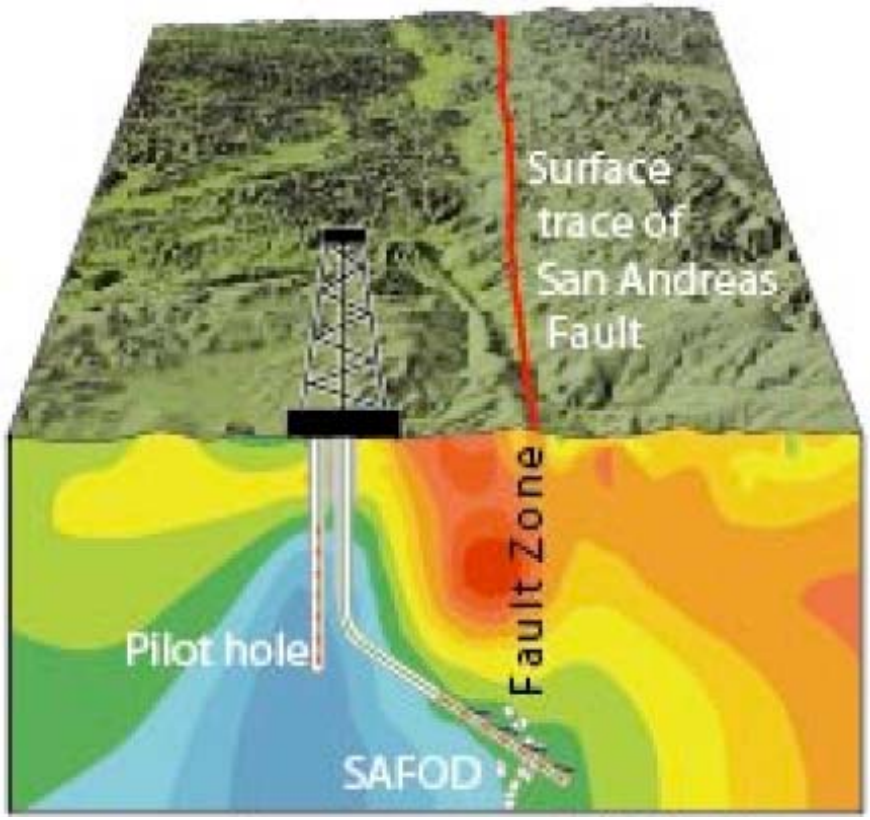

Schematic cross section of the San Andreas Fault Zone at Parkfield, showing the drill hole for the San Andreas Fault Observatory at Depth (SAFOD) and the pilot hole drilled in 2002. Red dots in drill holes show sites of monitoring instruments. White dots represent area of persistent minor seismicity at depths of 2.5 to more than 10 km. The colors in the subsurface show electrical resistivity of the rocks as determined from surface surveys; the lowest-resistivity rocks (red) above the area of minor earthquakes may represent a fluid-rich zone.

[Hickman & Zoback, *GRL* 2004]

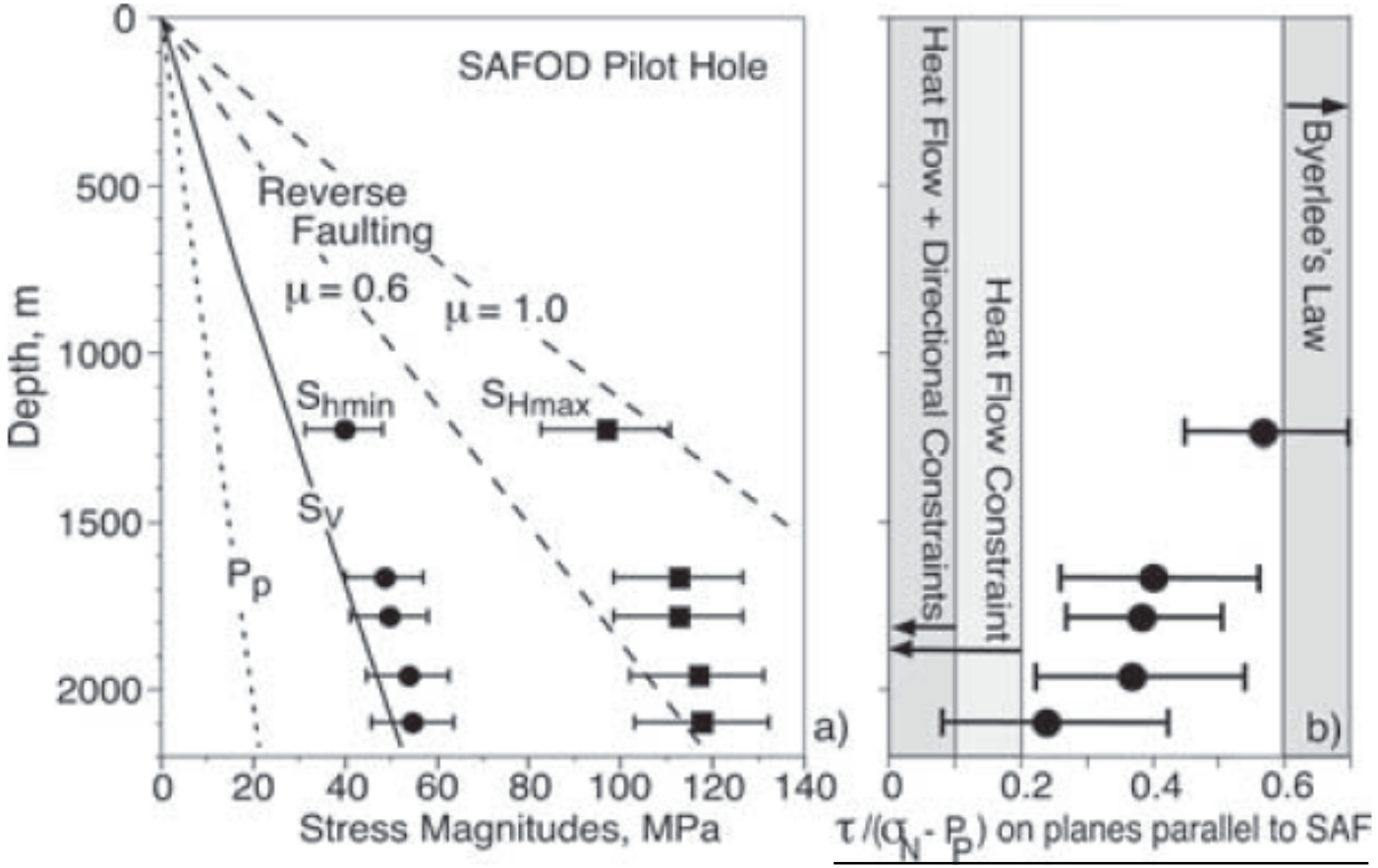

Simulations show growing pulse for ~ 0.22-0.24

Summary:

The simulations are based on laboratory friction and poromechanical studies, on geological characterizations of major fault zones, and on mathematical modeling of heating and weakening and of elastodynamics.

They have *no* input from seismology, heat flow, or regional stress magnitude/direction studies!

Yet they predict results, in particular:

- fault operation at low overall shear stress,
- self-healing rupture mode,
- magnitude of static stress drop,
- scaling of slip with rupture extent, and
- scaling of slipping pulse length with rupture extent (too small?),

which look somewhat like earthquakes on major faults as constrained by seismology, heat flow and stress studies.

Topics addressed:

• Rate- and state-dependent friction formulation: Physical and experimental background; applications to earthquake nucleation and earthquake sequences, aseismic deformation transients, and seismicity changes in response to stress transfers.

• Resolving a quandary in seismology: Major faults operate under low overall driving stress, in a manner that generates negligible heat outflow -- what fault zone physics (i.e., what thermo-hydro-mechanical processes) could allow that?

For publications by James R. Rice and collaborators mentioned here:

- Full citations are listed at http://esag.harvard.edu/rice/RicePubs.html
- Most items can be downloaded from that site.